

2012

Infrared laser ablation for biological mass spectrometry

Fan Huang

Louisiana State University and Agricultural and Mechanical College, fanchem@gmail.com

Follow this and additional works at: https://digitalcommons.lsu.edu/gradschool_dissertations



Part of the [Chemistry Commons](#)

Recommended Citation

Huang, Fan, "Infrared laser ablation for biological mass spectrometry" (2012). *LSU Doctoral Dissertations*. 2235.
https://digitalcommons.lsu.edu/gradschool_dissertations/2235

This Dissertation is brought to you for free and open access by the Graduate School at LSU Digital Commons. It has been accepted for inclusion in LSU Doctoral Dissertations by an authorized graduate school editor of LSU Digital Commons. For more information, please contact gradetd@lsu.edu.

INFRARED LASER ABLATION FOR BIOLOGICAL MASS SPECTROMETRY

A Dissertation

Submitted to the Graduate Faculty of the
Louisiana State University
Agricultural and Mechanical College
in partial fulfillment of the
requirements for the degree of
Doctor of Philosophy

in

The Department of Chemistry

by

Fan Huang

B. S., Peking University, China, 2000

M. S., University of Science and Technology of China, 2005

May 2012

ACKNOWLEDGEMENTS

This dissertation could not have been completed without the help and support of many people that I truly thank, from the bottom of my heart:

To my dear wife Tingting Jia, I am so blessed to have met you, and I cannot imagine the world without you. To my mom Yufang Liu and my dad Zhenjia Huang, you have always believed in me and given me your endless love and support. You are the greatest parents in the world.

To my advisor Professor Kermit Murray, I am very grateful for your invaluable guidance and encouragement throughout my Ph.D program studies. You are deeply appreciated. I am also thankful to my committee members, Professor Bin Chen, Professor Jayne Garno, Professor Megan Macnaughtan, and Professor Ernest Mendrela, for your time and helpful advice. Special thanks to Dr. Azeem Hasan for allowing me to work in the mass spectrometry facility and giving me help.

To the Murray Research Group both past and present: Mark, Damien, Jae-Kuk, John, Jerrell, Jianan, Xing, Jeonghoon, Jaye, Lancia, Udaya, Nicole, Thabiso, Xin, Sung-gun, Jon, Salla, Pratap, Yonathan, and Chinthaka. You are like brothers and sisters to me here at LSU. I will always remember the time we spent together in the lab, and I sincerely wish you all a great future. Special gratitude goes to post-doctoral researcher Yohannes who taught me how to use the trap instrument, Xing who taught me how to use the infrared lasers, and Zhe from the Mathematics Department at LSU who helped me with MATLAB calculations.

Finally, I want to thank all my family and friends, especially those of you in my hometown of Beijing, China. You all have given me much help and support. I will always miss you.

TABLE OF CONTENTS

ACKNOWLEDGEMENTS	ii
LIST OF TABLES	v
LIST OF FIGURES	vi
LIST OF ABBREVIATIONS	viii
ABSTRACT.....	xi
CHAPTER 1. INTRODUCTION.....	1
1.1. Mass Spectrometry	4
1.1.1. Electrospray Ionization.....	11
1.1.2. Matrix-assisted Laser Desorption Electrospray Ionization	14
1.2. Fundamentals of Laser Desorption and Ablation	15
1.3. Research Objectives.....	22
CHAPTER 2. EXPERIMENTAL	24
2.1. Time-of-flight Mass Spectrometry	24
2.2. IR/UV Two-laser MALDI TOF Mass Spectrometer	26
2.3. Three-dimensional Quadrupole Ion Trap	29
2.4. Continuous Flow IR MALDESI Mass Spectrometry	31
2.5. Reagents and Standards	37
CHAPTER 3. MATRIX-ASSISTED LASER DESORPTION IONIZATION OF INFRARED LASER ABLATED PARTICLES.....	38
3.1. Introduction.....	38
3.2. Experimental.....	40
3.3. Results and Discussion	42
3.4. Summary.....	49
CHAPTER 4. CONTINUOUS FLOW INFRARED MATRIX-ASSISTED LASER DESORPTION ELECTROSPRAY IONIZATION MASS SPECTROMETRY	51
4.1. Introduction.....	52
4.2. Experimental.....	55
4.3. Results and Discussion	57
4.4. Summary.....	68
CHAPTER 5. FINITE ELEMENT SIMULATION OF INFRARED LASER ABLATION OF GLYCEROL	69
5.1. Introduction.....	69
5.2. Ablation Model.....	72
5.3. Results and Discussion	74
5.4. Summary.....	84

CHAPTER 6. CONCLUSIONS AND FUTURE DIRECTIONS	86
REFERENCES.....	91
APPENDIX A. MATLAB PROGRAM FOR CALCULATING ABLATED SAMPLE VOLUME.....	105
APPENDIX B. LETTERS OF PERMISSION.....	109
VITA.....	128

LIST OF TABLES

Table 1-1 Commonly used UV MALDI matrices.....	8
---	---

LIST OF FIGURES

Figure 1-1 Schematic diagram of MALDI.....	7
Figure 1-2 Schematic diagram of ESI.....	12
Figure 1-3 Schematic diagram of IR-MALDESI.....	15
Figure 1-4 Phase diagram near the critical point indicating normal heating and superheating	18
Figure 2-1 Schematic layout of the IR/UV two-laser matrix-assist laser desorption ionization linear time-of flight mass spectrometer	26
Figure 2-2 Block diagram of the OPO laser	28
Figure 2-3 Schematic diagram of the IR/UV two-laser arrangement	29
Figure 2-4 Cross-section view of an ion trap mass analyzer	31
Figure 2-5 Schematic of the Hitachi M8000 3DQ ion trap mass spectrometer	32
Figure 2-6 Schematic (top) and photograph (bottom) of the CF IR MALDESI MS interface showing the nanospray source, capillary, liquid sample bead, and mass spectrometer orifice	34
Figure 2-7 Optical layout diagram of the OPO laser	35
Figure 2-8 Schematic (top) and photograph (bottom) of the on-line CF IR MALDESI reaction monitoring setup showing the nanospray, 6-port valve, nano mixer, and the MS orifice	36
Figure 3-1 Bradykinin mass spectra with different laser conditions: (a) 2.94 μm IR laser only, (b) 351 nm UV laser only, and (c) IR and UV lasers at $\Delta t = 50 \mu\text{s}$	43
Figure 3-2 Signal intensity of singly-charged molecular bradykinin ions as a function of delay time	44
Figure 3-3 Signal intensity of singly-charged molecular bradykinin ions as a function of IR laser fluence.....	45
Figure 3-4 Signal intensity of singly-charged molecular bradykinin ions as a function of UV laser fluence	46
Figure 3-5 IR/UV two-laser mass spectra of (a) cytochrome c at $\Delta t = 70 \mu\text{s}$ and (b) insulin at $\Delta t = 60 \mu\text{s}$	48
Figure 4-1 Scheme of 1,10-phenanthroline reaction with Fe^{2+}	58
Figure 4-2 On-line CF IR MALDESI mass spectra of the chelation of 1,10-phenanthroline (PA) with iron (II) in water. Positive-ion CF IR MALDESI mass spectra were recorded at three reaction stages: (a) 2 mM PA solution only before reaction, (b) PA solution after mixing with 20 mM FeSO_4 solution, and (c) after FeSO_4 solution depleted	59

Figure 4-3 Ion signals for (a) $[PA + H]^+$ and (b) $[(PA)_3 + Fe]^{2+}$ ions during the chelation reaction recorded as a function of reaction time.....	60
Figure 4-4 CF IR MALDESI mass spectra of (a) 500 μ M insulin in 50 mM NH_4HCO_3 water buffer solution, (b) 500 μ M insulin mixed with 100 mM 1,4-dithiothreitol (DTT) reducing agent, and (c) denatured insulin b chain after on-line mixing of 500 μ M insulin with 100 mM DTT solution.....	63
Figure 4-5 (a) CF IR MALDESI mass spectrum of 600 μ M cytochrome c in 50 mM NH_4HCO_3 water buffer solution with +10 through +18 charge states. (b) CF IR MALDESI mass spectrum of 600 μ M cytochrome c 1:10 (v/v) mixed with 600 mM trypsin. Peaks labeled with asterisks are assigned to tryptic peptides.....	64
Figure 4-6 CF IR MALDESI mass spectra of on-line digested cytochrome c solutions with different cytochrome c concentrations: (a) 600 μ M, (b) 500 μ M, (c) 400 μ M, and (d) 300 μ M. Peaks labeled with asterisks are assigned to tryptic peptides	66
Figure 4-7 Comparison of CF IR MALDESI mass spectra of a digested 500 μ M cytochrome c solution at flow rates: of (a) 4 mL min^{-1} and (b) 2 mL min^{-1}	67
Figure 5-1 Glycerol temperature with a 2.94 μ m flat-top profile laser at 6000 J/m^2 fluence for times of (a) 2 ns, (b) 5 ns, (c) 5 μ s, (d) 50 μ s, and (e) 1 ms.....	75
Figure 5-2 Glycerol temperature a) at the surface ($y = 0$) and b) as a function of depth ($x = 0$) for different times ((■) 5 ns, (Δ) 50 μ s, (\square) 20 ms, and (\blacktriangle) 0.1s) with a 2.94 μ m flat-top laser and 6000 J/m^2 fluence.....	76
Figure 5-3 Glycerol temperature after 5 ns for a) 2.94 μ m and b) 3.4 μ m wavelengths at 3000 J/m^2 fluence.....	77
Figure 5-4 Glycerol temperature versus sample depth after 5 ns for a) 2.94 and b) 3.40 μ m laser with different fluences: (■) 1000 J/m^2 , (\circ) 3000 J/m^2 , and (\blacktriangle) 5000 J/m^2	79
Figure 5-5 Laser wavelength dependence of glycerol surface temperature for fluences: (■) 1000 J/m^2 , (\circ) 2000 J/m^2 , (\blacktriangle) 3000 J/m^2 , (\square) 4000 J/m^2 , (\bullet) 5000 J/m^2 , and (Δ) 6000 J/m^2	80
Figure 5-6 Glycerol temperature for a 2.94 μ m wavelength Gaussian profile laser: a) temperature profile at 5 ns; b) temperature distribution along at the surface: (■) 5 ns, (Δ) 50 μ s, (\square) 20 ms, and (\blacktriangle) 0.1 s.....	81
Figure 5-7 Laser energy dependence of the a) depth and b) volume of glycerol subject to phase explosion at 2.94 μ m wavelength for flat-top (■) and Gaussian (\circ) laser profile	82

LIST OF ABBREVIATIONS

3D	three-dimensional
APCI	atmospheric pressure chemical ionization
APPI	atmospheric pressure photoionization
CF	continuous flow
CHCA	α -cyano-4-hydroxycinnamic acid
CI	chemical ionization
CRM	charge residue model
Da	dalton
DART	direct analysis in real time
DESI	desorption electrospray ionization
DHB	2,5-dihydroxybenzoic acid (Gentisic acid)
DSMC	direct simulation Monte Carlo
DTT	1,4-dithiothreitol
EESI	extractive electrospray ionization
EI	electron ionization
ELDI	electrospray-assisted laser desorption ionization
ESI	electrospray ionization
FAB	fast atom bombardment
FEM	finite element method
FT-ICR	Fourier-transform ion cyclotron resonance
GD	glow discharge
GPIB	general purpose interface bus
HPA	3-hydroxypicolinic acid

ICP	inductively coupled plasma
IEM	ion evaporation model
IR	infrared
IT	ion trap
KTP	potassium titanyl phosphate
LA	laser ablation
LADESI	laser-assisted desorption electrospray ionization
LAESI	laser ablation electrospray ionization
LDI	laser desorption ionization
LIBS	laser induced breakdown spectrometry
LMMS	laser microprobe mass spectrometry
<i>m/z</i>	mass-to-charge ratio
MALDESI	matrix-assisted laser desorption electrospray ionization
MALDI	matrix-assisted laser desorption ionization
MCP	microchannel plate
MD	molecular dynamics
MS	mass spectrometry
NBA	nitrobenzyl alcohol
Nd:YAG	neodymium-doped yttrium aluminium garnet
NRO	non-resonant oscillator
OPA	optical parametric amplifier
OPO	optical parametric oscillator
PA	1,10-phenanthroline
RF	radio frequency
SA	trans-3,5-dimethoxy-4-hydroxycinnamic acid (Sinapinic

	acid, Sinapic acid)
TCEP	tris(2-carboxyethyl)phosphine
TFA	trifluoroacetic acid
TOF	time-of flight
UV	ultraviolet

ABSTRACT

Instrument and technique development and modeling of ionization methods using infrared (IR) laser desorption and ablation for mass spectrometry (MS) analysis of chemical and biochemical samples are described. Infrared lasers are highly efficient at sample removal and post-ablation ionization of materials removed by IR laser can be used to improve ionization efficiency. Fundamental studies of the physical processes in laser ablation mass spectrometry can help elucidate the mechanism. In this research, an infrared/ultraviolet two-laser matrix-assisted laser desorption ionization (MALDI) MS was developed for analysis of biomolecules. An infrared laser was used to ablate a mixture of analyte and matrix, and the ablated material was post-ionized by an ultraviolet (UV) laser. Factors affecting ion yield, including IR and UV laser fluences and the delay time between the laser pulses, were studied using a peptide standard. Protein samples were tested and the observed signals suggested that ionization occurs through a UV MALDI mechanism. A continuous flow infrared matrix-assisted laser desorption electrospray ionization (CF IR MALDESI) mass spectrometry was developed for study of chemical and biochemical reactions. Samples in aqueous solution were flowed through a silica capillary to form a liquid bead at the capillary tip. An IR laser was used for sample ablation and the ejected sample was entrained in an electrospray to form ions. Ions were sent to an ion trap mass spectrometer for analysis. The chelation reaction of 1,10-phenanthroline with iron (II), the denaturation reaction of insulin with 1,4-dithiothreitol, and tryptic digestion of cytochrome c were on-line monitored. A two-dimensional finite element model was developed to simulate IR laser ablation of glycerol. The laser fluence was varied from 1 to 6 kJ/m², and the wavelength was varied from 2.7 – 3.7 μm that covered the OH and CH stretch absorption region of glycerol. The results showed a strong temperature dependence on laser wavelength and fluence. The peak

temperature of glycerol was obtained as the laser wavelength tuned to OH stretch absorption at 3 μm , and was sufficient for phase explosion to occur. The simulation results showed a good agreement with previous particle sizing and plume imaging results.

CHAPTER 1. INTRODUCTION

Laser desorption and ablation are phenomenon of material ejection from a condensed sample upon irradiation with intense laser pulses,^{1, 2} and have been widely used in mass spectrometry (MS) for sampling and ionization. Initially laser ablation mass spectrometry was applicable only to compounds with molecular mass limited to about 1000 daltons (Da) due to the direct laser absorption by the sample that causes fragmentation.³ This limitation remained until the appearance of soft (limited fragmentation) laser desorption ionization methods.^{4,5} Today, the soft ionization technique of matrix-assisted laser desorption ionization (MALDI) is one of the two major ionization techniques that, along with electrospray ionization (ESI), are known as dominant, powerful, and sensitive mass spectrometry detection tools for analysis of high molecular weight compounds, such as biomolecules and polymers. In electrospray ionization, a high voltage is applied to a liquid which forms a spray of highly charged droplets and, after solvent evaporation, highly charged ions.

Despite their ability for ionizing large molecules, MALDI and ESI each has its own drawbacks.⁶ For example ESI has poor tolerance for impurities and usually requires sample treatment prior to ionization, such as liquid separation. MALDI is difficult to couple directly to on-line liquid sample analysis, and requires sample preparation steps such as dissolving the sample in a suitable solvent and deposition with a matrix solution.

In recent years, several ionization techniques have been developed that allow mass spectrometric analysis under ambient conditions with minimal sample preparation.⁶⁻⁹ These new approaches are called ambient ionization and offer unprecedented flexibility in direct sample analysis in the open environment and have made a significant impact on the world of analytical science. Desorption electrospray ionization (DESI) and direct analysis in real time (DART) are

two recently developed ambient ionization methods that have been considered as largely responsible for the rapid growth of this field.⁶ DESI produces ions by the bombardment of the sample surface with a stream of ESI-charged droplets. In DART, ionization occurs when the sample is exposed to a stream of metastable species containing excited state atoms and molecules.¹⁰ Both DESI and DART have been used in a number of diverse application areas, such as drug analysis, forensics, food safety, and homeland security.^{6, 8, 9}

Several ambient ionization techniques use laser ablation for sampling, such as matrix-assisted laser desorption electrospray ionization (MALDESI),^{11, 12} electrospray-assisted laser desorption ionization (ELDI),¹³ and laser ablation electrospray ionization (LAESI).¹⁴ These methods combine laser ablation at atmospheric pressure with electrospray ionization, and because laser ablation and ESI are two independent steps, they can be optimized individually. These laser ablation based ambient ionization methods have been used for different applications,^{8, 9} especially for the large biomolecule analysis. For example, MALDESI has been used for detection of multiply-charged peptides and proteins,¹¹ top-down proteomics analysis,¹⁵ polypeptides,¹⁶ and biological fluids.¹²

Currently, most laser ablation MS experiments utilize pulsed ultraviolet (UV) lasers.¹⁷ Alternatively, infrared (IR) lasers have also been used.^{17, 18} IR lasers are more efficient at material removal than UV lasers. This is a disadvantage for MALDI under vacuum because accelerating ions through the expanding plume can cause fragmentation.^{19, 20} However, the efficient removal of material can be an advantage for MALDESI because the ionization is independent of the laser ablation step.^{12, 21} In addition, the deeper penetration of IR lasers enables them to remove deeply embedded analytes from materials such as thin layer chromatography plates, polyacrylamide gels, and tissue.²²⁻²⁴ A unique capability of IR laser ablation is the ability

to alter the characteristics of the ablation plume by changing the IR laser wavelength.²⁵⁻²⁷ Using an IR laser for ablation in MALDESI is particularly favorable for the analysis of biological samples, because water can be used as an intrinsic IR matrix. Therefore, it is natural to develop IR laser ablation based ionization techniques for the MS analysis of chemical and in particular, biochemical compounds.

In spite of many advantages to IR laser ablation mass spectrometry, this approach cannot be fully exploited without a thorough understanding of the processes involved in ion formation. It is known that an expanding ablation plume consists of atoms, neutral molecules, clusters, and particles that are formed either directly by laser-sample interaction or later through condensation in the expanding plume and aggregation of smaller particles.^{28, 29} Different species can play a role in different ionization techniques such as MALDI and MALDESI, however the physical and chemical mechanisms of laser ablation are not yet fully understood.^{17, 30} It is important to understand how laser parameters such as energy, wavelength, fluence, and pulse width influence material ejection in laser ablation and how the size and quantity of ejected species affect the ion formation. Gaining this information requires not only the MS analysis, but also other means such as experimental studies of particle formation^{25, 28, 31-33} and plume imaging,^{26, 34-37} as well as computational simulations^{29, 38} of laser ablation.

The goal of the research described in this dissertation was to develop and understand ionization methods based on IR laser desorption and ablation coupled with post-ablation and ionization of the material in the desorption plume. In this chapter, an overview of mass spectrometry and various ionization methods is presented. Ionization techniques that involve laser ablation are presented in detail with their applications and mechanisms. Fundamental studies of the physical processes important in laser ablation mass spectrometry are also presented.

The study of these processes can help elucidate the mechanism, and thus extend the applications of laser mass spectrometry.

1.1. Mass Spectrometry

Mass spectrometry is an analytical techniques that is used to determine the molecular weight, quantity, and composition of atoms and molecules.³ Mass spectrometers measure the mass-to-charge ratio (m/z) of gas-phase ions. A mass spectrometer consists of three fundamental parts: the ion source, the mass analyzer, and the detector. Mass spectrometry analysis begins by converting the sample to ions in the ion source by inducing either the loss or gain of a charge to the sample analyte.³⁹ The gas-phase ions are extracted and separated in the mass analyzer according to their m/z . The ions are separated using electric or a combination of electric and magnetic fields and detected in a variety of ways that produce an electrical signal corresponding to the quantity of ions of a given mass to charge ratio, m/z . Commonly used mass analyzers include time-of flight (TOF), ion trap, quadrupole, Fourier-transform ion cyclotron resonance (FT-ICR), and magnetic sector.³

The mass spectrum is a plot of the ion signal as a function of m/z . Sampling and ionization can be accomplished under vacuum or at atmospheric pressure, whereas mass analysis and ion detection is conducted under high vacuum so that ions can traverse the instrument without collisions with background gas.

Soft Ionization Methods for Biomolecule Analysis

A wide variety of ionization sources that use different ionization mechanisms have been developed.^{3, 40, 41} The method of ionization is typically determined by sample type and the

information desired from the mass spectrum. Ionization methods that utilize high energy electron beams, for example electron ionization (EI),³ or high pressure discharges, for example glow discharge (GD),⁴² or inductively coupled plasma (ICP),⁴³ are considered to be “hard” ionization methods because ionization is accompanied by extensive molecular fragmentation. Hard ionization methods are not suitable for ionizing atoms or molecules that are thermally labile or have a high molecular weight. Ion formation by these methods usually involves high energy collision process that causes extensive fragmentation. The fragmentation can prevent the detection of large molecules, limiting the usefulness of these methods to the analysis of atoms or small volatile molecules with molecular weight below a few hundred Da.^{39,41}

Soft ionization refers to the formation of gas-phase ions without extensive fragmentation.⁴⁴ The first soft ionization method was chemical ionization (CI) that was developed in 1960s.⁴⁵ The ionization source of CI is similar to the electron ionization source, but the ionization process is different. In CI, a reagent gas, usually methane, isobutane or ammonia, is introduced and bombarded with an electron beam to produce reagent ions. The reagent ions ionize sample molecules through ion-molecule reactions to produce sample ions. A common mechanism of ion formation is the protonation of the sample molecule by transfer of a proton from a reagent ion. The amount of energy transferred to the sample ion under CI conditions is normally a few electron volts (eV), which is an order of magnitude lower than that of EI (~70 eV).³ Consequently, CI produces less fragments than EI; however, CI analysis is also limited to small volatile molecules.

Desorption ionization with a beam of fast atoms or ions is called fast atom bombardment (FAB).³ In FAB, the sample is dissolved in a nonvolatile liquid matrix solution such as m-nitrobenzyl alcohol (NBA) or glycerol. The liquid mixture is then bombarded with a kV energy

beam of Xe atoms or Cs⁺ ions. The sample ions as well as neutral species are sputtered from liquid surface after the bombardment.⁴¹ Although masses as high as 30 kDa have been observed in FAB experiments (not routinely), the signal intensity above 2000 Da is usually weak and this is considered the upper mass limit of FAB.³

Laser desorption ionization (LDI) is a technique that uses a pulsed laser beam to deposit energy into a sample inducing desorption of molecules into the gas phase to produce ions.⁴¹ The first application of laser ablation with mass spectrometry was demonstrated in 1970s.⁴⁶ In LDI, ions, neutral molecules as well as particles are removed from the sample surface as a plume. Because the sample molecules directly absorb energy from the laser, which can lead to the fragmentation, LDI is applicable to a limited number of compounds with molecular weight usually < 1000 Da.

Matrix-assisted Laser Desorption Ionization

The MALDI concept was first introduced in 1985 by Karas and Hillenkamp who used a 266 nm UV laser to analyze organic molecules.⁴⁷ The main difference between MALDI and LDI is that in MALDI sample is mixed with a light absorbing matrix. In MALDI process the analyte is typically co-crystallized with a solid matrix compound, often a small organic acid with strong absorption in the near UV. A schematic of MALDI is shown in Figure 1-1. The matrix isolates analyte molecules, absorbs energy from the laser, and provides protons for analyte ionization. MALDI usually produces singly protonated molecules. Localized ejection of the matrix and expansion of the matrix into the gas phase are induced by the energy transfer. Little internal energy is transferred to the analyte molecules, which therefore protects analyte from being damaged by direct absorption of photons.⁴⁸ MALDI is used for mass spectrometric analysis of

large, non-volatile and thermally labile compounds such as proteins,^{4, 5} synthetic polymers,⁴⁹ oligonucleotides,⁵⁰ polysaccharides⁵¹ and lipids.⁵² MALDI has significantly increased the upper mass limit for the MS analysis of biomolecules to greater than 500,000 Da.^{53, 54}

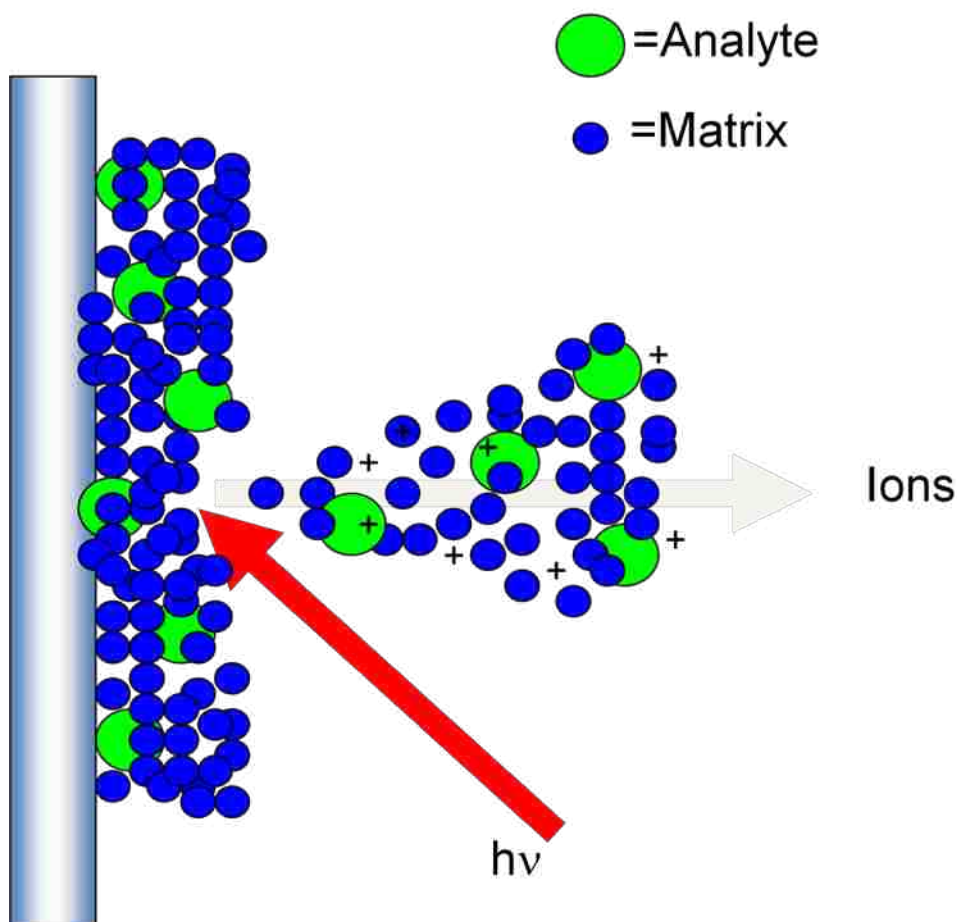
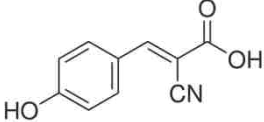
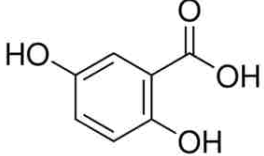
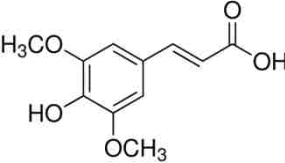
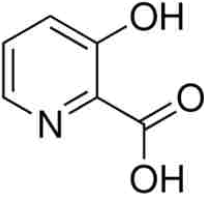


Figure 1-1 Schematic diagram of MALDI.

Desirable characteristics of a MALDI matrix include a strong light absorption at the wavelength of the laser, the ability to form crystals with the analyte, low sublimation temperature, and the ability to participate in photochemical reactions so that analytes can be ionized with high yields.³ Table 1-1 lists several commonly used UV matrices and their properties.

Table 1-1 Commonly used UV MALDI matrices

Matrix	Structure	Wavelength	Major applications
α -cyano-4-hydroxycinnamic acid CHCA		337 nm, 355 nm	Peptides, fragmentations
2,5-dihydroxybenzoic acid (Gentisic acid) DHB		337 nm, 355 nm	Proteins, peptides, carbohydrates, synthetic polymers
Trans-3,5-dimethoxy-4-hydroxycinnamic acid (Sinapinic acid, Sinapic acid) SA		266 nm, 337 nm, 355 nm	Proteins, peptides
3-hydroxypicolinic acid HPA		337 nm, 355 nm	Best for nucleic acids

To prepare a MALDI sample, matrix and analyte solutions are deposited on a probe at a matrix to analyte molar ratio between 100:1 to 50,000:1. Upon solvent evaporation, the mixture

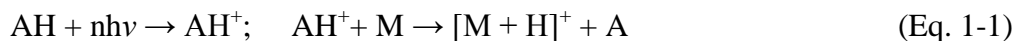
dries and co-crystallizes on the target surface. Once the target is inserted into the ion source of a mass spectrometer, the crystals on the target are irradiated with the pulsed laser.⁵⁵

A typical MALDI mass spectrometer uses a pulsed UV laser. Two of commonly used lasers are the nitrogen laser (337 nm) and frequency tripled Nd:YAG (355 nm). MALDI has also been performed using lasers operating in the infrared (IR) wavelength range.⁵⁶⁻⁵⁸ The penetration depth of an IR laser under MALDI conditions is several orders of magnitude larger than for UV lasers.⁵⁵ Although IR and UV lasers produce comparable MALDI mass spectra, the propensity for IR lasers to remove large quantities of material makes this approach more difficult to use for routine analysis.^{19, 20} However, the deeper penetration enables an IR laser to remove deeply embedded analytes from materials such as thin layer chromatography plates, polyacrylamide gels, and tissue.²²⁻²⁴ In addition, the ability to use intrinsic solvents as the matrix and the relatively soft ionization of large biomolecules make IR lasers attractive in certain cases.

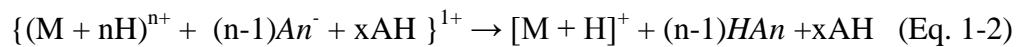
MALDI experiments are usually carried out under vacuum, which makes MALDI difficult for the analysis of liquid samples and on-line coupling to liquid separations. However, there have been a few approaches that combine MALDI with liquid sample introduction,⁵⁹⁻⁶³ such as aerosol MALDI and continuous flow (CF) MALDI. In the aerosol method for MALDI liquid introduction, the matrix and analyte are dissolved in a solution that is sprayed directly into the mass spectrometer.⁶⁰⁻⁶² The solvent evaporates when the aerosol passes through a heated drying tube, and ions are formed by pulsed UV laser irradiation. CF MALDI was first introduced in 1993 by Li et al.⁶⁴ In CF MALDI the analyte and matrix are delivered into the ion source using a continuous flow probe that consists of a capillary that is either terminated with a frit or left open and mounted in a stainless steel tube. Being delivered through the capillary, analytes are ablated with a UV laser and then subsequently mass analyzed. Ions of large molecules such as

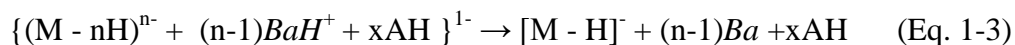
myoglobin were detected using CF MALDI, although the signal intensity was about an order of magnitude lower than static MALDI, due to the higher system pressure and the relatively higher concentration of volatile solvent when sample was continuously introduced. Later on CF was used with IR MALDI using a syringe pump to deliver analyte and matrix solution, such as insulin and myoglobin solution mixed with glycerol, to a stainless steel frit in vacuum.⁶⁵

The mechanism of MALDI is still under investigation.^{30, 48, 66, 67} Two major models have been proposed to explain experimental results: photochemical ionization and cluster ionization. The photochemical ionization model assumes the generation of neutral analyte molecules in the matrix crystals and a photoionization of the matrix molecules as the first step, followed by charge transfer to the analyte in the plume.^{68, 69} The photochemical ionization processes are expressed as:⁶⁹ (A: matrix; M: analyte)



The more recent cluster ionization model proposes that analytes such as proteins retain their solution charge state upon incorporation into the matrix.⁴⁸ The analyte molecules are entrained in a dense plume of the desorbed matrix clusters. A break-up of the crystal lattice into small clusters upon desorption with some of them having only a single analyte ion is assumed. In the expanding plume the clusters are assumed to lose neutral matrix and solvent molecules as well as counter ions as free acids or bases after their proton-transfer neutralization with analyte protonation sites.⁷⁰ This assumption is supported by experimental results where pH indicator molecules retain their color and charge state upon crystal incorporation for acidic, neutral, or basic matrices.⁷¹ The possible reactions of cluster ionization model are expressed as (M: analyte, AH: matrix, *An*: anion, *Ba*: base; shown in the bracket is a cluster):⁴⁸





Ion yields in the 10^{-6} to 10^{-4} range have been reported in MALDI.⁷²⁻⁷⁵ Many Factors can affect MALDI ion yields, such as laser fluence, pulse width, and the choice of matrix.⁴⁸ Recently a model was developed to investigate laser pulse width and fluence effects on MALDI ionization process.⁶⁷ The results showed that picosecond pulses lead to much higher initial ion concentrations than nanosecond pulses, but the differences rapidly disappear as a result of the phase change. The ion velocity is fluence dependent in the early stage of simulation, but the later time difference is not significant. Another factor that affects ion yield in MALDI is the positive and negative charge recombination, which was modeled recently.⁶⁶ The result suggests that electron tunneling (a physical process that occurs when potential donors and acceptors are in near contact) is a likely mechanism in MALDI that leads to charge recombination and ion loss. Proper experimental parameters such as laser fluence and matrix selecting need to be chosen to make sure ion formation exceeds ion loss in MALDI.

1.1.1. Electrospray Ionization

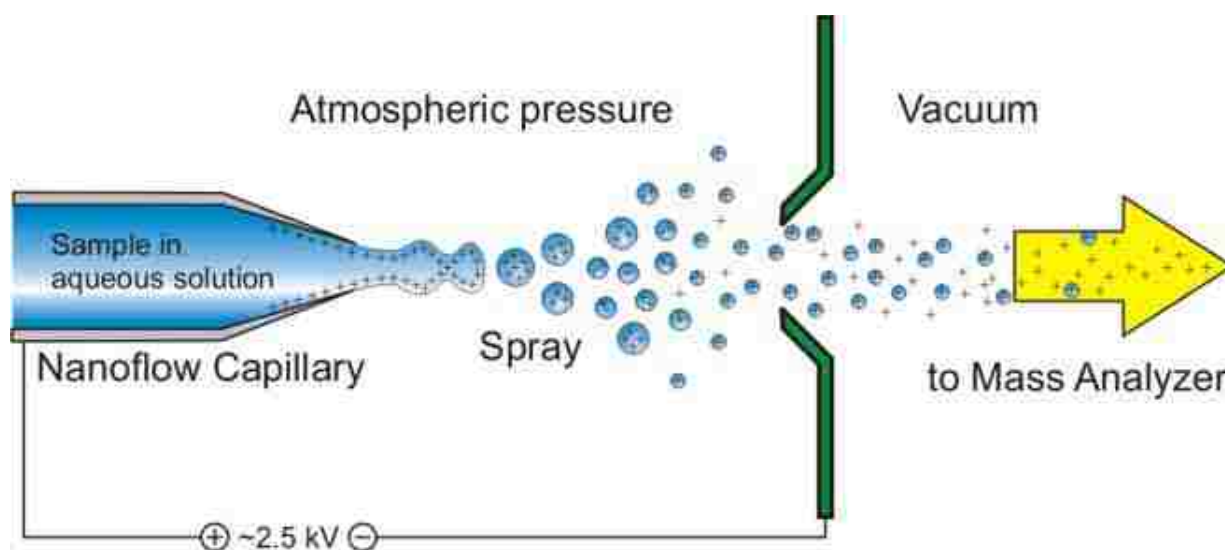


Figure 1-2 Schematic diagram of ESI.

Electrospray ionization is a method used to ionize molecules, especially macromolecules from a liquid solution.⁷⁶ In late 1980s, Fenn and co-workers used ESI for the analysis of biological macromolecules,⁷⁷ and he was co-awarded the Nobel Prize in Chemistry in 2002 for this development.

A schematic of ESI is shown in Figure 1-2. The sample solution is carried through an ESI needle that has a potential of a few kilovolts applied on it. The droplets coming out of the needle are charged and, as the solvent evaporates, the droplets shrink in size until the repelling Coulombic force is large enough to exceed the surface tension and the droplets disintegrate to produce smaller and more highly charged droplets.⁷⁸ This process repeats itself many times until highly charged solute molecules remain. This ion creation mechanism is known as charge residue model (CRM).⁷⁸ Alternatively, ion formation can proceed by the ion evaporation model (IEM), in which the droplet reaches a certain size and the field at the surface of the droplet becomes sufficiently large enough to eject highly charged ions.⁷⁹

One important feature of ESI is that it produces multiply-charged ions, which makes it compatible with mass spectrometers with a relatively low m/z range. In addition, because ESI uses liquid sample introduction and ionization is at atmospheric pressure, it is well suited for coupling to liquid separation.⁸⁰

Ambient Ionization

Ambient ionization is the direct analysis of materials in their native environment with ions created outside the mass spectrometer.^{6, 8, 9, 81, 82} Ambient techniques allow the ionization of untreated samples in the open environment. As a result, analysis is rapid with the time scale

governed by the time needed to bring the sample to the mass spectrometer.⁸² Moreover, ambient ionization can be a soft ionization method, with internal energy deposited lower than for ESI, therefore very little fragmentation can occur in some ambient ionization methods.^{8, 82}

The first two ambient ionization techniques for biological molecule analysis were desorption electrospray ionization (DESI) and direct analysis in real time (DART).⁹ DART is a glow discharge-based ambient ionization method that was first introduced by Cody and co-workers in 2004.¹⁰ DESI ionization is carried out by directing pneumatically assisted electrosprayed droplets onto a sample surface. The charged solvent droplets pick up analytes while in contact with the surface, and after secondary droplets are removed from the surface by the shear of the pneumatic assist gas, analyte ions are formed and delivered to a mass spectrometer. The multiply-charged ESI-like ions in DESI suggest that DESI ionization mechanism is an ESI-like ionization process in its final stages.⁸³ DESI has been applied to diverse samples and mixtures, and can be performed directly with analytes on glass, paper, metal, plastic, and silica plates.⁸³

DART has applications in different fields such as forensics, pharmaceuticals, biological chemistry, and food chemistry.⁹ In DART, a glow discharge with a potential usually between 1 and 5 kV is created to form a plasma in nitrogen or helium gas to produce ionized gas, electrons, and metastable species. The plasma passes through electrostatic lenses, which removes charged particles. The remaining metastable species are aimed directly at the sample, which can be a solid, liquid or gas, to desorb and ionize the analyte.^{10, 84} When helium is used, the excited helium atoms react with water molecules in the air, forming protonated water cluster ions.⁹ The ions then transfer a proton to an analyte molecule to form a protonated molecule.

1.1.2. Matrix-assisted Laser Desorption Electrospray Ionization

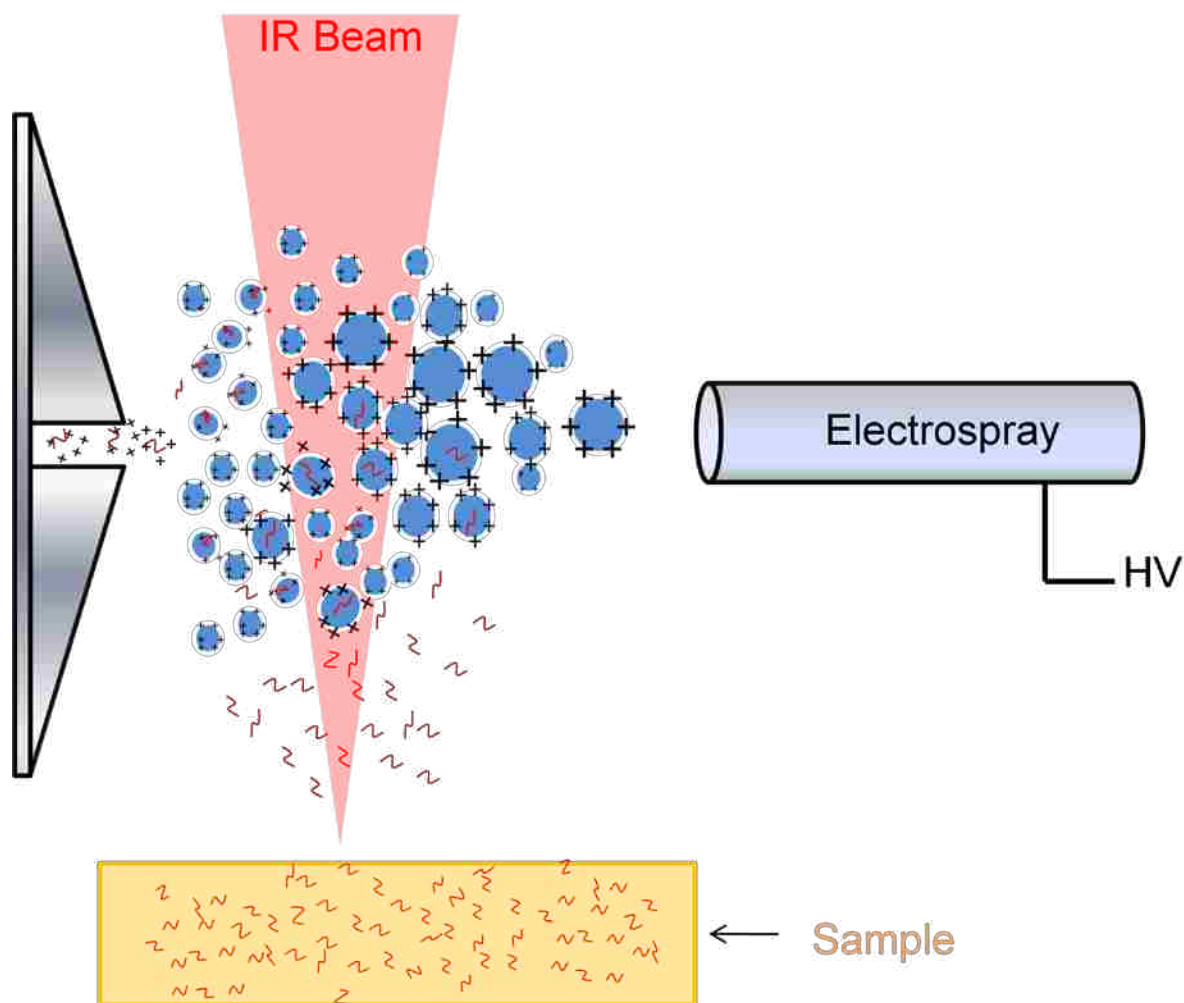


Figure 1-3 Schematic of IR-MALDESI.

By combining the sample removal ability of lasers with the ionization ability of highly-charged ESI droplets, several new ambient ionization methods have been developed. The method called electrospray-assisted laser desorption ionization (ELDI) was developed in 2004 by Shiea and co-workers.¹³ In ELDI, no matrix is used and a UV laser is used to ablate to form a sample plume that subsequently interacts with a solvent electrospray to produce ionization. Two years later, Muddiman and co-workers used matrix to aid the sample removal by laser ablation, and they termed this method matrix-assisted laser desorption electrospray ionization (MALDESI).¹¹

In MALDESI or ELDI, a UV laser is used. When using an IR laser, this approach has been called IR LADESI,¹² laser ablation ESI (LASEI),¹⁴ or IR MALDESI, but the processes are the same. In this work, we use the term IR MALDESI. A schematic of IR MALDESI is shown in Figure 1-3. Water can be used as a matrix, and several biological and pharmaceutical samples were directly analyzed without any sample treatment.¹² It has been suggested that the ionization mechanism is similar to electrospray with the analyte material incorporated as neutral molecules or through a droplet merging mechanism in which the material ablated from the target in the form of particles interacts with the ESI droplets.^{12, 14}

1.2. Fundamentals of Laser Desorption and Ablation

Since the introduction of the first ruby laser in early 1960s, numerous applications of laser desorption and ablation have been established in diverse areas, such as pulsed laser deposition,⁸⁵ nanoparticle manufacturing,⁸⁶ micromachining,^{87, 88} surgery,⁸⁹ and chemical analysis.⁹⁰⁻¹⁰¹ Laser desorption refers to laser-induced thermal evaporation of individual molecules from the outermost layers of the sample.^{46, 55} When laser energy is rapidly transferred to the sample, ablation occurs, leading to massive material ejection, mainly in the form of clusters and particles.^{1, 2, 89} As compared with conventional dissolution techniques, the unique advantage of laser ablation for analytical sampling is that nearly any sample can be ablated with minimal sample preparation and often under ambient conditions. In addition, analysis using laser ablation requires a smaller amount of sample than that required for solution nebulization, and a focused laser beam permits resolution and sample spatial characterization.

In spite of many applications, the exact mechanisms of laser ablation are still under investigation. To facilitate further optimization of experimental parameters in current

applications as well as developments of new techniques based on laser ablation, fundamental studies aimed at understanding the physical processes involved in material desorption, ablation, and ion formation are needed.

Energy Deposition and Material Ejection

The first step of laser ablation is laser energy deposition from the laser in the material, which is strongly affected by the optical properties of material at the wavelength of the laser radiation. Under conditions such as MALDI and MALDESI, the optical absorption of the material is governed by Beer's Law:⁴⁷

$$H = H_0 e^{-\alpha z} \quad (\text{Eq. 1-4})$$

where H_0 is the laser fluence at the sample surface, H is the laser fluence at depth z in the sample, and α is the attenuation coefficient (the product of the molar absorption α_n and the concentration of the absorbing molecules c_n in the sample). The molar absorption α_n is a wavelength dependent property.⁴⁷

In addition to the laser energy and the optical properties of the material, the rate of energy deposition also strongly affects laser desorption and ablation. In many laser ablation applications such as MALDI, the laser pulse duration is typically shorter than the time of dissipation of the absorbed laser energy by the thermal conduction. This condition is commonly referred as thermal confinement.^{2, 89, 102} The condition for thermal confinement can be expressed as:²

$$t_p < t_{th} = 1/(\alpha^2 D_T) \quad (\text{Eq. 1-5})$$

where t_p is the laser pulse, t_{th} is energy dissipation time in regime of thermal confinement, α is the absorption coefficient of the ablated material, and D_T is the thermal diffusivity.

In the regime of thermal confinement, material can be overheated far beyond the boiling temperature.¹⁰² For most UV matrices, t_{th} is about 1 μ s, which is much longer than the ns laser pulse width.² For IR lasers and IR matrices such as glycerol, t_{th} is even longer due to the deeper penetration (smaller α).

If the rate of energy flow into the sample is shorter or comparable to the time that is needed for a mechanical relaxation of the absorbing volume, the laser heating takes place at nearly constant volume conditions, causing a high thermoelastic pressure buildup. This condition is stress confinement.^{2, 89, 102} The condition for the stress confinement can be expressed as:²

$$t_p < t_s = l/(\alpha C_s) \quad (\text{Eq. 1-6})$$

where t_s is energy dissipation time (acoustic time constant) in the regime of stress confinement, C_s is the speed of sound in the irradiated material. t_s is usually a few hundred of ps under conditions of UV MALDI, and a few ns under conditions of IR MALDI and IR MALDESI.^{2, 89} For laser ablation of metals in ICP MS, t_s is usually in femtosecond range.²⁹

During and after the energy deposition by laser irradiation, materials can be ejected in different forms, such as atoms, molecules, clusters, and particles. The quantity and size distribution of material that is removed has a strong dependence on the laser irradiation conditions, such as laser fluence, pulse width, laser wavelength, and background pressure.^{2, 17, 29, 38, 89} In general, material ejection occurs through two physical processes: desorption and ablation.

Laser desorption occurs in the low laser fluence regime, and the desorbed materials are usually small species such as atoms and molecules.^{38, 55, 89} The dependence of the yield of ejected molecules N on fluence F can be well described by an Arrhenius-type expression.^{74, 103}

$$N = A \exp \left[\frac{E_S^*}{k_B(T_0 + BF)} \right] \quad \text{for } F < F_{th} \quad (\text{Eq. 1-7})$$

where N is the number of desorbed molecules, E_S^* is the activation energy, A is a pre-exponential factor, B is a factor that describes the conversion energy into a surface temperature, T_0 is the initial temperature of the system, k_B is Boltzmann's constant, and F_{th} is a threshold fluence, which defines the upper limit of validity of the desorption model.

When the rate of volumetric energy deposition is more rapid than the rate of energy consumed by melting, vaporization and normal boiling of the irradiated material, the material is overheated and ablation occurs.⁸⁹ Compared to desorption, ablation is a more violent process. More material is removed by ablation and the ejected species are usually clusters and particles.^{29,}

55, 89

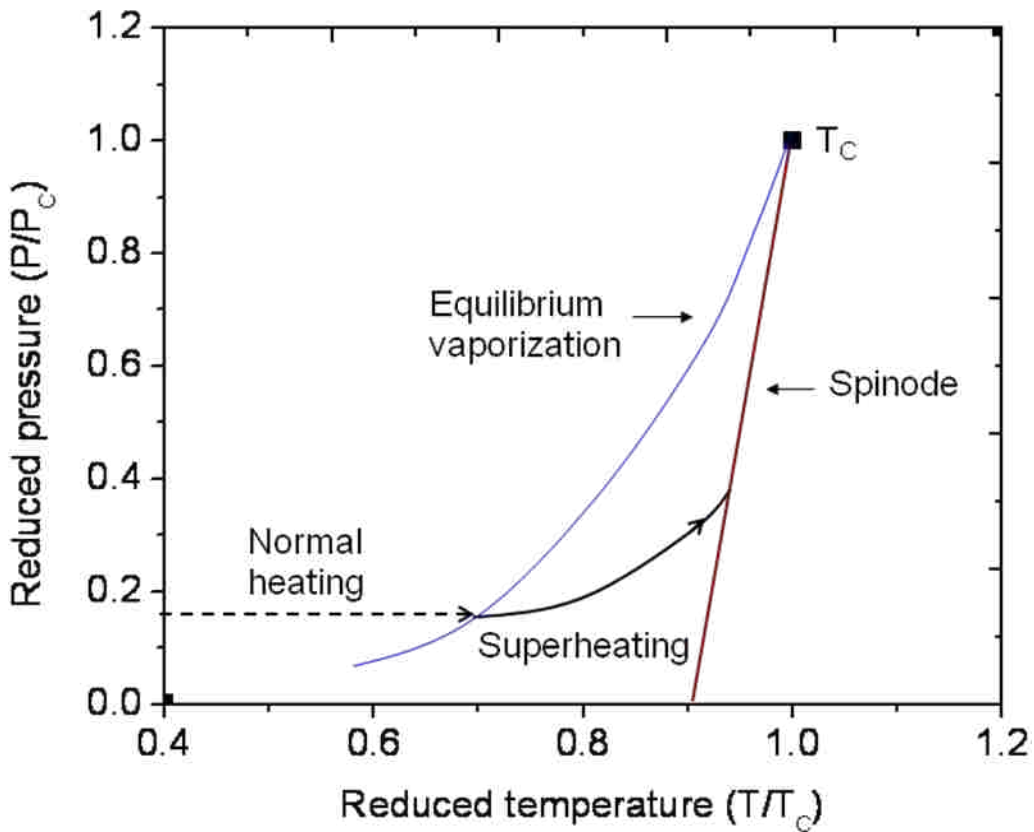


Figure 1-4 Phase diagram near the critical point indicating normal heating and superheating.

Phase explosion is a major process of laser ablation. The mechanism of phase explosion can be explained using a phase diagram such as that shown in Figure 1-4. In a normal heating process, when the temperature of the material reaches the boiling temperature, the liquid and the vapor phases are in equilibrium (equilibrium vaporization line in Figure 1-4).¹⁰⁴ For a solid material, the top layer melts after its temperature reaches the melting point, forming a liquid layer. However, because of the fast energy deposition from the laser pulse, it is possible to superheat this layer above the boiling point at heating rates in excess of 10^6 K/s.⁴⁶ If the temperature exceeds 90% of the critical temperature T_c , the phase of the superheated material breaks through the spinode line, which is the upper boundary of metastable equilibrium.¹⁰⁴ The superheated liquid material becomes unstable and catastrophically relaxes to a liquid-vapor mixture.¹⁰³ Under this conditions, phase explosion occurs that transits the superheated liquid to a mixture of gas phase molecules, clusters and liquid droplets.^{38, 89}

Phase explosion can occur in both thermal confinement and stress confinement regimes. In the thermal confinement regime, the threshold fluence for laser ablation is defined as the energy required to heat the sample surface to the limit of metastable equilibrium, leading to the ejection of a mixture of vapor, clusters, and particles.^{38, 89, 105} Compared with thermal confinement, the particles ejected in the stress confinement regime are larger in size and can be orders of magnitude more numerous.³⁸ Particle emission through phase explosion under MALDI and MALDESI conditions has been experimentally observed and studied.^{25, 28, 29, 31-33, 55, 93, 106}

Besides phase ablation, other physical processes involved in laser ablation are hydrodynamic sputtering and photomechanical spallation. Hydrodynamic sputtering refers to the process in which droplets of material are formed and expelled from a target as a consequence of transient melting. This process is distinct from phase explosion and is mainly caused by

hydrodynamic instabilities.¹⁰⁷ Photomechanical spallation refers to the removal of the sample surface layer caused by reflection of the laser-induced pressure wave from the back surface of the sample.^{38, 89} Hydrodynamic sputtering and photomechanical spallation are usually less effective than phase explosion,⁸⁹ and thus are considered as minor processes in laser ablation.

Recoil-induced material ejection is another important material removal process in laser ablation, which is a secondary material expulsion induced by the formation of recoil stresses due to the rapidly expanding vapor plume and the ejected droplets during phase explosion.^{89, 108} Recoil-induced material ejection is most pronounced during ablation of liquids and of materials for which a molten layer is formed.⁸⁹ Distinct from phase explosion that occurs across the entire ablation area, recoil-induced material ejection is found to occur preferentially at the ablation crater rim and include the ejection of droplets much larger than those from the initial phase explosion. As a result, it leads to a transient indentation of the surface.^{26, 34, 109}

Computational Simulations of Laser Ablation

A number of models and simulation methods have been developed to study laser ablation under conditions suitable for chemical analysis. Atomistic simulations have been used to study the channels and rates of vibrational relaxation of excited molecules and the redistribution of the deposited energy between the translation and internal degrees of freedom.^{110, 111} For example, femtosecond laser-induced transient melting and atomic mixing in a gold film deposited on a bulk copper substrate have been investigated at the atomic level.¹¹² Because of the long computational time required, atomic-level simulations are limited to small systems and short simulation times.³⁸

A simplified model has been developed that treats each matrix molecule as a breathing sphere with a single vibrational degree of freedom represented by the molecular radius which allows modeling of large ensembles over experimental relevant times.^{38, 113} This approach uses molecular dynamics (MD) and provides information on the time evolution of a system of interacting atoms through the numerical integration of the equations of motion for all atoms in the system. Numerous molecular dynamics simulations have been reported for the investigation of laser desorption and ablation,^{17, 30, 67, 114-116} such as laser-material interaction,¹⁰² early stage material ejection,^{38, 117, 118} ion formation,^{17, 30, 114} ion yield dependence,^{67, 119} and ion recombination.⁶⁶ The challenges in application of the MD method for simulation of laser ablation are the limitations of time and length scales. Most systems studied in MD simulations do not exceed hundreds of nanometers in size and tens of nanoseconds in time.¹¹⁶ These limitations make MD simulation problematic for the study of IR laser ablation, in which many particles up to micron size are formed,^{25, 26} and the laser pulse can be hundreds of nanoseconds long.¹²

In addition to MD simulations for analytical sampling, a few models concentrate on the laser-generated plasma.^{120, 121} Because this plasma can absorb a fraction of the incoming laser intensity before it reaches the target, this effect is called plasma-shielding.¹²¹ Several models focus not only on the laser-sample interaction, but also describe the expansion of the plumes, for example in hydrodynamic models (an approach that considers the solutions of the hydrodynamic equations for an unsteady adiabatic expansion with the correct boundary conditions)¹²²⁻¹²⁴ and direct simulation Monte Carlo (DSMC) models.¹²³⁻¹²⁶ In DSMC, plume expansion is divided into a number of cells with the cell size determined by the local mean free path. The flow field is reproduced using a large number of simulated particles that are characterized by coordinates, velocities, internal energies, species types and weight factors. The evolution of the system is split

into collisionless streaming and collisions. At each time step, all particles are moved as if they do not interact, and after that a given number of particles are selected for collisions. Collisions pairs are selected at random from the same cell regardless of the positions of the particles. New velocities are calculated as a result of each collision event.

The finite element method (FEM) is a procedure for obtaining numerical solutions to partial differential equations by dividing the system into small finite elements to which simplifying approximation can be made. FEM doesn't have the short time and length limitations in MD, therefore can be used to study laser ablation in a much larger scale. In the past few years, a number of FEM models have been developed to study laser ablation for different applications. For instance, a study of explosive boiling, temperature distribution and ablation depth of pulsed Nd:YAG laser ablation of titanium carbide (TiC) has been reported recently.^{127, 128} Another example is a model developed to study the shape and stress distributions in laser machining of ceramic substrates.¹²⁹ Most recently, a bio-heat model was developed to study the temperature and damage distribution involved in laser ablation of prostate tumors and the results established a clear correlation between simulation and *in vivo* experiments.¹³⁰

1.3. Research Objectives

The overall objective of this research was to develop infrared laser ablation based ionization techniques for chemical and biological analysis. Infrared lasers are highly efficient at sample removal and post-ionization can be used to improve ionization efficiency. To achieve this goal, the specific components of the project were 1) to develop an IR/UV two-laser MALDI MS for the study of IR laser ablated particles; 2) to develop an on-line continuous flow interface based on IR matrix-assisted laser desorption electrospray ionization (IR MALDESI) for reaction

monitoring; 3) to model IR laser ablation involved in ambient ionization conditions using finite element method (FEM). Experimental setups used in this research are described in Chapter 2. The IR/UV two-laser MALDI study is described in Chapter 3. The on-line continuous flow IR MALDESI study is described in Chapter 4. The FEM simulation study is described in Chapter 5. A summary and conclusions for the entire research as well as future study of IR laser ablation mass spectrometry is included in Chapter 6.

CHAPTER 2. EXPERIMENTAL

The goal of the research described in this dissertation was to study and develop new ionization techniques that use infrared laser ablation for sampling, and apply these techniques to chemical and biochemical analysis. Two experimental setups were developed and used: an IR/UV two-laser matrix-assisted laser desorption ionization mass spectrometer and a continuous flow IR matrix-assisted laser desorption electrospray ionization mass spectrometer. The IR/UV two-laser MALDI system was based on a home-built linear time-of-flight (TOF) mass spectrometer and used to study IR laser ablated particles. Factors that affect the two-laser ion yield were studied, including the fluence of the IR and UV lasers and the delay time between the laser pulses. The CF IR MALDESI ion source was coupled with a commercial quadrupole ion trap mass spectrometer. Chemical and biochemical reactions were monitored using this setup. In this chapter, a description of the fundamentals of TOF and quadrupole ion trap mass spectrometers along with detailed information on the IR/UV two-laser MALDI and CF IR MALDESI setups are presented.

2.1. Time-of-flight Mass Spectrometry

Time-of-flight mass spectrometry (TOF MS) is a method in which mass to charge ratio (m/z) of ion is determined via a time measurement.¹³¹ The TOF mass analyzer separates ions in a field free flight tube after ions are accelerated to a constant energy, and theoretically, the TOF analyzer has an unlimited mass range. The primary advantage of TOF over other mass analyzers is the acquisition speed.¹³² Unlike scanning mass analyzers, such as ion traps or sectors, an entire mass spectrum of TOF can be obtained at once within hundreds of microseconds and is only limited by the repetition rate of the laser in the case of MALDI and the speed at which the data

can be recorded. The flight tube of a TOF MS is a vacuum chamber with a pressure usually below 10^{-6} torr to prevent collisions with background gas molecules. The length of the flight tube is based on the desired ion separation resolution over a given mass range. Ions are generated in the ion source. Before they are transferred to the flight tube for separation, all ions are accelerated with the same kinetic energy that is defined by the acceleration voltage. Lighter ions travel faster and arrive at the detector first due to their higher velocity. The energy of the accelerated ions depends on their mass according to Equation 2-1:¹³¹

$$E_{KE} = \frac{1}{2}mv^2 \quad (\text{Eq. 2-1})$$

where E_{KE} is the kinetic energy, m is ion mass, and v is the velocity of the ion. Considering the equation:

$$E_{KE} = zeV \quad (\text{Eq. 2-2})$$

where z is the charge number of the ion, e is the charge of an electron, and V is the acceleration voltage, the Equation 2-1 can be rearranged to solve for the velocity of a singly charged ion ($z = 1$):

$$v = \left[\frac{2eV}{m} \right]^{\frac{1}{2}} \quad (\text{Eq. 2-3})$$

Neglecting the time spent in ion source, Equation 2-3 can be rearranged to solve for the flight (t):

$$t = \left[\frac{m}{2eV} \right]^{\frac{1}{2}} L \quad (\text{Eq. 2-4})$$

where L is the length of the flight tube.

The overall time for an ion to travel in the source and the flight tube can be calibrated for mass using Equation 2-5:

$$t = a^2\sqrt{m} + b \quad (\text{Eq. 2-5})$$

where a and b are constants and found from fitting the m/z values of two known peaks. Mass resolution (R) is usually reported using the full-width at half-maximum (fwhm) method and can be calculated from either flight times or masses, as shown in Equation 2-6:

$$R = \frac{m}{\Delta m} = \frac{t}{2\Delta t} \quad (\text{Eq. 2-6})$$

2.2. IR/UV Two-laser MALDI TOF Mass Spectrometer

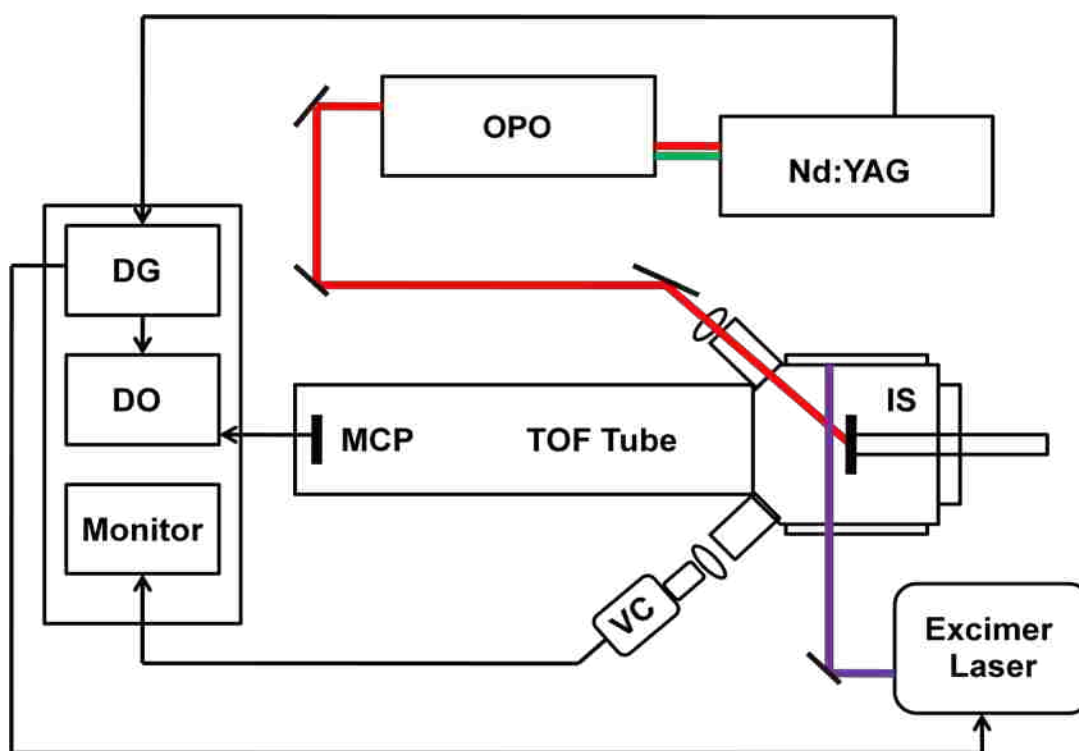


Figure 2-1 Schematic layout of the IR/UV two-laser matrix-assist laser desorption ionization linear time-of flight mass spectrometer.

The experiment involving matrix-assisted laser desorption ionization of IR laser ablated material discussed in Chapter 3 was performed on a home-built linear TOF mass spectrometer combined with a tunable pulsed IR optical parametric oscillator (OPO) laser system used for

sample ablation, and a 351 nm UV excimer laser used for post-ionization. A schematic diagram of the IR/UV two-laser MALDI setup is shown in Figure 2-1.

The mass spectrometer was maintained under vacuum with the pressure of the ion source and the flight tube at 1×10^{-6} and 1×10^{-7} torr, respectively. The vacuum was generated by two 1200 L/s diffusion pumps (VHS-4, Varian, Palo Alto, CA). The ion source consisted of a sample target holder followed by a grid at a distance of 18 mm. A CCD camera with macro zoom lens was placed at a 45° port to view placement and irradiation of the sample target. Positive ions were accelerated into a 1 m TOF tube where they were mass separated. At the other end of the TOF tube, a dual microchannel plate (MCP) assembly (Galileo, Sturbridge, MA) was used for ion detection. Ions were accelerated into a dual 25 mm diameter MCP detector, the front of which was held at -2.2 kV. A grounded grid was located approximately one centimeter in front of the MCP. The back of the second 25 mm diameter MCP is held at -220 V and the collection anode is held at ground. The detector output was coupled to the 50 Ω input of a 500 MHz digital oscilloscope (9350CM LeCroy, Chestnut Ridge, NY) for data acquisition. The digitized data were downloaded to a computer via a general purpose interface bus (GPIB), using Labview software (National Instruments, Austin, TX), for storage and further manipulation.

A wavelength tunable optical parametric oscillator (OPO, Mirage 3000B, Continuum, Santa Clara, CA, USA) IR laser was used for sample ablation. A block diagram of the OPO laser is shown in Figure 2-2.

The OPO laser was pumped by a 1064 nm fundamental and 532 nm second harmonic of an Nd:YAG laser (Powerlite 8000, Continuum, Santa, Clara, CA, USA). After entering the Mirage 3000B, the 1064 and 532 nm beams is split into two beams that are routed through attenuators and beam telescopes. The energy of the 1064 and 532 nm beams is 270 and 80 mJ after

attenuation, respectively. The 532 nm beam is used to pump a potassium titanyl phosphate (KTP) non-resonant oscillator (NRO). In this process, the KTP crystals convert the 532 nm radiation into tunable IR radiation ranging from 1.45 to 2.16 μm . The 1.45 to 2.16 μm NRO output signal enters a KTP optical parametric amplifier (OPA) cavity that is pumped by the 1064 nm beam. The OPA amplifies the 1.45 to 2.16 μm OPA signal and produces 2.16 to 4.00 μm . This NRO and OPA arrangement allows the Mirage 3000B to produce tunable IR radiation from 1.45 to 4.00 μm .

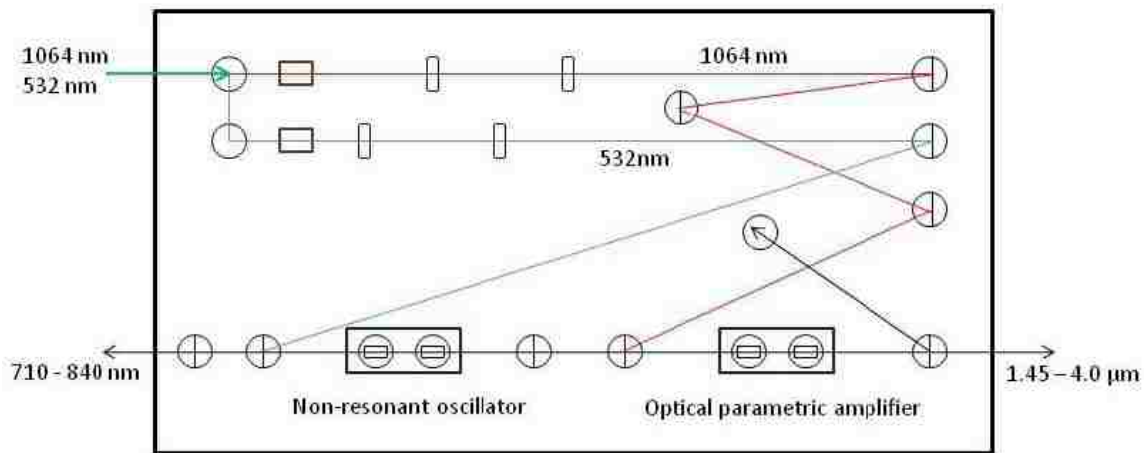


Figure 2-2 Block diagram of the OPO laser.

The UV laser used was a 351 nm XeF excimer laser (Optex, Lambda Physik, Gottingen, Germany). The laser has a maximum energy of 8 mJ, a maximum repetition rate of 200 Hz, and a pulse width of 8 ns.

In this study, the OPO laser was run at a 2 Hz repetition rate with 5 ns pulse width. The IR beam was attenuated using a combination of optical flats and focused using a 250 mm spherical lens onto the sample surface at an angle of 45° , as shown in Figure 2-3. The spot size was $200 \times 280 \mu\text{m}$, measured using laser burn paper. The 351 nm UV excimer laser was synced with the IR laser using a delay generator (DG535; Stanford Research Systems, Sunnyvale, CA, USA). The

UV laser was attenuated using a variable number of glass microscope slides. The UV beam was directed above and parallel to the sample surface with a distance of 1.4 mm between the center of the UV beam and the sample surface. Focusing of the UV beam was achieved using a 254 mm focal length fused-silica lens and the spot size was $500 \times 1000\mu\text{m}$ with the long axis parallel to the target surface. The laser energy for both lasers was measured using a pyroelectric joule meter (Model ED-104AX, Gentec, Palo Alto, CA).

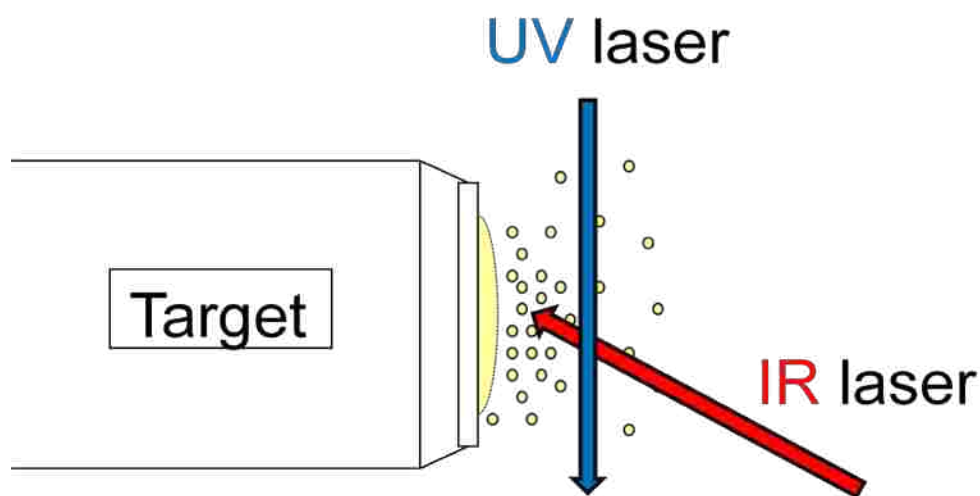


Figure 2-3 Schematic of the IR/UV two-laser arrangement.

2.3. Three-dimensional Quadrupole Ion Trap

A three-dimensional quadrupole ion trap (3DQ IT) is a mass analyzer and detector that consists of two hyperbolic metal electrodes with their foci facing each other and a hyperbolic ring electrode between these two electrodes.¹³³ A diagram of the 3D ion trap is shown in Figure 2-4. In a 3D ion trap mass analyzer, the ions are trapped in the space between three electrodes by AC and DC electric fields. An AC radio frequency (RF) voltage oscillates between two end cap electrodes if ion excitation is desired, and the driving AC voltage is applied to the ring electrode.

The motion of ions in a quadrupole field can be described by solutions to the Mathieu equation:¹³³

$$\frac{d^2u}{d\xi^2} + [a_u - 2q_u \cos 2\xi]u = 0 \quad (\text{Eq.2-7})$$

where u represents the x , y and z coordinates, ξ is a dimensionless parameter given by $\xi = \beta t/2$, and a_u and q_u are dimensionless trapping parameters. The parameter β is the radial frequency of the potential applied to the ring electrode.

In a cylindrical coordinate system, the quadrupolar potential is given by:

$$\phi_{r,z} = \frac{\phi_0}{r_0^2} (r^2 - 2z^2) \quad (\text{Eq. 2-8})$$

where r and z are the radial and axial dimensions, and Φ_0 the applied electric potential. The applied potential Φ_0 is a combination of radio frequency and DC, and is given by:

$$\phi_0 = U + V \cos \Omega t \quad (\text{Eq. 2-9})$$

where $\Omega = 2\pi\nu$ and ν is the applied frequency, U and V are DC and AC voltages, respectively.

Ejection of ions from the ion trap is accomplished by changing the amplitude of the RF potential applied to the ring electrode. Each m/z is ejected from the trap at a specific RF amplitude. The motion of ions in the trap is expressed in terms of trapping parameters: a_z and q_z , as given by:

$$a_z = \frac{8eU}{mr_0^2\Omega^2} \quad (\text{Eq. 2-10})$$

and

$$q_z = \frac{4eV}{mr_0^2\Omega^2} \quad (\text{Eq. 2-11})$$

The locus of all trapped ions is on the q_z axis. The basis of mass analysis is the relation given by rewriting equation 2-11:

$$\frac{m}{z} = \frac{4V}{q_{max}r_0^2\Omega^2} \quad (\text{Eq. 2-12})$$

where q_{max} (equal to 0.908) is the maximum value of q_z at which ions exit the trap. At a given value of an AC voltage V , all ions for which q_z lies between 0 and 0.908 are trapped with the quadrupole field. By increasing V , ions of successively increasing m/z exit the ion trap along the z direction.

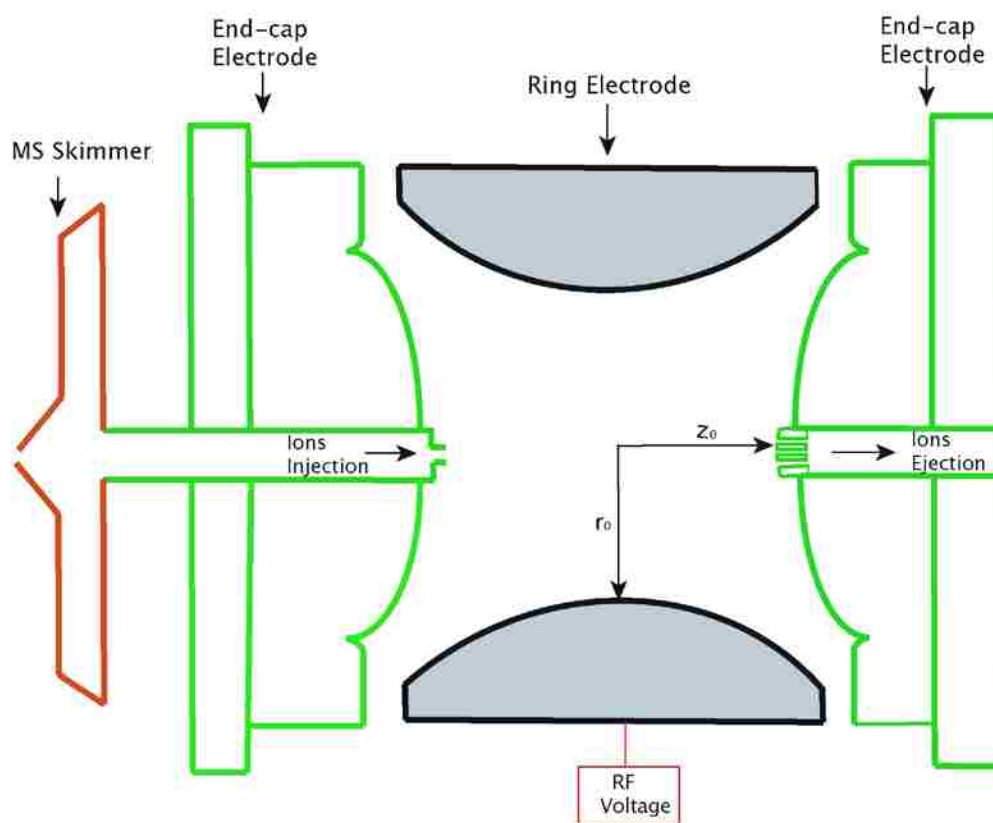


Figure 2-4 Cross-section view of an ion trap mass analyzer.

2.4. Continuous Flow IR MALDESI Mass Spectrometry

The experiment of continuous flow (CF) IR MALDESI was performed using a Hitachi M8000 3DQ ion trap mass spectrometer with a modified nano-electrospray source. Using CF IR MALDESI, several chemical and biochemical reactions were monitored on-line and off-line.

The Hitachi M8000 3DQ quadrupole ion trap mass spectrometer (Hitachi, Tokyo, Japan) is equipped with an electrospray ionization source and a conversion dynode detector. A schematic diagram of this instrument is shown in Figure 2-5.

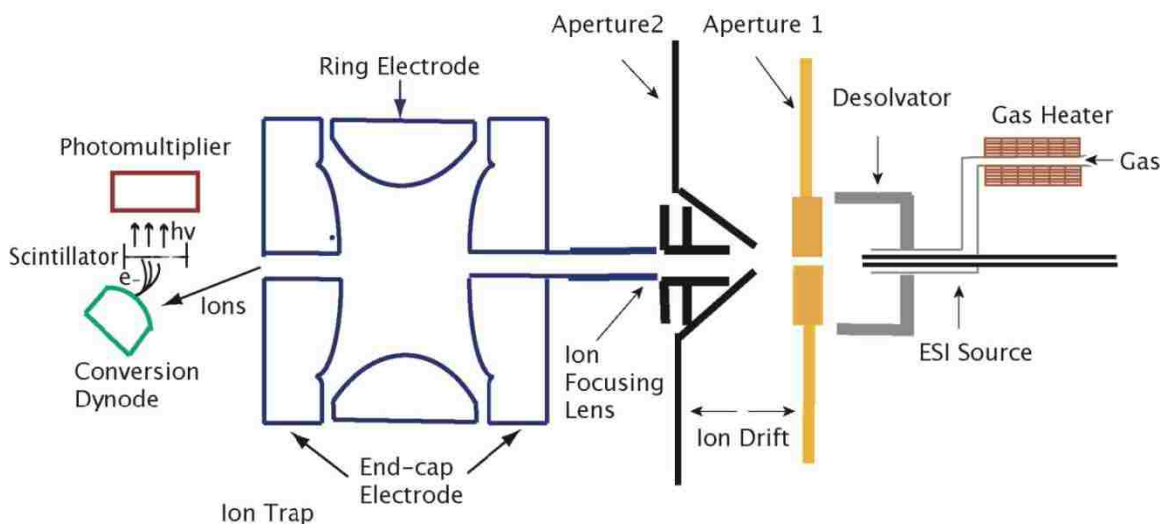


Figure 2-5 Schematic of the Hitachi M8000 3DQ ion trap mass spectrometer.

As shown in Figure 2-5, before entering the trap, ions generated from the ESI source pass through a drift region between aperture 1 and 2 and a set of lenses for ion beam focusing. The temperatures on the gas heater, aperture 1, and aperture 2 were at 180 °C, 150 °C and 120 °C, respectively. The ion drift voltage and ion focus voltage were set to 100 V and 30 V, respectively. After entering the trap, ions are trapped, and then sequentially ejected into a photomultiplier conversion dynode detector. Helium gas at 10^{-3} torr pressure is used as the buffer gas in the trap. The maximum m/z range of Hitachi M8000 IT MS is 2000.

To perform CF IR MALDESI analysis, the original ESI source on the Hitachi ion trap was replaced with a nanoelectrospray emitter (PV 300, New Objective, Woburn, MA, USA).¹² This nanoelectrospray emitter had a 50 μm i.d. fused-silica capillary that was tapered at the tip to 30 μm i.d. and was fitted in a stainless steel sleeve. The emitter was mounted perpendicular to the

MS skimmer cone and the tip faced the MS skimmer orifice at distance of 8 mm. The skimmer cone voltage was held at 40 V and heated to a temperature of 180 °C. The ESI solution was a 1:1 (v/v) mixture of acetonitrile and water with 0.2% formic acid. The solution was flowed through a 50 µm i.d. fused-silica capillary (Polymicro Technologies, Phoenix, AZ, USA) using a syringe pump (55-1111; Harvard Apparatus, Holliston, MA, USA). No nebulizing gas was used. The voltage on the ESI needle was 3.5 kV and the capillary was at ground.

A schematic and photograph of the CF IR MALDESI interface is shown in Figure 2-6. An open fused silica capillary (50 µm i.d., 360 µm o.d.) was prepared by removing the polyimide coating from the tip before it was mounted 7 mm below the spray axis pointing upward and 6 mm from the tip of the spray cone. A sample solution was flowed through the capillary, forming bead of liquid at the capillary tip. Material was ablated from the liquid bead and entrained in the electrospray to form ions by MALDESI.

The laser system was a pulsed infrared optical parametric oscillator (OPOTEK, Carlsbad, CA) operating at a 20 Hz repetition rate. It is an integrated tunable laser system in which the output of an Nd:YAG laser is used to pump an OPO, converting it into a tunable beam. The overall working mechanism of this laser is similar to the Mirage OPO system that is described in Section 2.2. A schematic of the laser optical layout is shown in Figure 2-7. The laser wavelength was set at 2.94 µm to overlap with the OH stretch absorption of the water matrix. The laser beam was directed downward toward the capillary tip at a 10° angle from normal. The spot size of the laser beam at the capillary tip was approximately 210 µm as determined with laser burn paper. The maximum laser energy was 2 mJ with no attenuation, and it was found that the maximum laser energy resulted in the largest signal intensity. Therefore, all the experiments were carried out at 2 mJ.

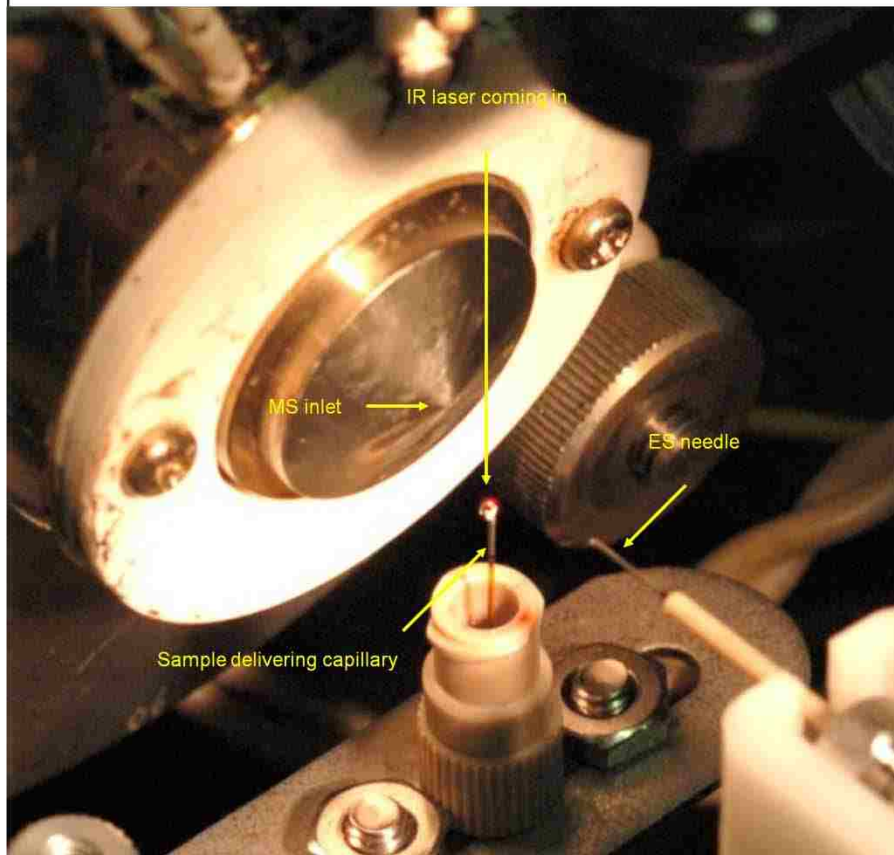
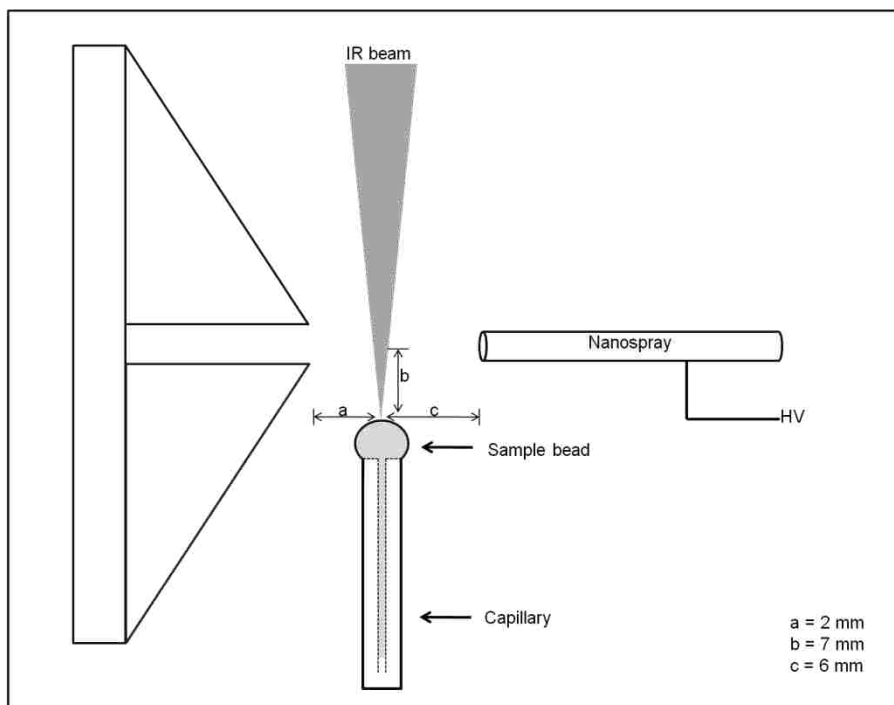


Figure 2-6 Schematic (top) and photograph (bottom) of the CF IR MALDESI MS interface showing the nanospray source, capillary, liquid sample bead, and mass spectrometer orifice.

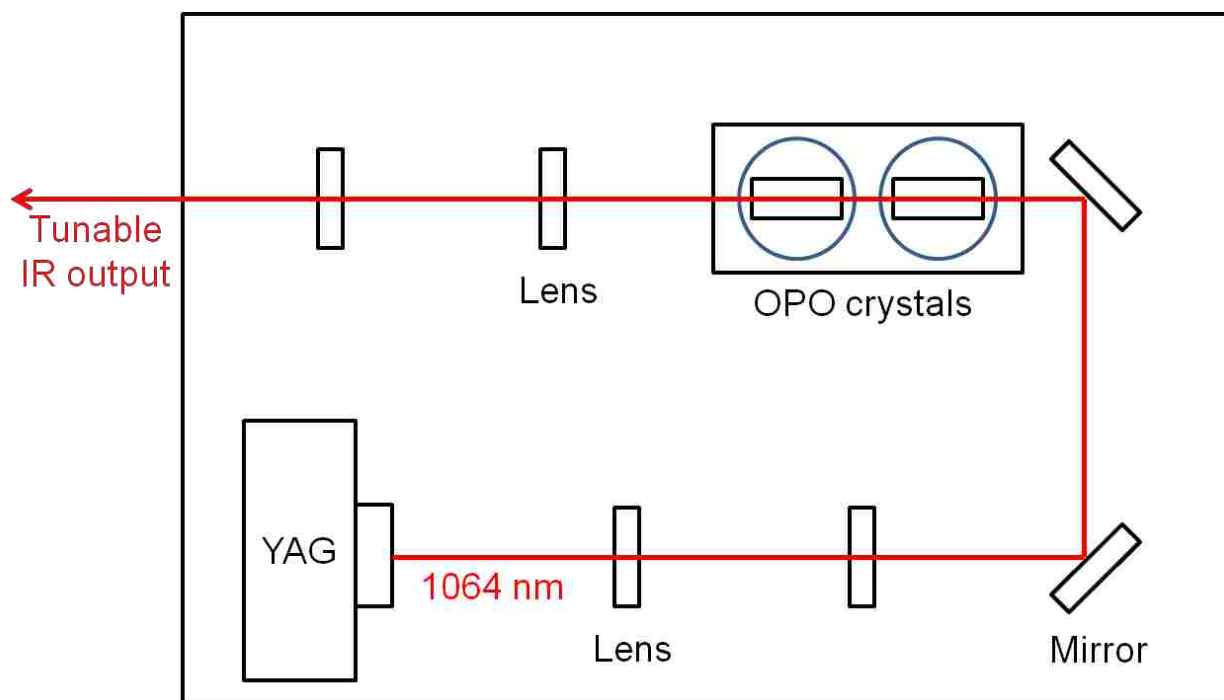


Figure 2-7 Optical layout diagram of the OPO laser.

A low flow-rate mixer (Nanomixer; Upchurch Scientific, Oak Harbor, WA, USA) was used to mix reactants. The mixer has a three-layer silicon-glass structure that with two inlet channels and one outlet channel. The flow at each inlet channel was $3 \mu\text{L min}^{-1}$, resulting in a $6 \mu\text{L min}^{-1}$ sample flow rate of the outlet capillary. When the solution enters the mixer through the inlet channels, it is split into 32 smaller channels then recombined in an interdigitated fashion, which promotes mixing even under conditions of reduced diffusion distances and laminar flow.¹³⁴ In the reaction monitoring studies discussed in Chapter 4, reaction solution flowed into the mixer through one inlet channel, and solvent flowed through the other inlet channel, which was connected to the output of a 6-port injection valve with a $3 \mu\text{L}$ loop (Model 7010, Rheodyne, Oak Harbor, WA). The other reaction solution was injected through the 6-port valve. The reaction started when two solutions were combined in the mixer.

A schematic and photograph of the on-line CF IR MALDESI reaction monitoring setup is shown in Figure 2-8. For protein digestion, the protein solution was flowed directly through a $250\ \mu\text{m} \times 150\ \text{mm}$ trypsin column with a $7\ \mu\text{L}$ bed volume (Orachrom, Woburn, MA).

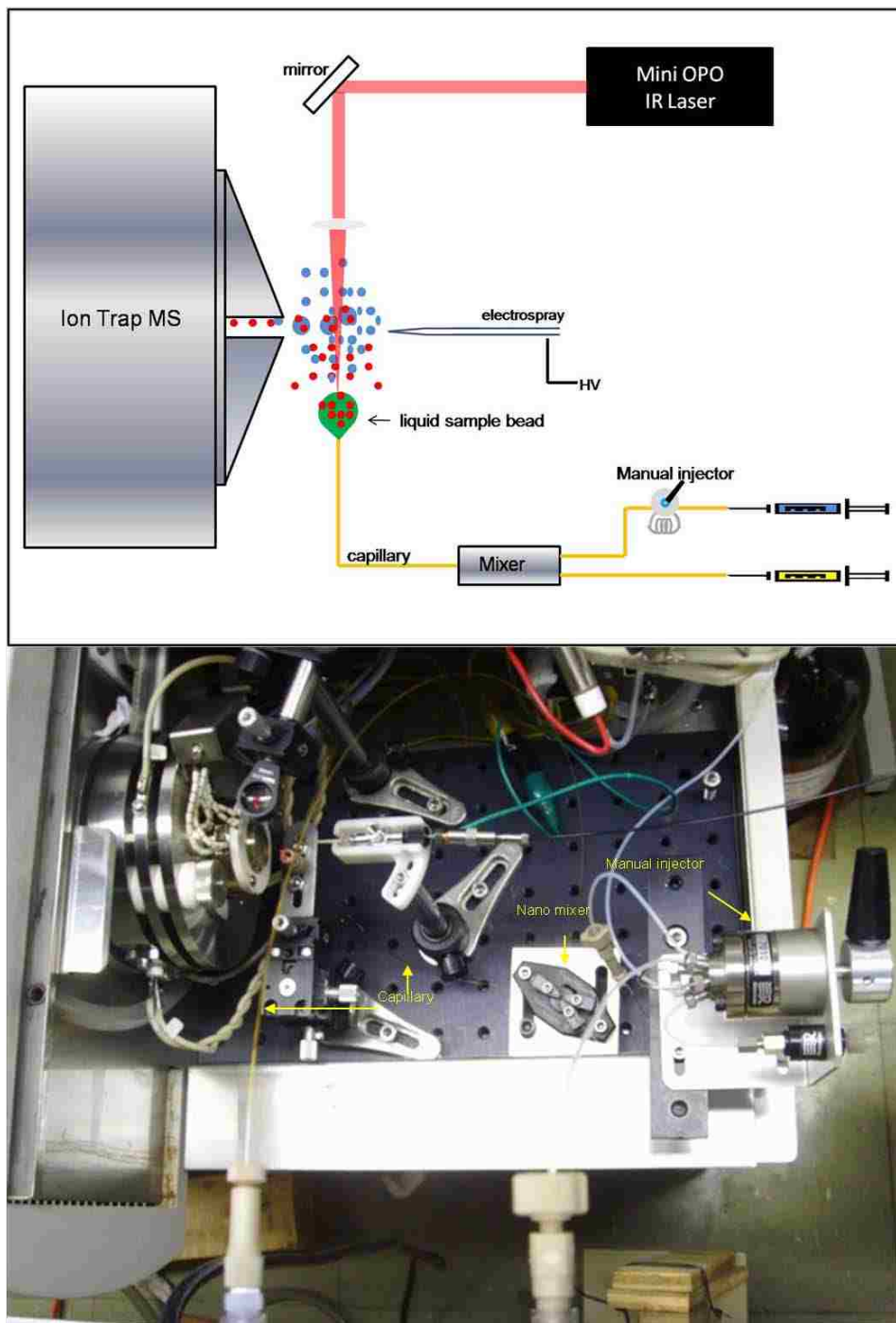


Figure 2-8 Schematic (top) and photograph (bottom) of the on-line CF IR MALDESI reaction monitoring setup showing the nanospray, 6-port valve, nano mixer, and the MS orifice.

2.5. Reagents and Standards

The following reagents used in IR/UV two-laser MALDI experiments were obtained from Sigma Aldrich (St. Louis, MO, USA) and used without further purification: bradykinin (B3259), cytochrome c from bovine heart (C3131), bovine insulin (I5500) and 2,5-dihydroxy benzoic acid (G5254). Analyte and matrix solutions were prepared in 970 μl methanol + 30 μl 1% trifluoroacetic acid (TFA; Fisher, Fair Lawn, NJ, USA) in distilled water (house supply).

The reagents 1,10-phenanthroline (PA), iron (II) sulfate heptahydrate ($\text{FeSO}_4 \cdot 7\text{H}_2\text{O}$), 1 mM 1,4-dithiothreitol (DTT) solution, insulin, cytochrome c, trypsin, ammonium bicarbonate (NH_4HCO_3), and formic acid used in CF IR MALDESI experiments were obtained from Sigma Aldrich and used without further purification. HPLC grade methanol and acetonitrile were purchased from Mallinckrodt Baker (Phillipsburg, NJ). House purified water (18 $\text{M}\Omega\text{-cm}$, Barnstead E-pure, Dubuque, IA) was used for aqueous solution preparation.

CHAPTER 3. MATRIX-ASSISTED LASER DESORPTION IONIZATION OF INFRARED LASER ABLATED PARTICLES*

In this chapter, the use of an IR laser to ablate biomolecules that were subsequently ionized by UV MALDI is described. Infrared light from a pulsed OPO laser system was directed at a solid sample containing a DHB matrix and peptide or protein analyte. The sample was placed under vacuum. A pulsed 351 nm UV excimer laser that was directed 1.4 mm above and parallel to the sample surface was used to irradiate the ablated material in the desorption plume. Ions created by post-ablation ionization were detected with a linear TOF mass spectrometer. Mass spectra of the peptide bradykinin and proteins bovine insulin and cytochrome c, were recorded. Under these conditions, two simultaneous mass spectra were generated: an IR-MALDI mass spectrum from the OPO and a UV post-ablation spectrum generated by irradiating material in the plume. Factors affecting the two-laser ion yield were studied, including the delay time between the laser pulses and the fluence of the IR and UV laser.

3.1. Introduction

Matrix-assisted laser desorption/ionization (MALDI) mass spectrometry (MS) has become a standard technique for the study of large biological and synthetic macromolecules.¹³⁵ MALDI is typically performed with a single laser operating in the ultraviolet (UV) wavelength range between 260 and 360 nm, and matrices absorbing in this wavelength range are used in almost all UV MALDI studies.⁵⁵ Alternatively, MALDI has been performed using lasers operating in the infrared (IR) wavelength range.^{136, 137} Although IR and UV lasers produce comparable MALDI mass spectra, the propensity for IR lasers to remove large quantities of material makes this approach more difficult to use for routine analysis.^{19, 20} However, the ability to use intrinsic

*The work reported in this chapter has been published in *International Journal of Mass Spectrometry*. Reprinted by permission of the Elsevier.

solvents as the matrix and the relatively soft ionization of large biomolecules make it attractive in certain cases.^{23, 138, 139} IR lasers have also been used with success for atmospheric pressure MALDI^{140, 141} and IR laser assisted desorption electrospray ionization.^{12, 14}

IR lasers can be used in combination with UV lasers to combine the material heating and removal ability of the former with the ionization efficiency of the latter. The two lasers can be directed at the same spot on the sample target and the energy adjusted so that ions are produced only when both lasers are fired.¹⁴² The time delay between the two pulses is adjusted to maximize the ion signal. An IR laser directed at the sample target heats and, in some cases, melts the sample material, which results in more efficient UV laser ionization.²⁷ Another two-laser approach uses the IR laser to desorb and ablate material, and the second laser to irradiate the plume of material.^{143, 144} With this approach the desorption and ionization processes are separated, allowing them to be optimized independently. Using this approach, many low mass (typically a few thousand Da) compounds can be post-ionized with good signal intensity.¹⁴⁵

Large molecules can be ionized from suspended particulate material that has been sprayed or ablated. For example, particles sprayed from a solution containing matrix and analyte⁶¹ or coated with matrix by condensation¹⁴⁶ will produce ions from relatively large biomolecules when irradiated with a UV laser. A similar result was obtained when an IR laser was used to desorb and ablate material from a solid sample and a second IR laser was used for ionization.¹⁴⁷ Ions from large biomolecules were observed that are not expected from multiphoton ionization of free molecules. It is known that IR lasers ablate large quantities of particulate,³¹ suggesting that laser desorption ionization of the ablated particulate is a key component of the ionization process. Ablation of material into a continuous electrospray has also been performed using IR lasers to ablate the analyte as particulate.^{12, 14} An improved understanding of the processes involved in the

ablation of particulate and subsequent ionization has the potential to lead to better IR laser ablation and ionization in mass spectrometry.

In this chapter, we report IR laser ablation with UV laser irradiation of the desorbed and ablated plume of material. A tunable pulsed IR optical parametric oscillator (OPO) laser was used for sample ablation, and a 351 nm UV excimer laser was used for post particle ablation and ionization. The matrix 2,5-dihydroxybenzoic acid (DHB) and peptide and protein molecular weight standards bradykinin, bovine insulin and cytochrome c were used to demonstrate the process. The relation between ion yield and such factors as delay time between the IR and UV lasers and IR and UV laser fluence was explored.

3.2. Experimental

All experiments were carried out on the IR/UV two-laser MALDI TOF mass spectrometer that was described in detail in Chapter 2, Section 2.2. Briefly, ions that were generated by the IR laser or the IR and UV laser in combination were accelerated to 18 kV using a single stage of acceleration with an 18 mm gap. The ions were mass separated in a field free region of 1 m flight tube with a 25 mm microchannel plate detector. Data were recorded with a 500 MHz digital oscilloscope that was triggered by a pulse delay generator that also controlled the laser timing. Mass spectra were averaged on the oscilloscope and transferred to a computer or, for ion yield measurements, peak areas were integrated on the oscilloscope and the results were transferred to the computer. The IR laser system was an OPO running at a 2 Hz repetition rate. In this study, the data were acquired at IR wavelength of either 2.94 μm or 3.05 μm . The IR beam was focused onto the sample surface at an angle of 45°. The IR laser pulse width is 5 ns. The UV laser was 351 nm excimer laser with 8 ns pulse width that was synced with the IR laser. The UV beam was

directed above and parallel to the sample surface with a distance of 1.4 mm between the center of the UV beam and the sample surface.

Each mass spectrum shown below in the Results and Discussion section was an average of 20 single laser shots. For the UV ionization ion yield studies, Δt refers to the time difference between IR and UV laser pulses, and was set by a pulse delay generator. The pulse generator and oscilloscope were both controlled by the data acquisition computer that set the delay between the IR and UV laser pulses at the pulse generator. The integrated peak area for the selected time range was then read from the oscilloscope and recorded on the computer. The delay time was incremented and the peak integration process was repeated at the new Δt . After one sweep through the full range of Δt values, the pulse generator was reset to the starting Δt and the data acquisition process was repeated. The sequence of data acquisition over the full range of delay time values was repeated five times to generate each plot and each data point resulted from an average of 20 laser shots. The sample target was rotated at one revolution every two minutes using a variable speed motor to provide a fresh sample spot for each laser shot. For the study of ion yield as a function of fluence, the peak area values were recorded from the oscilloscope without being transferred to the computer. The laser energy measurements were repeated five times and the average laser energy was combined with laser spot size to obtain the fluence.

Three biological samples were ablated and tested: bradykinin, bovine insulin, and cytochrome c from bovine heart. The analyte solutions and DHB matrix solution were prepared in 970 μl methanol + 30 μl 1% trifluoroacetic acid in distilled water. The concentration for each solution was 0.5 mM for bradykinin, 0.52 mM for insulin, 0.42 mM for cytochrome c and 0.44 M for DHB. The analyte to matrix molar ratio of each matrix and analyte solution mixture was 1:1500 for bradykinin, 1:1000 for insulin and 1:2000 for cytochrome c. After the solution was

mixed well, 24 μl mixture was deposited on a stainless steel sample target with a diameter of 8 mm for a typical dried droplet spot.

3.3. Results and Discussion

Mass spectra of the peptide bradykinin with a DHB matrix using IR, UV and both IR and UV lasers are shown in Figure 3-1. Figure 3-1a was obtained using only the IR laser at 2.94 μm with a fluence of 5.2 kJ/m^2 ; the zero of the x-axis corresponds to the firing of the IR laser. The peaks with flight times less than 10 μs correspond to matrix ions and associated adducts with masses less than 300 Da. The protonated bradykinin molecule, $[\text{M} + \text{H}]^+$, that results from IR laser desorption ionization is observed at a flight time of 19.7 μs . Figure 3-1b was obtained with only the UV laser at a fluence of 1.4 kJ/m^2 ; no peaks are observed in the spectrum. Figure 3-1c was obtained using both IR and UV lasers at a delay time of 50 μs with IR and UV laser fluences of 5.2 and 1.4 kJ/m^2 , respectively. Under these conditions, a mass spectrum similar to that observed in Figure 1a is observed in the time region below 20 μs , but new features are observed between 50 and 80 μs . The additional peaks resemble those resulting from the IR laser radiation, but are displaced by the 50 μs time delay. The cluster of peaks between 52 and 60 μs are displaced by about 50 μs from the IR laser generated matrix peaks and the peak at 71 μs is displaced by 51.3 μs from the IR laser generated bradykinin peak. This latter peak is assigned as protonated bradykinin that was ablated from the target by the IR laser and ionized by the UV laser. The longer flight time for the bradykinin produced with the UV laser is due to the fact that the ions are formed above the target surface and are therefore accelerated through a lower potential difference. It was in all cases nearly impossible to suppress the IR MALDI signal

because the IR laser energy required for the two-laser signal was in most cases sufficient for the production of ions.

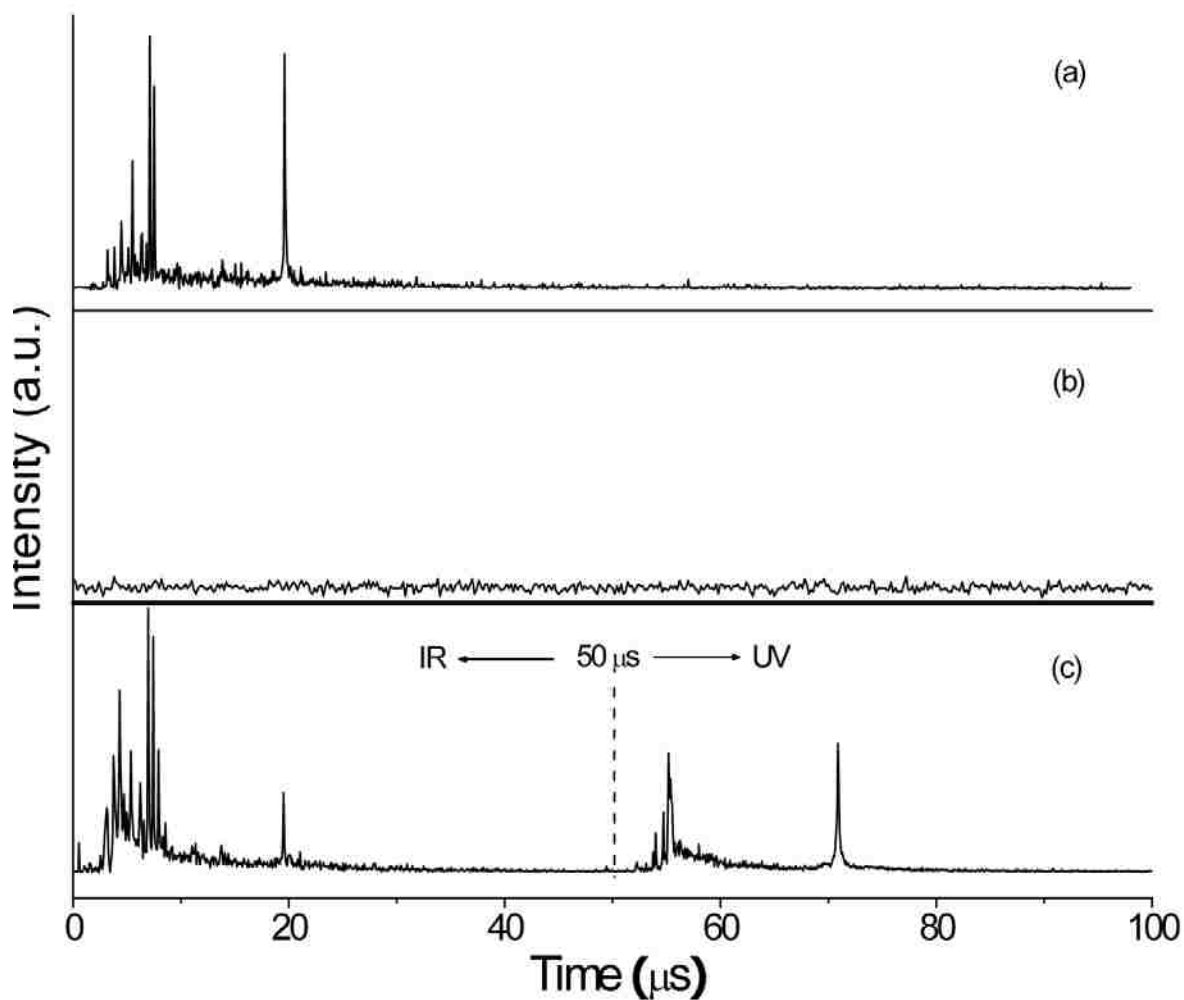


Figure 3-1 Bradykinin mass spectra with different laser conditions: (a) 2.94 μm IR laser only, (b) 351 nm UV laser only, and (c) IR and UV lasers at $\Delta t = 50 \mu\text{s}$.

Figure 3-2 shows the delay time dependence of intensity of the two-laser protonated bradykinin peak under conditions similar to those used to obtain Figure 3-1c. The IR fluence was 5.6 kJ/m^2 , the UV fluence was 1.4 kJ/m^2 and delay time ranged from 20 to 300 μs . Although signal from protonated bradykinin could be obtained with delay times as low as 12 μs ,

interferences from the IR laser mass spectrum prevented accurate measurements of the peak area below 20 μs . The peak area rises as delay time increases from 20 to 50 μs and the signal reaches a maximum near 50 μs . The signal drops rapidly between 50 and 120 μs and then more slowly after that to 300 μs . After 300 μs , signal could be observed, but it was weak and not reproducible.

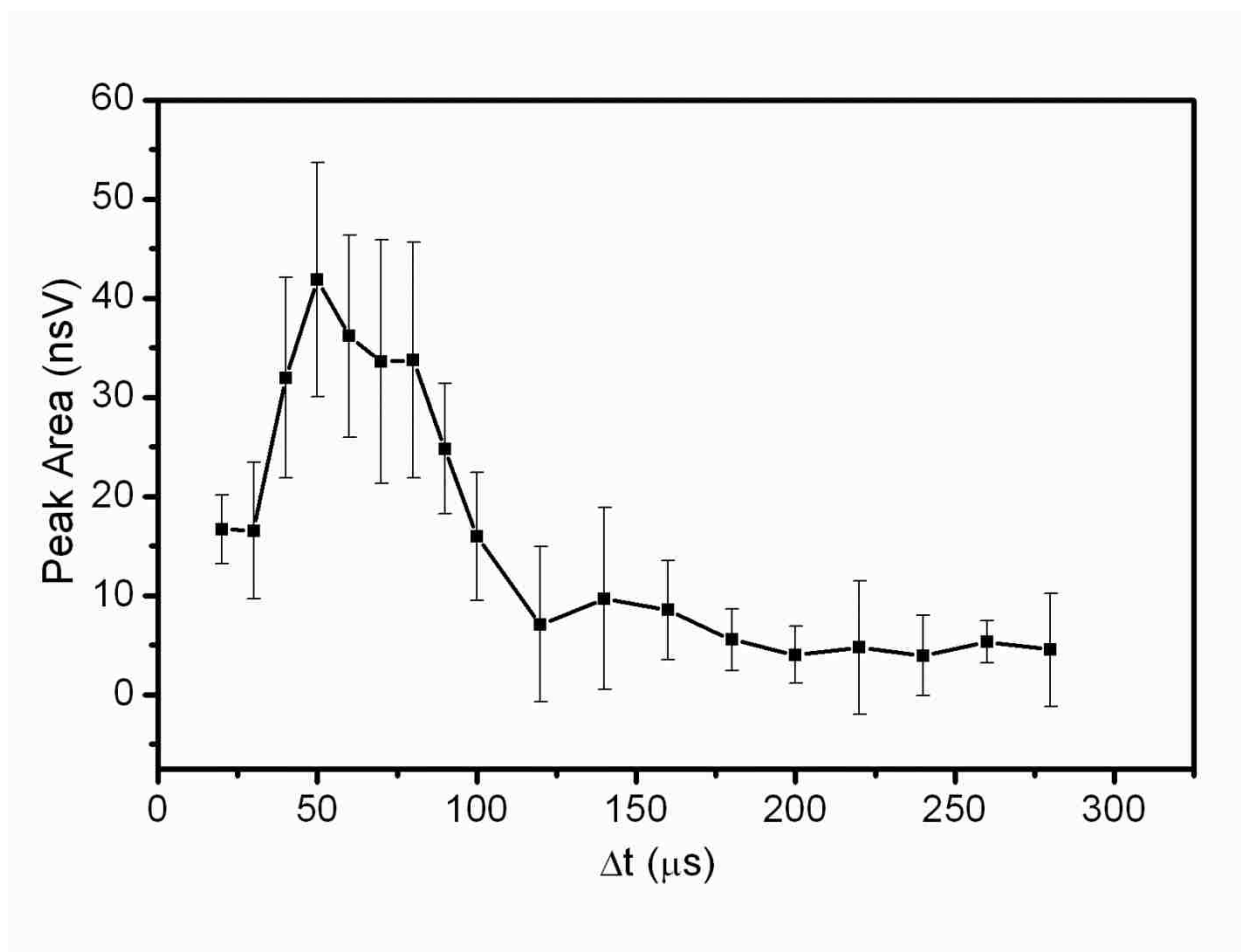


Figure 3-2 Signal intensity of singly-charged molecular bradykinin ions as a function of delay time.

Figure 3-3 displays a plot of the two-laser bradykinin $[\text{M} + \text{H}]^+$ peak area, plotted as a function of the IR laser fluence. The delay time was 50 μs and the UV laser fluence was 1.4 kJ/m^2 . This figure indicates that, in order to achieve optimum signal intensity, the IR laser energy

must be in a relatively narrow range between 5 and 7 kJ/m². Under these conditions, the maximum two-laser signal occurred at an IR fluence of 5.6 kJ/m².

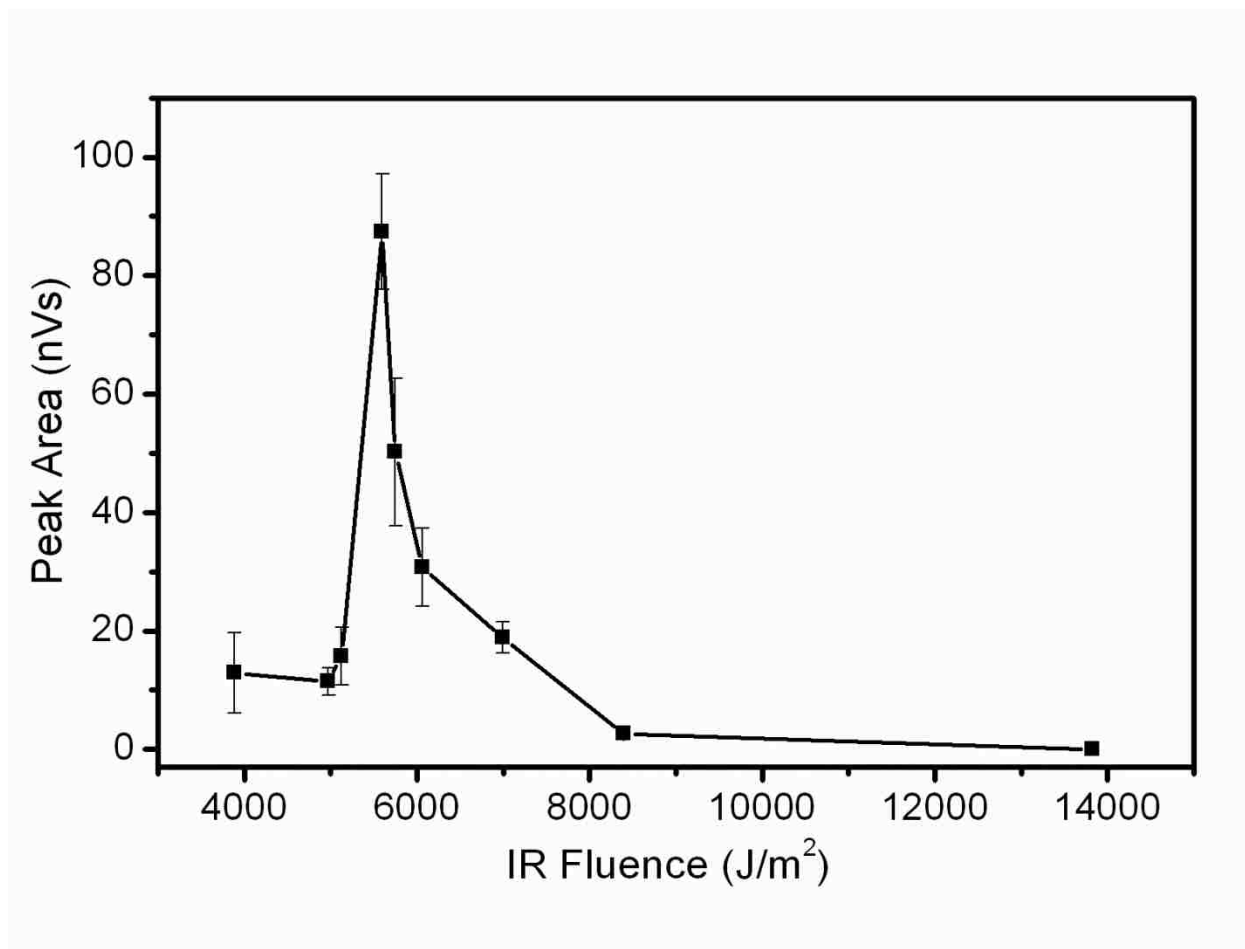


Figure 3-3 Signal intensity of singly-charged molecular bradykinin ions as a function of IR laser fluence.

The bradykinin two-laser $[M + H]^+$ peak area plotted as a function of the UV laser fluence is shown in Figure 3-4. The delay time was 50 μ s and the IR laser fluence was 5.6 kJ/m². The UV laser fluence dependence shows a gradual rise starting at the threshold of 0.8 kJ/m², below which no signal was observed. Above this threshold fluence, the peak area increases linearly with the UV fluence. In the range tested up to 2 kJ/m², the signal continued to rise with laser fluence, suggesting that a better signal intensity might be obtained if the UV fluence were

increased to still higher levels. The need for high UV laser energies has been observed previous in aerosol MALDI.¹⁴⁸

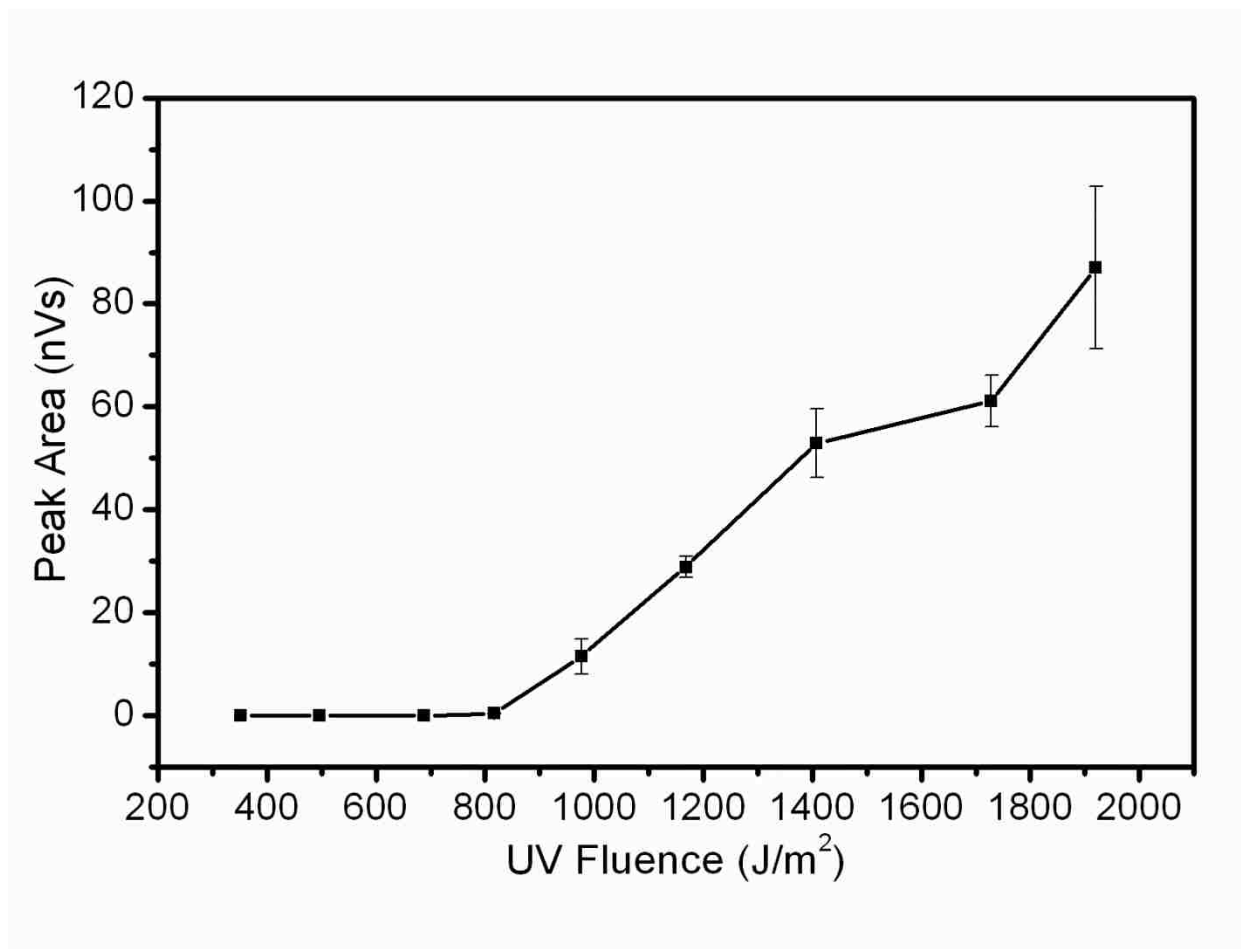


Figure 3-4 Signal intensity of singly-charged molecular bradykinin ions as a function of UV laser fluence.

Protein standards were investigated using the post-ablation ionization method. Figure 3-5 displays two representative mass spectra of cytochrome c (Figure 3-5a) and insulin (Figure 3-5b) in a DHB matrix with IR wavelength at 3.05 μm . It was found that this wavelength, which corresponds to the IR absorption maximum of DHB,¹⁴⁹ gave the best results for the two-laser protein mass spectra. The peaks at 139 μs in Figure 3-5a and at 107 μs in Figure 3-5b correspond to cytochrome c and insulin, respectively. For the cytochrome c mass spectrum, the delay time

was 70 μs , and the IR and UV fluencies were 8.4 and 1.4 kJ/m^2 , respectively. For the insulin mass spectrum, the delay time was 60 μs and the IR and UV fluences were 3.8 and 1.4 kJ/m^2 , respectively. Although the maximum in the ion signal was obtained with an approximately 50 μs delay, an additional delay was added for the larger proteins to avoid overlap of the one and two laser mass spectra. Factors affecting the protein mass spectra were not studied since the signal intensity under our experimental conditions was not high and it was therefore difficult to obtain reproducible results.

Two possibilities for ionization of biomolecules in the plume of desorbed and ablated material are the multiphoton ionization of free molecules and the ionization of particles containing matrix and analyte. The observation of biomolecules of the size of insulin and cytochrome c (Figure 3-5) argues strongly against a multiphoton ionization mechanism. Molecules of this size are difficult to ionize through the absorption of multiple photons due to the efficient energy dissipation in the large number of vibrational degrees of freedom.¹⁴⁵ Instead, these results suggest that particles containing a UV MALDI matrix and analyte, when irradiated with the UV laser, form ions by a MALDI process. It has been observed that particles containing matrix and analyte, when sprayed into vacuum and irradiated with a UV laser, form ions by MALDI.^{61, 148} A particle MALDI mechanism has been suggested previously for IR laser ablated particles that were irradiated with a second IR laser. However, in this case, the absorption of the second IR laser energy by the analyte molecule²⁷ or waters of hydration¹³⁸ cannot be ruled out. The observation of ions from proteins by UV irradiation of the ablated material strongly suggests that the ionization mechanism is MALDI of the ablated particles. This hypothesis is supported by results of time-resolved fast-flash photography of the glycerol plume^{26, 35} and by measurements

of the particle size and number ablated by an IR laser from a MALDI matrix,^{25,31} which show a large number of particles in the IR ablation plume.

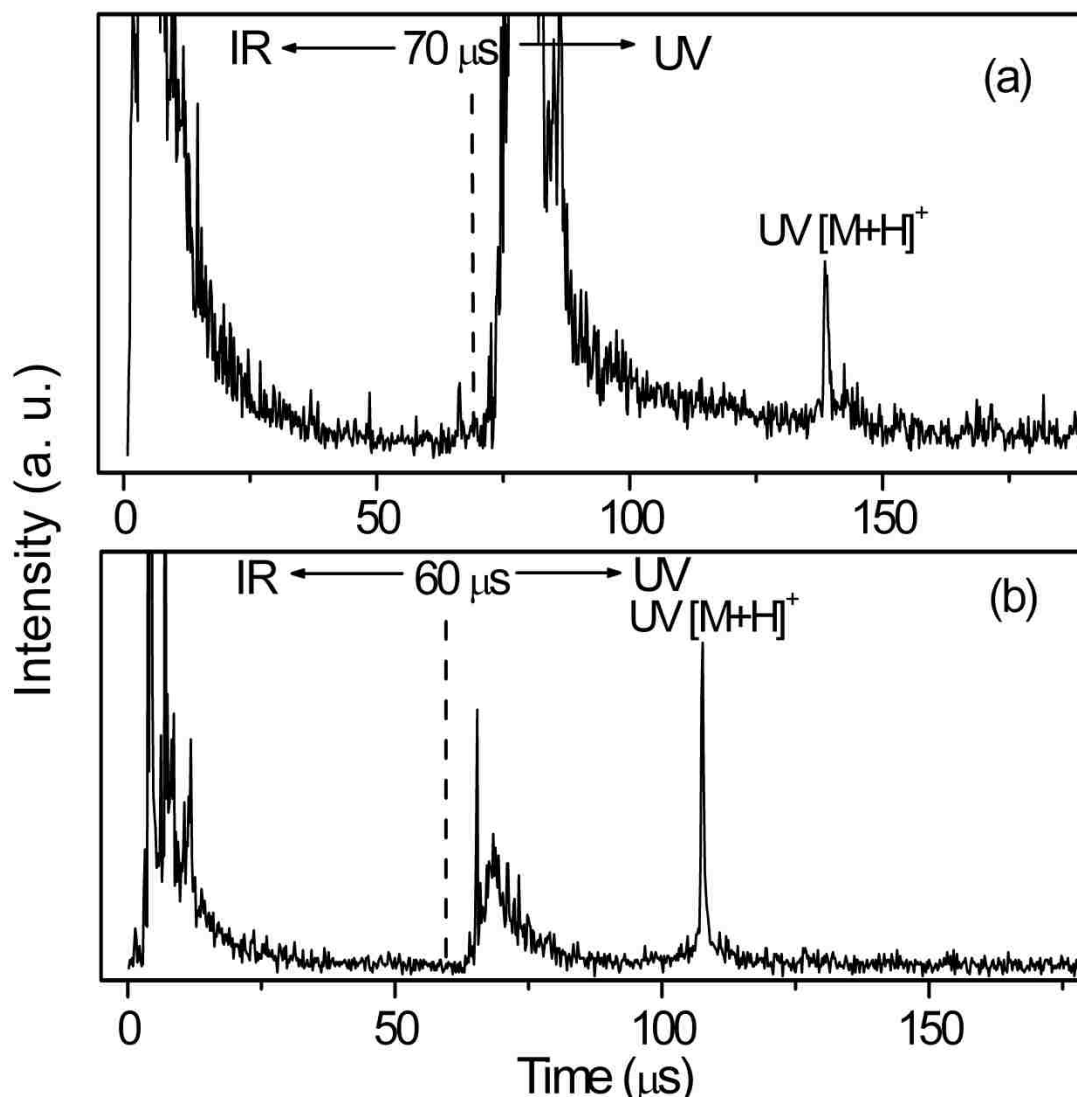


Figure 3-5 IR/UV two-laser mass spectra of (a) cytochrome c at $\Delta t = 70 \mu\text{s}$ and (b) insulin at $\Delta t = 60 \mu\text{s}$.

The velocity of the IR laser desorbed material can be estimated using the appearance of two laser signal as an indication for the arrival time of the plume front. For UV MALDI, the axial velocity is between 200 and 1000 m/s for ions, 600 and 800 m/s for neutrals.⁵⁵ A previous study

of IR laser ablation and IR ionization found that the axial velocity of the plume front corresponding to the initial rise in ion signal represented a plume front velocity of 1000 m/s.¹⁴⁷ A fast photography study of IR laser ablation of glycerol showed a plume front velocity of 400 m/s in the air.²⁶ In our work, the velocity of the plume expansion can be calculated by dividing the distance between the UV beam center and the sample surface (1.4 mm) by the delay time for observation of UV ions (50 μ s for the maximum ion yield in Figure 3-2). The calculated velocity is about 30 m/s, which is more than an order of magnitude slower than expected. However, it is also possible that material is ejected after the end of the laser pulse, which would lead to an anomalously low estimate to the ejection velocity.¹⁰⁶ Such delayed emission of IR ablated particulate has been observed using fast photography,³⁴ photoacoustic,¹⁵⁰ and time-resolved particle size measurements.¹⁰⁶ It is possible that the UV laser is less efficient at ionizing biomolecules in the early part of the plume compared to the IR laser used in the previous study. This would lead to the delayed signal onset and the low apparent particle velocity observed in this study.

3.4. Summary

An infrared ablation of biomolecules that was post ionized by ultraviolet matrix-assisted laser desorption ionization method is presented. Using this method, mass spectra of biomolecules including bradykinin, insulin, and cytochrome c were obtained with a 2, 5-dihydroxybenzoic acid matrix. Two-laser signal could be obtained at IR laser fluences between 5 and 8 kJ/cm². The signal increased with UV laser fluence and was the optimum at the maximum of 2 kJ/cm². The observation of signal from proteins larger than 10 kDa suggests that ionization proceeds through

the ablation particles containing a mixture of matrix and analyte followed by UV MALDI of these particles.

CHAPTER 4. CONTINUOUS FLOW INFRARED MATRIX-ASSISTED LASER DESORPTION ELECTROSPRAY IONIZATION MASS SPECTROMETRY*

In the previous chapter, UV MALDI analysis of IR laser ablated protein and peptide samples was described. It has been noted that IR lasers are efficient for sample removal, and the ablated material contains a significant quantity of particulate. The fact that the signal was still observed with a delay time as long as several hundreds of microseconds indicates that IR laser ablation generated sample plume expands for hundreds of μs and several millimeters above the sample surface. This long duration of the sample plume generated by the IR laser ablation has been seen and confirmed by particle sizing and fast photography experiments.^{25, 26, 34} Although UV lasers, such as the excimer laser used in the work described in the previous chapter, are efficient in terms of ion formation, their ns pulse width is short as compared to the hundreds of μs plume duration. One problem of IR/UV two-laser MALDI discussed in the previous chapter therefore is that even with the UV laser post-ionization, still a large fraction of the sample in the plume is not used and doesn't make ions due to the temporal mismatch. This problem has been addressed with the development of IR MALDESI,¹² which uses a continuous source, electrospray, to ionize infrared laser ablated materials.

In this chapter, a continuous flow (CF) IR MALDESI method was used for the on-line and off-line analysis of liquid, chemical and biochemical sample reactions. Samples in aqueous solution were flowed through a 50 μm ID silica capillary at a 1–6 $\mu\text{L}/\text{min}$ flow rate. As analyte aqueous solution flowed through the capillary, a liquid sample bead formed at the capillary tip. A pulsed OPO laser with wavelength of 2.94 μm and a 20 Hz repetition rate was focused onto the capillary tip for sample desorption and ablation. The plume of ejected sample was entrained in an

*The work reported in this chapter has been published in *Rapid Communication in Mass Spectrometry*. Reprinted by permission of the John Wiley.

electrospray to form ions by MALDESI. The resulting ions were sampled into an ion trap mass spectrometer for analysis. Using CF IR MALDESI, several chemical and biochemical reactions were monitored on-line: the chelation of 1,10-phenanthroline with iron (II), insulin denaturation with 1,4-dithiothreitol (DTT), and tryptic digestion of cytochrome c.

4.1. Introduction

Over the past several decades, mass spectrometry (MS) has been used increasingly with direct liquid introduction for coupling to separations such as liquid chromatography and capillary electrophoresis.¹⁵¹⁻¹⁵³ In addition to separation methods, mass spectrometry has also been used extensively for monitoring liquid reactions on-line.¹⁵⁴⁻¹⁵⁷ The spray ionization methods such as atmospheric pressure chemical ionization (APCI), atmospheric pressure photoionization (APPI), thermospray ionization and electrospray ionization (ESI) that are highly effective for coupling to liquid separations also have great utility for reaction monitoring. ESI and APCI are the most widely used, with the former better suited to larger and more highly charged species such as proteins or peptides and the latter to smaller, less polar species such as small organic molecules. For on-line analysis, it is advantageous for the reaction to occur immediately before the solution is sprayed for ionization. Over the past few years, different types of sources coupled to either APCI or ESI have been developed to for on-line study of organic reaction mechanisms, which include microreactors, capillary mixers, photolysis cells, photochemical reactors and electrochemical cells.^{157, 158} Reactions that involve large molecules have also been studied on-line by ESI MS, such as peptide and protein reactions with nitric oxide.¹⁵⁹

Desorption ionization methods such as fast atom bombardment (FAB) and matrix-assisted laser desorption/ionization (MALDI) can also be used for on-line reaction monitoring. The on-

line versions of FAB and MALDI use a capillary and frit to deliver the liquid into the vacuum of the mass spectrometer for ionization,⁵⁹ although aerosol^{60, 61} and rotating ball interfaces¹⁶⁰ have also been developed for MALDI. FAB has been used to monitor biochemical reactions on-line,¹⁶¹ most notably in combination with microdialysis to monitor penicillin G in the bloodstream of a live rat.¹⁶² There are a number of methods for off-line MALDI analysis of chemical reactions,¹⁶³ but on-line analysis is more difficult. On-line reaction monitoring with microfluidic chip was accomplished by inserting the device into the source of a MALDI time-of-flight mass spectrometer.¹⁶⁴ Both organic and biochemical reactions were demonstrated.

As discussed in Chapter 1, ambient mass spectrometry is the direct analysis of materials in their native environment with ions created outside the mass spectrometer.^{6, 8, 81} With these methods, material is removed from solid or liquid samples that are bombarded with ions, charged droplets, or a pulsed laser; sample preparation is minimal and in some cases unnecessary.⁸ The use of ambient ionization MS for on-line reaction monitoring has recently been reported. Direct analysis in real-time (DART) is a method that uses metastable ions directed at a surface to produce secondary analyte ions.¹⁰ DART has been used to monitor organic reactions important in drug discovery under ambient conditions.¹⁶⁵ With extractive electrospray ionization (EESI), a spray of solvent droplets containing the analyte interacts with charged droplets from an electrospray to form analyte ions.¹⁶⁶ EESI was recently demonstrated for on-line monitoring of organic chemical reactions.¹⁶⁷ Electrospray laser desorption ionization (ELDI) uses a ultraviolet laser to desorb material deposited on a target that reacts with charged electrosprayed droplets to form ions.¹³ In the reactive ELDI approach, one of the reactants is contained in the electrospray while the other is deposited on the target. The reaction occurs when the desorbed reactant enters

the electrosprayed droplet. The reactive ELDI technique has also been demonstrated for biochemical reactions in peptide and protein analysis.¹⁶⁸

The matrix-assisted laser desorption electrospray ionization approach to ambient ionization (MALDESI) uses a matrix to aid in the removal of material for subsequent ionization through interaction with an electrospray.¹¹ This approach was recently extended to infrared (IR) laser desorption,¹⁵ facilitating the use of liquid matrix materials such as water and other solvents.¹² It has been suggested that the MALDESI ionization mechanism is similar to electrospray with the analyte material incorporated as neutral molecules¹¹ or through a droplet merging mechanism in which the material ablated from the target in the form of particles interacts with the ESI droplets.^{12, 14} For large ablated particles, the small ESI droplets may collide with the particles, extract material, and thereafter expel ions via the DESI mechanism.¹⁶⁹ Studies of plume imaging²⁶ and particle detection and sizing²⁵ show that a large fraction of the material removed by the IR laser is in the form of particulate; however, the particle size range conducive to ion formation is not clear.

We have adapted IR MALDESI for the on-line continuous flow analysis of chemical and biochemical reactions. The approach is similar to those used for CF FAB and MALDI: reagents in aqueous solution were flowed through a fused silica capillary and mixed in a microfluidic device. The mixed solution formed a bead at the tip of a capillary beneath the electrospray plume. A pulsed IR laser was directed at sample bead to desorb and ablate the solution that was entrained in the electrospray to form ions by MALDESI. Several chemical and biochemical reactions were monitored on-line using this CF IR MALDESI approach.

4.2. Experimental

The experiment was carried out on the Hitachi 3DQ ion trap mass spectrometer coupled with the CF IR MALDESI interface that was described in detail in Chapter 2, Section 2.4. The ESI solution was a 1:1 (v/v) mixture of acetonitrile and water with 0.2% formic acid that was flowed through a 50 μm i.d. fused silica capillary using a syringe pump; no nebulizing gas was used. The voltage on the ESI needle was 3.5 kV and the capillary was at ground. Mass spectra were acquired in positive-ion mode and ions were accumulated for 100 ms in the trap.

The continuous flow IR MALDESI interface is similar to the MALDESI configuration published previously¹² with the addition of the continuous flow capillary. This open fused silica capillary (50 μm i.d., 360 μm o.d.) was prepared by removing the polyimide coating from the tip and was mounted 7 mm below the spray axis pointing upward and 6 mm from the tip of the spray cone. A sample solution was flowed through the capillary, forming bead of liquid at the capillary tip. The laser system was a wavelength tunable pulsed IR OPO operating at 20 Hz repetition rate. The wavelength was set at 2.94 μm to overlap with the OH stretch absorption of the water matrix, and the laser energy was 2 mJ with no attenuation that resulted in the largest signal intensity. The laser was directed downward toward the capillary tip at an 80° angle from horizontal. When the laser was on, material was ablated from the liquid bead and entrained in the electrospray to form ions by MALDESI.

Two of the chemical reactions studied, chelation of 1,10-phenanthroline (PA) with Fe^{2+} and insulin denaturation, were carried out using a low flow-rate mixer. The mixer had two inlet channels and one outlet channel. The flow at each inlet channel was 3 $\mu\text{L min}^{-1}$, resulting in a 6 $\mu\text{L min}^{-1}$ sample flow rate of the outlet capillary. In the studies described below, one reaction solution flowed into the mixer through one inlet channel, and solvent flowed through the other

inlet channel, which was connected to the output of a 6-port injection valve with a 3 μL loop. For protein digestion, a cytochrome c solution was flowed directly through a 250 μm \times 150 mm trypsin column with a 7 μL bed volume.

The reagents 1,10-phenanthroline (PA), iron (II) sulfate heptahydrate ($\text{FeSO}_4 \cdot 7\text{H}_2\text{O}$), 1 mM 1,4-dithiothreitol (DTT) solution, insulin, cytochrome c, trypsin, ammonium bicarbonate (NH_4HCO_3), and formic acid were obtained from Sigma Aldrich and used without further purification. HPLC grade methanol and acetonitrile were purchased from Mallinckrodt Baker. House purified water was used for aqueous solution preparation.

For the chelation reaction, a 1,10-phenanthroline (PA) solution with a concentration of 2 mM was prepared by dissolving PA in methanol and water (1:1 v/v). A Fe^{2+} solution with a concentration of 20 mM was prepared in the same manner. The on-line monitoring of this chelation reaction was done by continuously delivering 2 mM PA solution through the mixer to the tip of the capillary. The IR laser was continuously fired to ablate the solution emerging at the capillary tip and the ESI was continuously running. To initiate the reaction, a 20 mM Fe^{2+} solution was injected to the mixer through the 6-port valve. Mass spectra were acquired immediately after the Fe^{2+} solution was injected at $t = 0$. The chelation reaction took place once PA and Fe^{2+} solutions were mixed in the mixer, and the product of this reaction, $[(\text{PA})_3 + \text{Fe}]^{2+}$, was formed.

The reagents for the insulin denaturation reaction consisted of an aqueous solution of insulin that was prepared by dissolving insulin in a 50 mM NH_4HCO_3 solution to give a final concentration of 500 μM . A 100 mM DTT solution was prepared by diluting a 1 M DTT solution with water. Static (off-line) denaturing of insulin was carried out by mixing equal volumes of 500 μM insulin solution with 100 mM DTT. The mixture was delivered through a fused silica

capillary to the IR MALDESI source for analysis. On-line CF IR MALDESI insulin denaturation was performed in the same manner as the chelation reaction. A 500 μM insulin solution was continuously flowed through one mixer inlet and a 100 mM DTT solution was injected through the 6-port valve and delivered to the other mixer inlet port. The mixed solutions were then delivered to the IR MALDESI source for analysis.

Reagents for the cytochrome c digestion reaction were prepared using aqueous solutions of cytochrome c in 50 mM NH_4HCO_3 solutions to give final concentrations of 300, 400, 500 and 600 μM for the protein. The trypsin solution was prepared by dissolving the dry reagent in a 100 mM NH_4HCO_3 solution to give a final trypsin concentration of 600 μM . Static cytochrome c trypsin digestion was performed by mixing 600 μM trypsin with 600 μM cytochrome c solution at a 1:10 (v/v) ratio. The mixture was delivered through a fused silica capillary directly to the IR MALDESI source. On-line CF IR MALDESI analysis of cytochrome c tryptic digestion was performed by continuously flowing the cytochrome c solution through the immobilized trypsin column. The tryptic peptides and undigested cytochrome c exiting the column flowed through the fused silica capillary to the IR MALDESI source for analysis.

4.3. Results and Discussion

Three reactions were investigated using IR MALDESI: chelation of 1,10-phenanthroline (PA) with Fe^{2+} , insulin denaturation, and cytochrome c digestion. The chelation reaction of 1,10-phenanthroline (PA) with Fe^{2+} is typically studied off-line by absorption spectroscopy due to the strong absorption of $[(\text{PA})_3 + \text{Fe}]^{2+}$ at wavelengths between 400–600 nm.¹⁷⁰ Insulin denaturation is commonly performed off-line by mixing insulin with reducing agents such as 1,4-dithiothreitol (DTT), or just simply by applying heat. The disulfide bonds of insulin break, resulting in the

formation of insulin α and β chains.¹⁷¹ The tryptic digestion of a proteins such as cytochrome c is a common step in proteomic analysis due to the robust nature of this enzyme and can be performed in solution or with support-bound reagents.¹⁷²

Chelation of 1,10-phenanthroline with Fe^{2+}

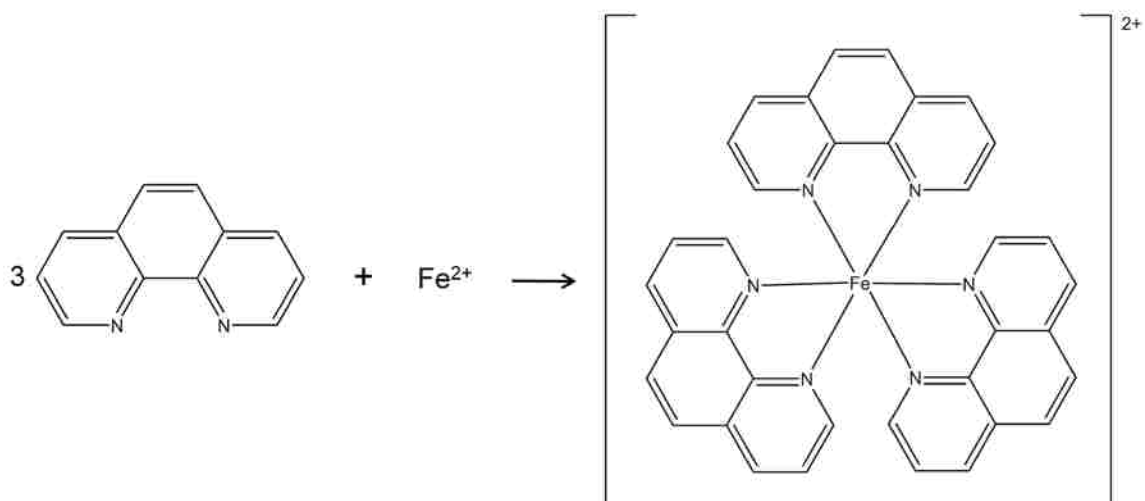


Figure 4-1 Scheme of 1,10-phenanthroline reaction with Fe^{2+} .

Chelation of PA with Fe^{2+} occurs when three PA molecules bind to one Fe^{2+} ion, forming the $[(\text{PA})_3 + \text{Fe}]^{2+}$ ion, as indicated in Figure 4-1. Three CF IR MALDESI mass spectra obtained at different points of the reaction are shown in Figure 4-2. The mass spectrum in Figure 4-2a, was obtained prior to the injection of the Fe^{2+} when only the PA solution was flowing to the capillary tip. The peak at m/z 181 corresponds to the $[\text{M} + \text{H}]^+$ peak of PA. A small peak corresponding to the sodium adduct with PA is observed at m/z 203. Figure 4-2b shows the mass spectrum that was obtained 4 minutes after the injection of the Fe^{2+} solution. The reaction between the PA and the Fe^{2+} resulted in the near complete disappearance of the protonated PA peak and the appearance of a strong $[(\text{PA})_3 + \text{Fe}]^{2+}$ peak at m/z 298. At a time of 18 min, shown in Figure 4-2c, nearly all of the Fe^{2+} had flowed through the system. Here, the PA peak

reappeared with an intensity close to that in Figure 4-2a, and the $[(PA)_3 + Fe]^{2+}$ peak was less than 10% of its intensity in Figure 4-2b.

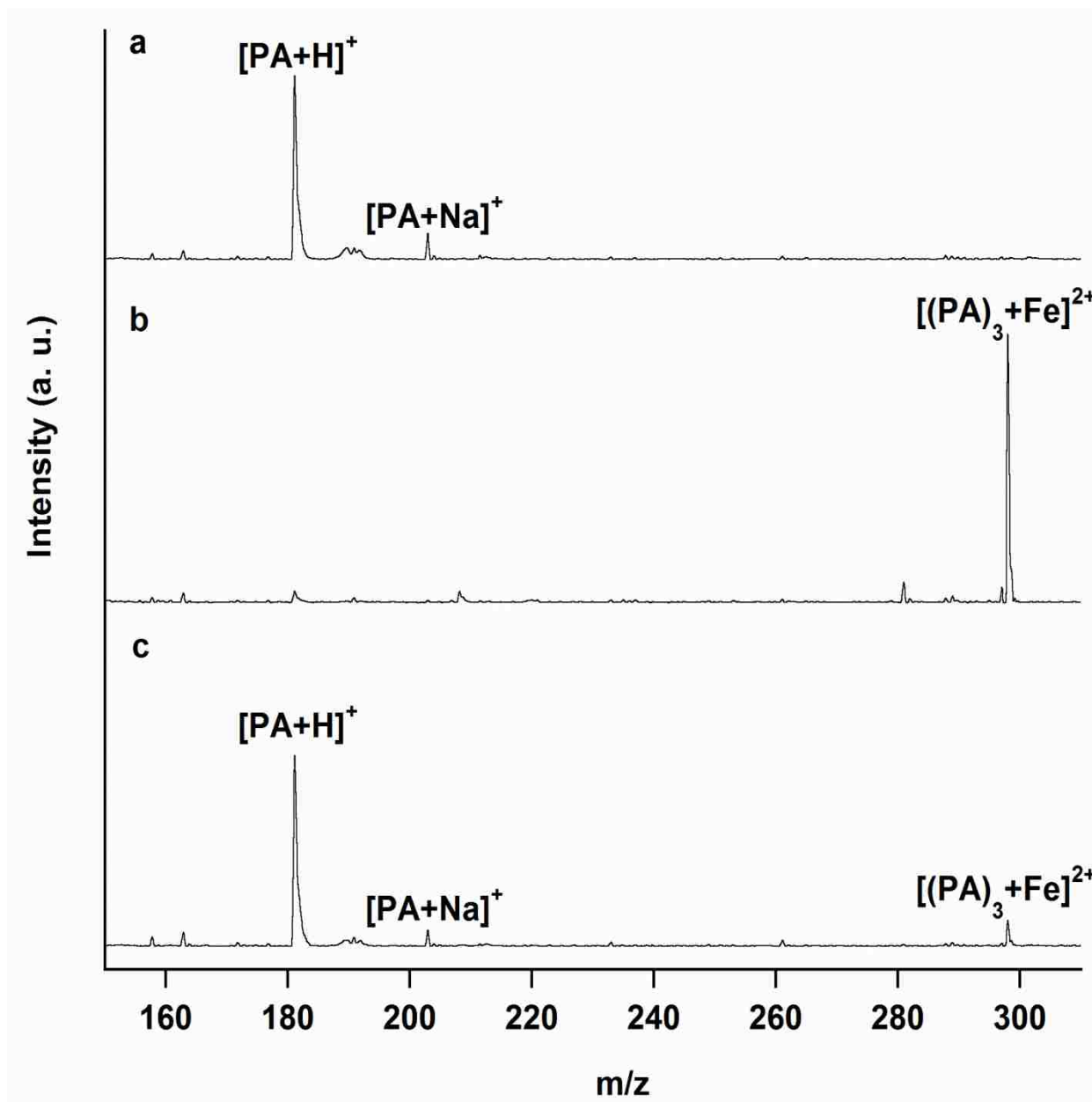


Figure 4-2 On-line CF IR MALDESI mass spectra of the chelation of 1,10-phenanthroline (PA) with iron (II) in water. Positive-ion CF IR MALDESI mass spectra were recorded at three reaction stages: (a) 2 mM PA solution only before reaction, (b) PA solution after mixing with 20 mM $FeSO_4$ solution, and (c) after $FeSO_4$ solution depleted.

A plot of the total ion currents of reactant and product are shown in Figure 4-3: Figure 4-3a shows the total ion current of PA and Figure 4-3b shows the total ion current of $[(PA)_3 + Fe]^{2+}$.

The Fe^{2+} solution was injected at 0 min, and theoretically, it required ~ 2 min to flow through a ~ 80 cm of $100 \mu\text{m}$ i.d. tubing from the injection valve to the mixer at a flow rate of $3 \mu\text{L min}^{-1}$ and an additional 0.2 min to flow through the 60 cm $50 \mu\text{m}$ i.d. capillary from the mixer to the capillary tip.

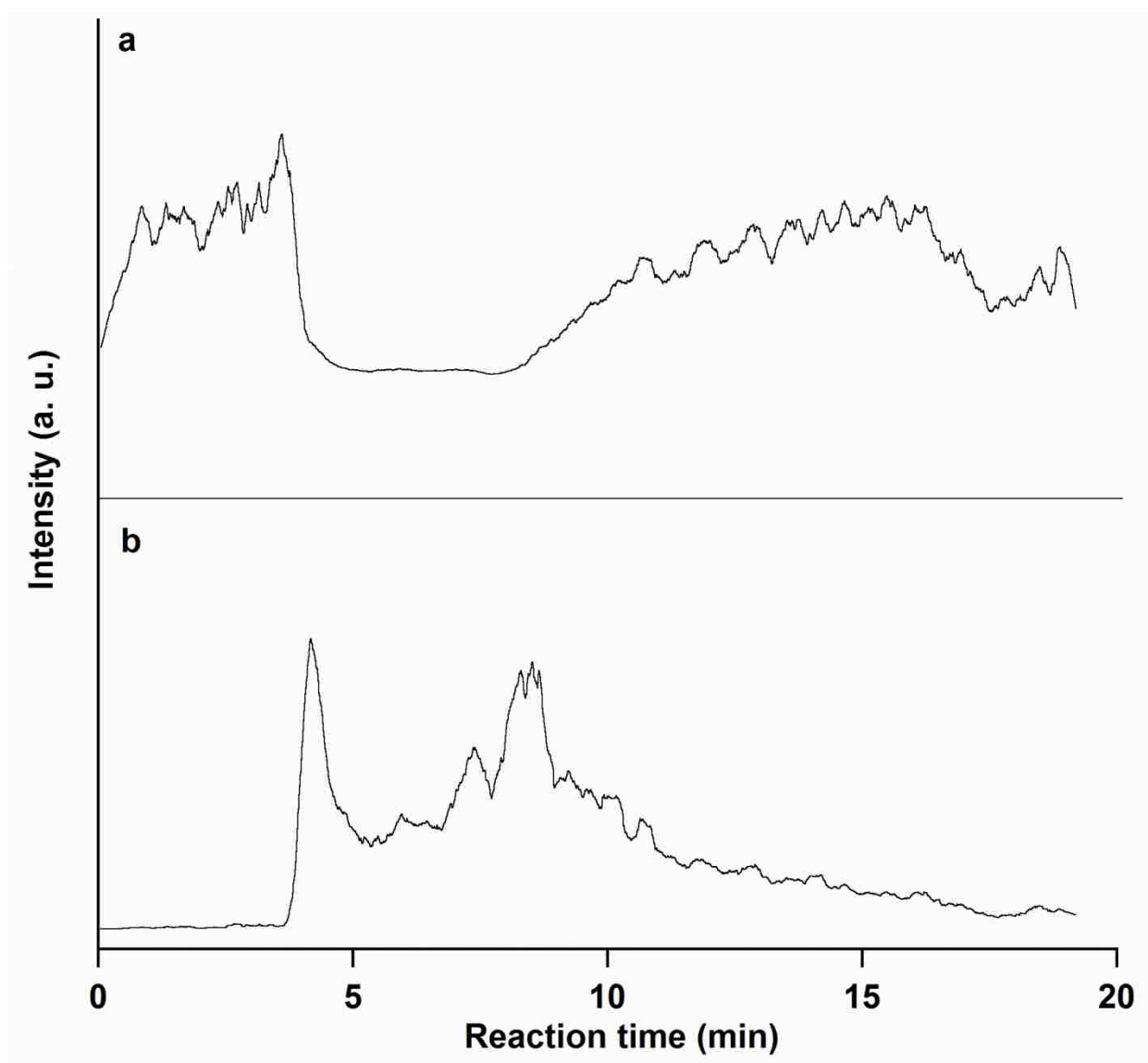


Figure 4-3 Ion signals for (a) $[\text{PA} + \text{H}]^+$ and (b) $[(\text{PA})_3 + \text{Fe}]^{2+}$ ions during the chelation reaction recorded as a function of reaction time.

As shown in Figure 4-3, between 0 and 4 min, the PA signal was strong whereas no $[(\text{PA})_3 + \text{Fe}]^{2+}$ signal was observed. From 4 to approximately 9 min, the PA signal dropped and then

rose slowly after the 3 μL plug of Fe^{2+} passed through the system. The product $[(\text{PA})_3 + \text{Fe}]^{2+}$ signal rose over 30 seconds to a maximum and then dropped to 40% within one minute. The signal increased to 92% of the maximum value at 8.5 min and then decreased slowly over the next 10 minutes. The anticipated time for PA signal drop was 30 seconds.

The delayed onset and extended signal measurement can be attributed to inefficient mixing of the product and reactant streams or sample memory effect. The sample memory effect has been observed and discussed in CF IR vacuum MALDI. It has been found in CF IR MALDI that the memory effect is affected by the sample concentration as well as the laser spot size compared to the sample spot.⁶⁵ Higher sample concentration and lower laser spot coverage on the target both resulted in a memory effect. In our case of CF IR MALDESI, the memory effect might partially result from the Fe^{2+} accumulation on the continuous flow capillary with the Fe^{2+} solution concentration 10 times higher than PA solution concentration. It was found that the memory effect could be reduced with a lower concentration of Fe^{2+} (data now shown). However, the signal intensity of $[(\text{PA})_3 + \text{Fe}]^{2+}$ also dropped. Laser spot coverage does not appear to be a likely reason for memory effect in CF IR MALDESI, because the laser energy and repetition rate was sufficient enough to remove the sample bead from the capillary tip, and the 210 μm laser spot size was large enough to cover the capillary exit.

Insulin Denaturation Reaction with 1,4-dithiothreitol

The results of off-line and on-line CF IR MALDESI studies of insulin denaturation are shown in Figure 4-4. Figure 4-4a displays a representative CF IR MALDESI mass spectrum of insulin before mixing with DTT. This spectrum is similar to that obtained with ESI and contains multiply-protonated insulin ions from $[\text{M} + 4\text{H}]^{4+}$ to $[\text{M} + 6\text{H}]^{6+}$. Figure 4-4b shows an IR

MALDESI mass spectrum of the static denaturation of insulin. The disappearance of insulin multiply protonated ion peaks and the appearance of insulin α chain doubly charged peak and β chain multiply charged peaks indicates that the denaturation reaction had progressed completely. Figure 4c shows an on-line CF IR MALDESI mass spectrum of denatured insulin after injecting DTT solution through 6-port valve. Again, insulin was completely denatured since only $\beta+3$ and $\beta+4$ peaks were observed. However, as compared with Figure 4b, peaks in Figure 4c were less intense and no α chain peak was observed. MS analysis of insulin denaturation has been reported using a ^{252}Cf ionization time-of-flight mass spectrometer.¹⁷¹ In this study, both intense α and β chain peaks were observed. In another insulin denaturation study reported by Fischer and co-workers, however, only β chain peak was observed in the positive ion spectrum 15 minutes after mixing and incubating in a test tube with tris(2-carboxyethyl)phosphine (TCEP), and both α and β chain peaks with approximately equal intensity were observed in the negative ion spectrum.¹⁷³ In the study by Peng and co-workers on insulin denaturation using ELDI,¹⁶⁸ only β chain peaks were observed when DTT solution was sprayed and protein solution was desorbed by the laser; both α and β chain peaks were observed when protein solution was sprayed and the DTT solution was laser desorbed. The reason for this difference is still not clear, but the authors have pointed out that the detection limit for positively charged α chain is higher compared to the β chain by conventional ESI MS. The relatively higher limit of detection is a possible explanation for our lack of observation of the α chain peaks in on-line CF IR MALDESI.

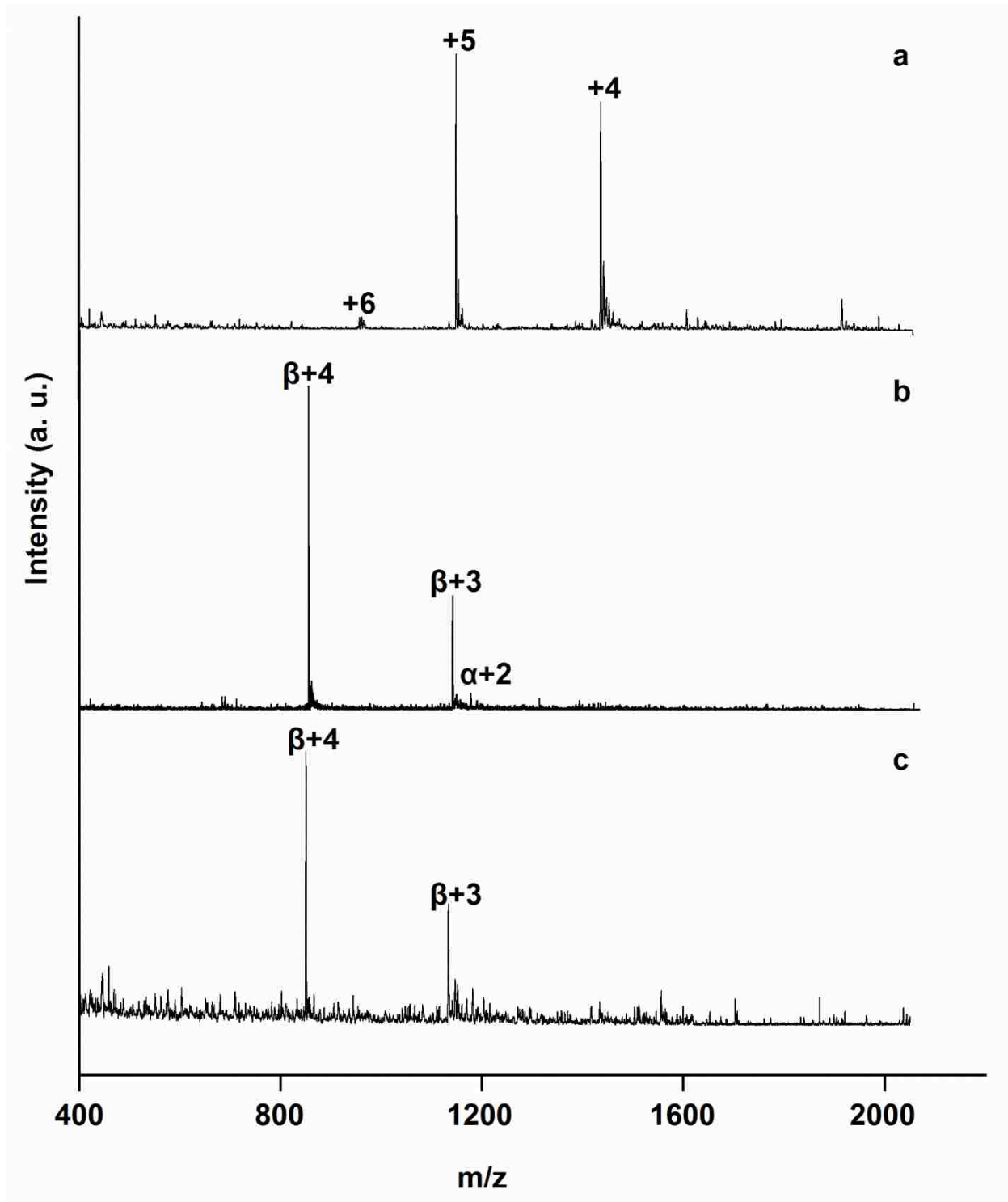


Figure 4-4 CF IR MALDESI mass spectra of (a) 500 μ M insulin in 50 mM NH_4HCO_3 water buffer solution, (b) 500 μ M insulin mixed with 100 mM 1,4-dithiothreitol (DTT) reducing agent, and (c) denatured insulin b chain after on-line mixing of 500 μ M insulin with 100 mM DTT solution.

4.3.3. Cytochrome c Trypsin Digestion Reaction

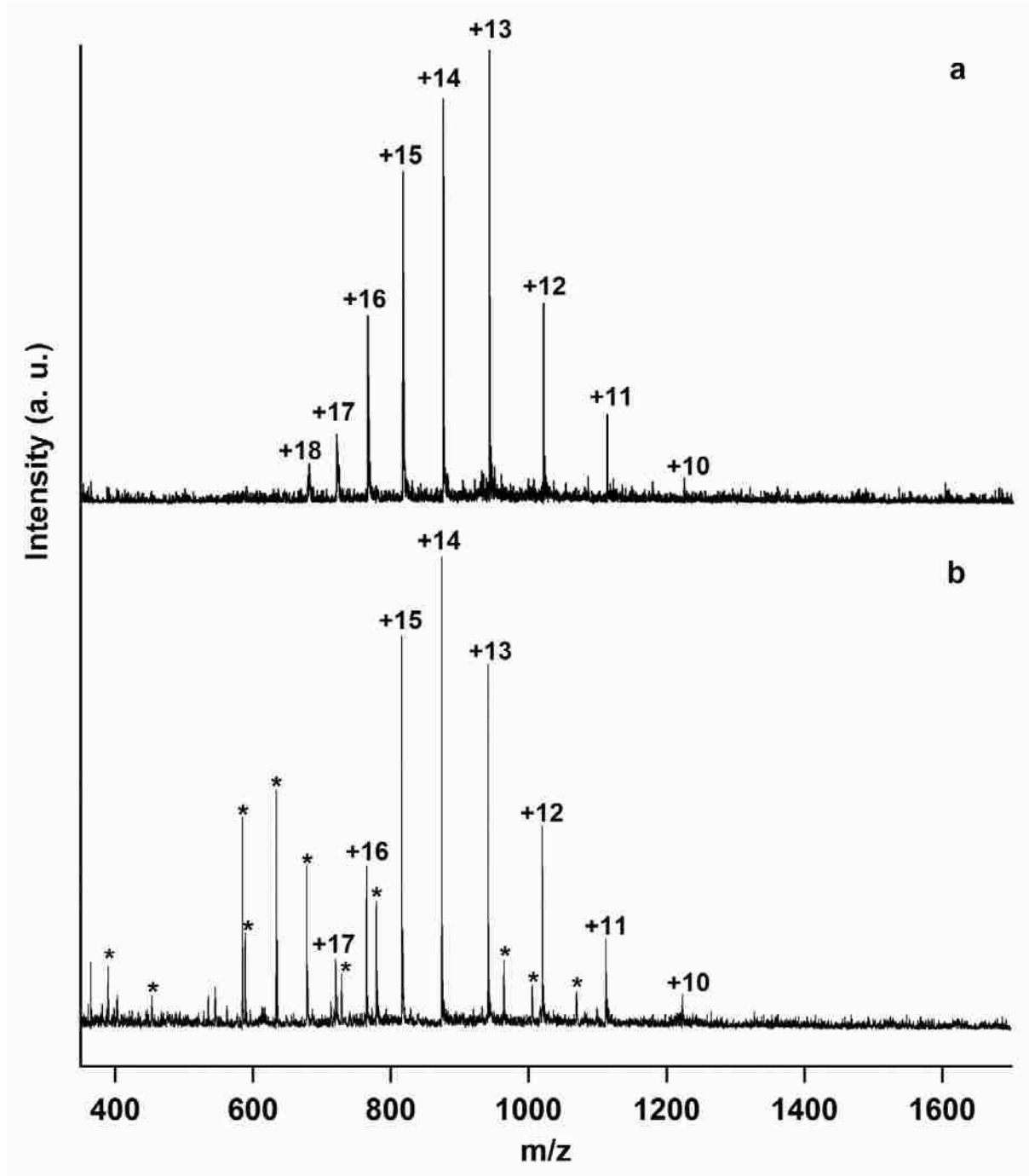


Figure 4-5 (a) CF IR MALDESI mass spectrum of 600 μM cytochrome c in 50 mM NH_4HCO_3 water buffer solution with +10 through +18 charge states. (b) CF IR MALDESI mass spectrum of 600 μM cytochrome c 1:10 (v/v) mixed with 600 mM trypsin. Peaks labeled with asterisks are assigned to tryptic peptides.

It was found that the detection limit of cytochrome c with IR MALDESI detection was about 300 μM when flowed directly to the capillary tip (data not shown). This is comparable to that reported for static IR MALDESI on this system. A representative CF IR MALDESI mass spectrum of 600 μM cytochrome c before digestion is shown in Figure 4-5a. This spectrum contains multiply-protonated cytochrome c ions from $[\text{M} + 10\text{H}]^{10+}$ to $[\text{M} + 18\text{H}]^{18+}$, which is similar to previous IR MALDESI results using this instrument.¹² The mass spectrum from a tryptic digest of 600 μM cytochrome c using static IR MALDESI is shown in Figure 4-5b. Eleven cytochrome c tryptic peptide peaks were observed, indicating digestion reaction had progressed. The sequence coverage was 92%.

On-line CF IR MALDESI mass spectra of cytochrome c digestion with different protein concentrations are shown in Figure 4-6. From Figure 4-6a to Figure 4-6d, the cytochrome c concentrations before digestion were 600, 500, 400, 300 μM , respectively. At low concentration, the cytochrome c peak intensity decreased relative to those of the tryptic peptide peaks, which is probably due to a more favorable substrate:enzyme ratio. For 300 μM initial cytochrome c concentration (Figure 4-6d), only tryptic peptide peaks were found. The sequence coverage for 600, 500, 400, and 300 μM cytochrome c solutions were 75%, 51%, 92%, and 81%, respectively.

The digestion efficiency is affected by the flow rate, since a lower flow rate corresponds to a longer residence time in the trypsin column. Figure 4-7 shows on-line CF IR MALDESI mass spectra of 500 μM cytochrome c digestions at flow rates of 4 $\mu\text{L min}^{-1}$ and 2 $\mu\text{L min}^{-1}$. As expected, the 2 $\mu\text{L min}^{-1}$ flow rate mass spectrum (Figure 4-7b) had a relatively higher intensity of peptide to protein compared to 4 $\mu\text{L min}^{-1}$ mass spectrum (Figure 4-7a). In addition, the sequence coverage was 51% at 4 $\mu\text{L min}^{-1}$ compared to 82% at 2 $\mu\text{L min}^{-1}$ flow rate.

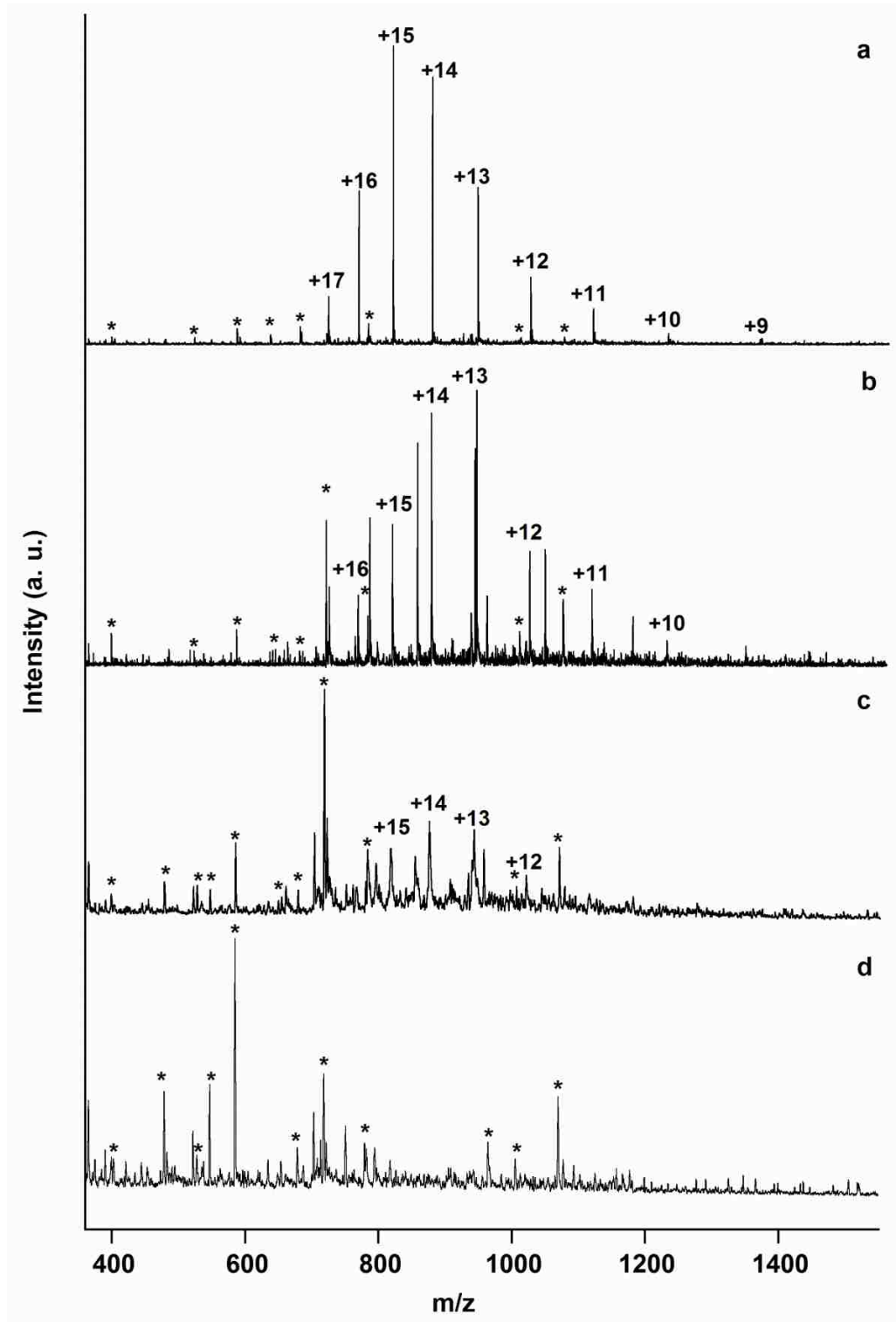


Figure 4-6 CF IR MALDESI mass spectra of on-line digested cytochrome c solutions with different cytochrome c concentrations: (a) 600 μM , (b) 500 μM , (c) 400 μM , and (d) 300 μM . Peaks labeled with asterisks are assigned to tryptic peptides.

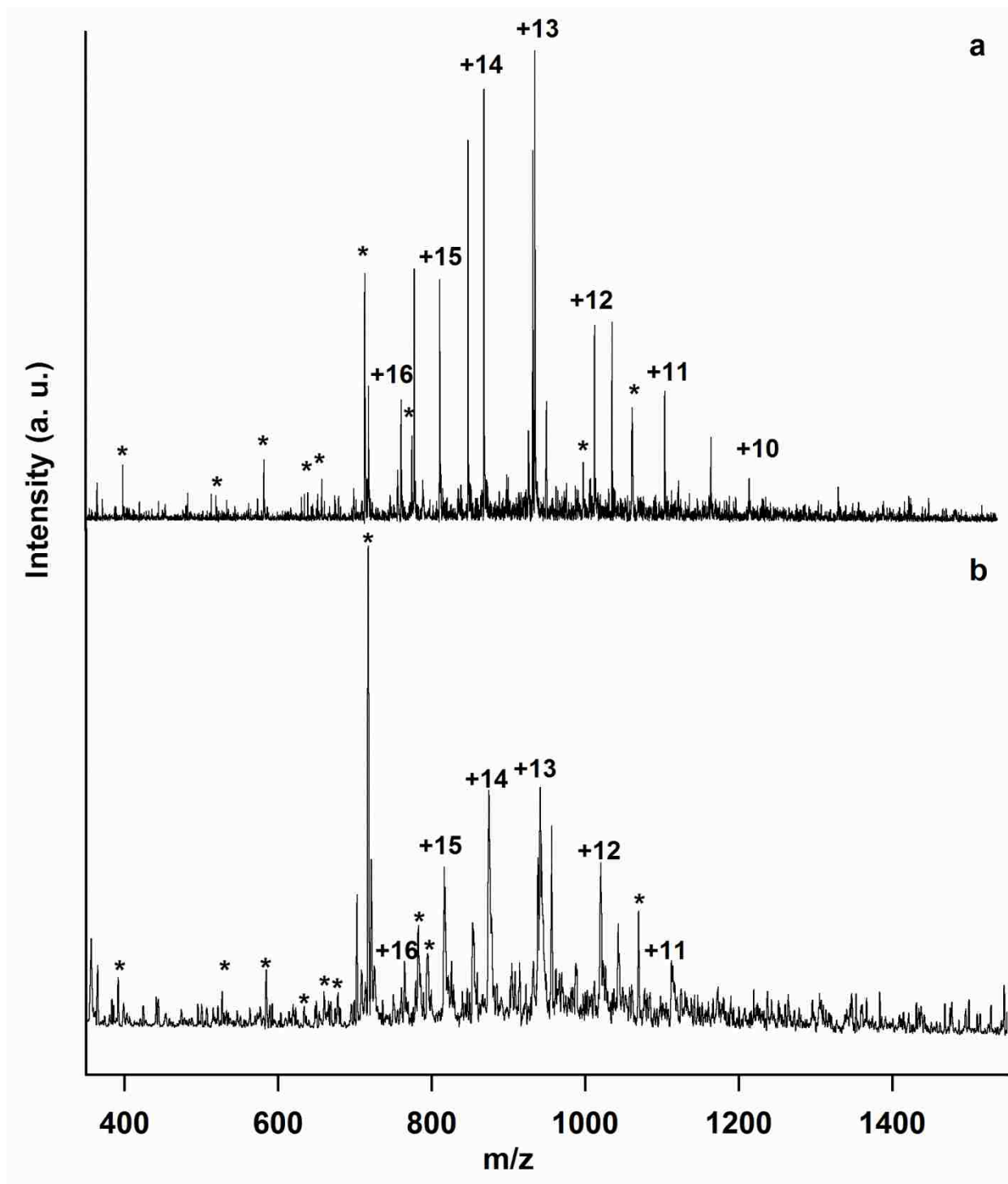


Figure 4-7 Comparison of CF IR MALDESI mass spectra of a digested 500 μM cytochrome c solution at flow rates: of (a) 4 mL min^{-1} and (b) 2 mL min^{-1} .

4.4. Summary

In this study, continuous flow was adapted to IR MALDESI for an on-line monitoring of reactions. Three chemical and biochemical reactions were monitored: the chelation of 1, 10-phenanthroline with iron (II), the insulin denaturation with 1, 4-dithiothreitol, and the tryptic digestion of cytochrome c. The detection limit of CF IR MALDESI was found to be in the micromolar range for peptides and sub-millimolar range for proteins. Considering the size of the liquid bead formed at the tip of capillary to observe a CF IR MALDESI signal was generally $3 \times 10^{-11} \text{ m}^3$, 7 picomole of cytochrome c was calculated in this liquid bead for 300 μM concentration. A better limit of detection is expected by increasing the laser intensity, replacing water matrix with a better IR matrix such as glycerol, and coupling CF IR MALDESI to mass analyzers with better sensitivities. A band broadening effect was observed for the chelation reaction, which can be attributed to either turbulent mixing or a sample memory effect.

CHAPTER 5. FINITE ELEMENT SIMULATION OF INFRARED LASER ABLATION OF GLYCEROL

The previous two chapters presented experimental results of infrared laser ablation mass spectrometry for analysis of chemicals and biomolecules. In order to better explore potential applications of IR laser ablation mass spectrometry, as well as to develop new IR laser ablation ionization techniques, fundamentals processes of IR laser ablation such as laser interaction with materials, ion and particle formation, and the plume ejection need to be better understood. This requires theoretical studies such as computational simulations. In this chapter, a two-dimensional finite element model was developed to simulate glycerol ablation using a wavelength tunable infrared laser under conditions used for mass spectrometry. The laser fluence used for the simulations was varied from 1 – 6 kJ/m², and the wavelength was varied from 2.7 – 3.7 μm. The temperature required for the phase explosion of glycerol is 689 K, which is 90% of the critical temperature. This condition was found for laser wavelengths near 3 μm, which corresponds to the OH stretch absorption of glycerol.

5.1. Introduction

Laser ablation (LA) refers to laser-induced material ejection and has been widespread and exploited as a sampling method in many fields of chemistry, biology, and medicine.¹ During the laser ablation process, the laser beam interacts with a surface to induce heating, melting, boiling, particle ejection, and vaporization of the target material.^{174, 175} The expanding ablation plume consists of atoms, neutral molecules, ions, clusters as well as particles that are formed either directly by laser-sample interaction or later through condensation in the expanding plume²⁹ and aggregation of smaller particles.²⁸ The quantity and size distribution of material that is ablated has a strong dependence on the laser irradiation conditions, such as laser fluence, pulse width,

laser wavelength, and background pressure.^{29, 38, 175} The mechanism of laser induced material ejection includes desorption of individual atoms and molecules, explosive decomposition of the superheated material surface, formation of large droplets due to a melting and hydrodynamic sputtering, photomechanical spallation of the surface layer caused by thermoelastic stresses, and recoil-induced expulsion induced by the formation of recoil stresses due to the rapidly expanding vapor plume and the ejected droplets during explosive decomposition.^{38, 89, 108, 109, 176}

In recent years laser ablation has been increasingly used in analytical chemistry. Compared with conventional dissolution techniques, laser ablation has many advantages.¹⁷⁴ For example nearly any sample can be ablated with minimal sample preparation and often under ambient conditions. The ablated material can be heated to the point at which it emits light that is detected such as in laser induced breakdown spectrometry (LIBS).^{98, 177} Mass spectrometry can be used to detect ions produced by laser ablation for example by laser microprobe mass spectrometry (LMMS),^{100, 178} and matrix assisted laser desorption ionization (MALDI) mass spectrometry.¹⁷⁹ Uncharged ablated material can be atomized and ionized in a plasma such as in laser ablation inductively coupled plasma mass spectrometry (LA ICP MS).^{93, 95} Several laser ablation ambient ionization mass spectrometry techniques have been developed, including matrix assisted laser desorption electrospray ionization (MALDESI),¹¹ and electrospray laser desorption ionization (ELDI).¹³

Many types of pulsed lasers have been used for ablation in analytical chemistry applications. A large number of studies use ultraviolet (UV) lasers because the high energy per photon results in both direct ionization and photon emission.¹⁷ Infrared lasers have also been used in cases where efficient removal of material is paramount.^{18, 23, 180, 181} Mid-IR laser systems such as the optical parametric oscillators and Er:YAG lasers with wavelengths near the 3 μm OH

stretch absorption are particularly useful for laser ablation. IR laser ablation has been used for MALDI,¹³⁷ but application is limited due to the large quantity of material removed and modest ionization efficiency. However, efficient material removal in IR laser ablation is an advantage for ambient ionization by MALDESI because the ionization is independent of the laser ablation step.^{12, 21} A unique advantage to IR laser ablation is the ability to alter the characteristics of the ablation plume by changing the IR laser wavelength when using a wavelength tunable IR laser source.²⁵⁻²⁷

A number of models and simulation methods have been developed to study laser ablation under conditions suitable for chemical analysis. For example, atomistic simulation¹¹⁰ and molecular dynamics simulation^{38, 67, 113-115} have been used to study laser-sample interaction, material in early stage,^{38, 117, 118} and ion formation.^{17, 30, 114} Hydrodynamic models^{123, 124} and Monte Carlo simulations^{125, 126} have been used to describe the expansion of the plume. The finite element method (FEM) is a procedure for obtaining numerical solutions to partial differential equations by dividing the system into small finite elements to which simplifying approximation can be made. A few FEM models have been developed in the past to simulate laser ablation for different applications, such as pulse laser ablation of titanium carbide (TiC)^{127, 128} and laser ablation removal of prostate tumors.¹³⁰ Recently a FEM model was developed to study the temperature rise of polystyrene during the process of resonant-infrared pulsed laser irradiation.¹⁰⁹ The result showed that after laser ablation the polystyrene surface was superheated and thermodynamically unstable, which leded phase explosion to occur. The simulation results showed a good agreement with the experimental results in which a strong phase explosion of polystyrene was observed after being ablated by an IR free-electron laser.

In this chapter, a 2D FEM model was developed to study the heat transfer involved in the IR laser ablation of glycerol under conditions used for mass spectrometry sampling applications. Heating of glycerol with both flat-top and Gaussian shape laser profiles was modeled at different laser fluences and wavelengths. The simulation results were compared with previous experimental data.

5.2. Ablation Model

The commercial FEM software Multiphysics (Comsol. Burlington, MA) was used to develop a two-dimensional model for the interaction of pulsed infrared laser light with glycerol. The thermal conductivity, density and heat capacity of glycerol used in the model are functions of temperature and were modeled by the FEM software. The initial temperature of glycerol was 298 K and the value of reflectivity (R) used was 0.1.¹⁸² It has been found that absorption coefficient (α) is temperature dependent and it usually drops as temperature increases.¹⁸³ In this work, α was assumed to be temperature independent in order to simplify the calculation. The value of the absorption coefficient for laser wavelengths from 2.7 – 3.7 μm were taken from the literature²⁵ and interpolated using infrared absorption profile.¹⁸⁴ The boiling point and critical temperature of glycerol are 563 K and 765 K, respectively.²⁶

To facilitate comparison with previous work on the laser ablation of glycerol, the laser parameters used in the model were the same as those of an OPO laser used in earlier experiments.^{25, 26} The OPO has a pulse temporal width of 5 ns and a 250 μm focused beam diameter with a near Gaussian profile. The laser wavelength range used in the model was from 2.7 μm to 3.7 μm , which covers the glycerol OH stretch vibration at 3.0 μm and the CH stretch vibration at 3.4 μm .^{25, 184} Laser ablation of glycerol was modeled using a Gaussian and flat-top

beam profile and the laser output energy was the same for both laser profiles. The laser fluence for the flat-top profile ranged from 1000 – 6000 J/m². No plasma shielding was considered in the simulation because the time required for plume and plasma formation at the fluences used is generally longer than 10 ns.^{26, 29}

The FEM model solved the two-dimensional heat conduction equations to determine temperature of the glycerol during and after laser pulse. The glycerol target geometry was represented by a rectangle 400 μm wide and 25 μm deep that was sufficient to extend beyond the 250 μm diameter laser spot and was deeper than the penetration of the IR laser. The center of the laser beam was aligned to the center of the rectangle. The upper half of glycerol was simulated by a 100 nm mesh and the lower half by a 250 nm mesh. A 50 nm mesh was used for the top 500 nm depth to allow a more precise estimation of laser-sample interaction. The boundary above the surface was modeled as air at 298 K and the boundary below the surface was glycerol at 298 K.

In two dimensions and neglecting convective and radiative energy transport the heat conduction equation can be written as:¹²⁷

$$\rho(T)C_p(T)\frac{\partial T(x,y,t)}{\partial t} - \nabla[k(T)\nabla T(x,y,t)] = Q(y,t) \quad (\text{Eq. 5-1})$$

where x and y are the horizontal and vertical spatial coordinates, ρ is the density, C_p is the specific heat capacity, T is the temperature, and k is the thermal conductivity of the sample. The quantity Q(y, t) is the heat source which in this model is the laser energy absorbed by the sample. For the surface layer, Q(y, t) can be expressed as:¹⁸²

$$Q(y,t) = 2.3 I_s(1 - R)\alpha e^{-\alpha y} \quad (\text{Eq. 5-2})$$

where R is the surface reflection, α is the absorption coefficient, and I_s is the laser irradiance at the sample surface. I_s is governed by Beer's law, and can be written as:

$$I_s(y) = I_0 e^{-\alpha|y|} \quad (\text{Eq. 5-3})$$

where I_0 is the maximal laser intensity and $|y|$ is the laser penetration depth.¹⁸⁵

5.3. Results and Discussion

The results of glycerol temperature calculations at different times after irradiation by a 5 ns pulsed laser at 2.94 μm wavelength are shown in Figure 5-1. The laser had a flat-top beam profile and the fluence is 6000 J/m^2 . During laser pulse at 2 ns (Figure 5-1a), the temperature of glycerol at the surface has risen from 298 K to 750 K. It reaches a maximum of 1450 K at the end of the laser pulse at 5 ns (Figure 5-1b). Although these temperatures are above the boiling point, the model does not account for this phase change. The surface temperature drops to 1220 K at 5 μs (Figure 5-1c) and 930 K at 50 μs (Figure 5-1d). At 1 ms (Figure 5-1e), heat transfer into the bulk results in a temperature within the laser irradiated area of approximately 500 K throughout, below glycerol boiling point.

Glycerol temperature distributions for a flat-top laser profile, wavelength of 2.94 μm , and a fluence of 6000 J/m^2 are plotted in Figure 5-2. The glycerol surface temperature ($y = 0$) as a function of the distance along the surface at different times is plotted in Figure 5-2a. The maximum temperature of 1450 K is obtained for the laser-irradiated area (x from -125 to 125 μm). Little thermal conduction occurs during the 5 ns laser irradiation. As time evolves, the surface temperature drops, through transfer into the bulk on a microsecond time scale and gradually dispersing laterally on the millisecond time scale. There is also some amount of heat lost at the surface to air boundary.

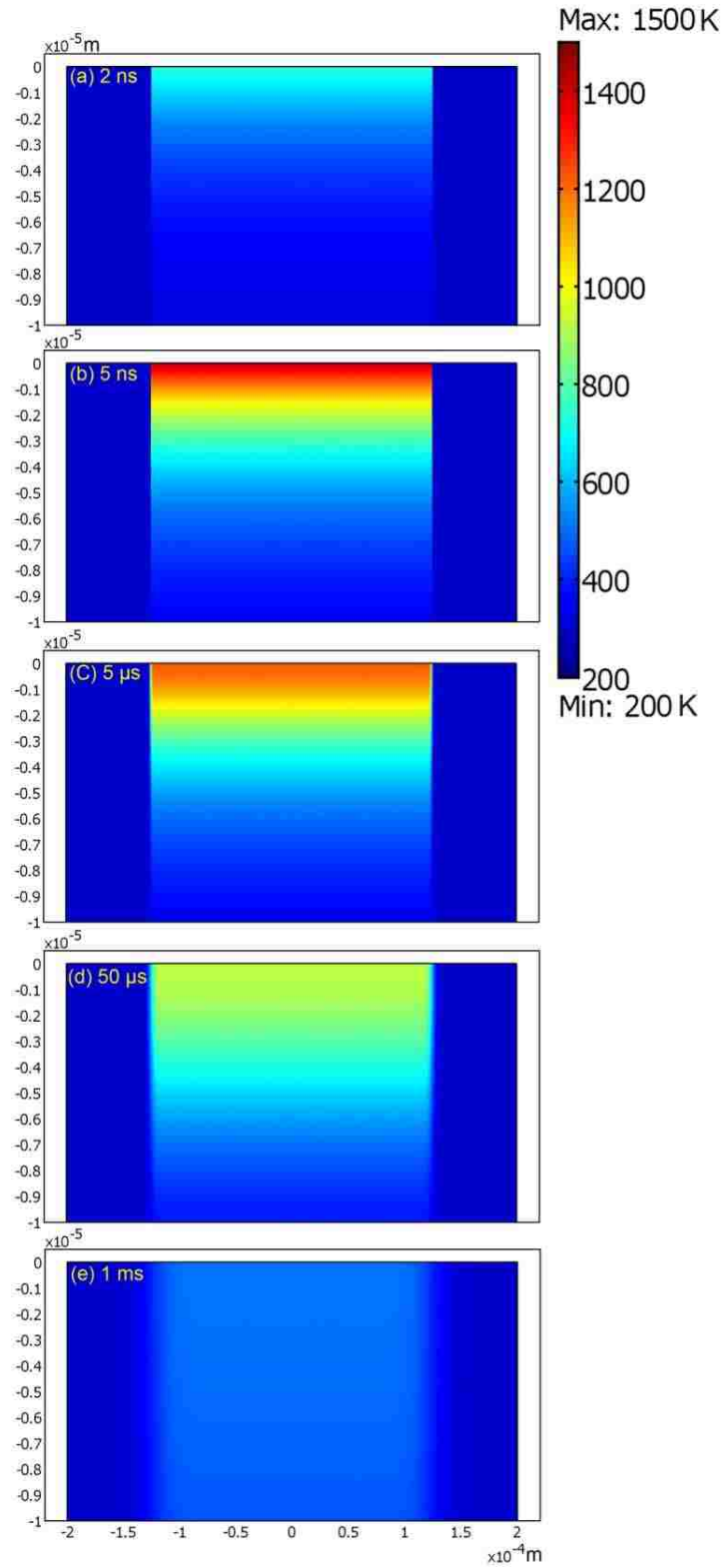


Figure 5-1 Glycerol temperature with a $2.94 \mu\text{m}$ flat-top profile laser at 6000 J/m^2 fluence for times of (a) 2 ns, (b) 5 ns, (c) 5 μs , (d) 50 μs , and (e) 1 ms.

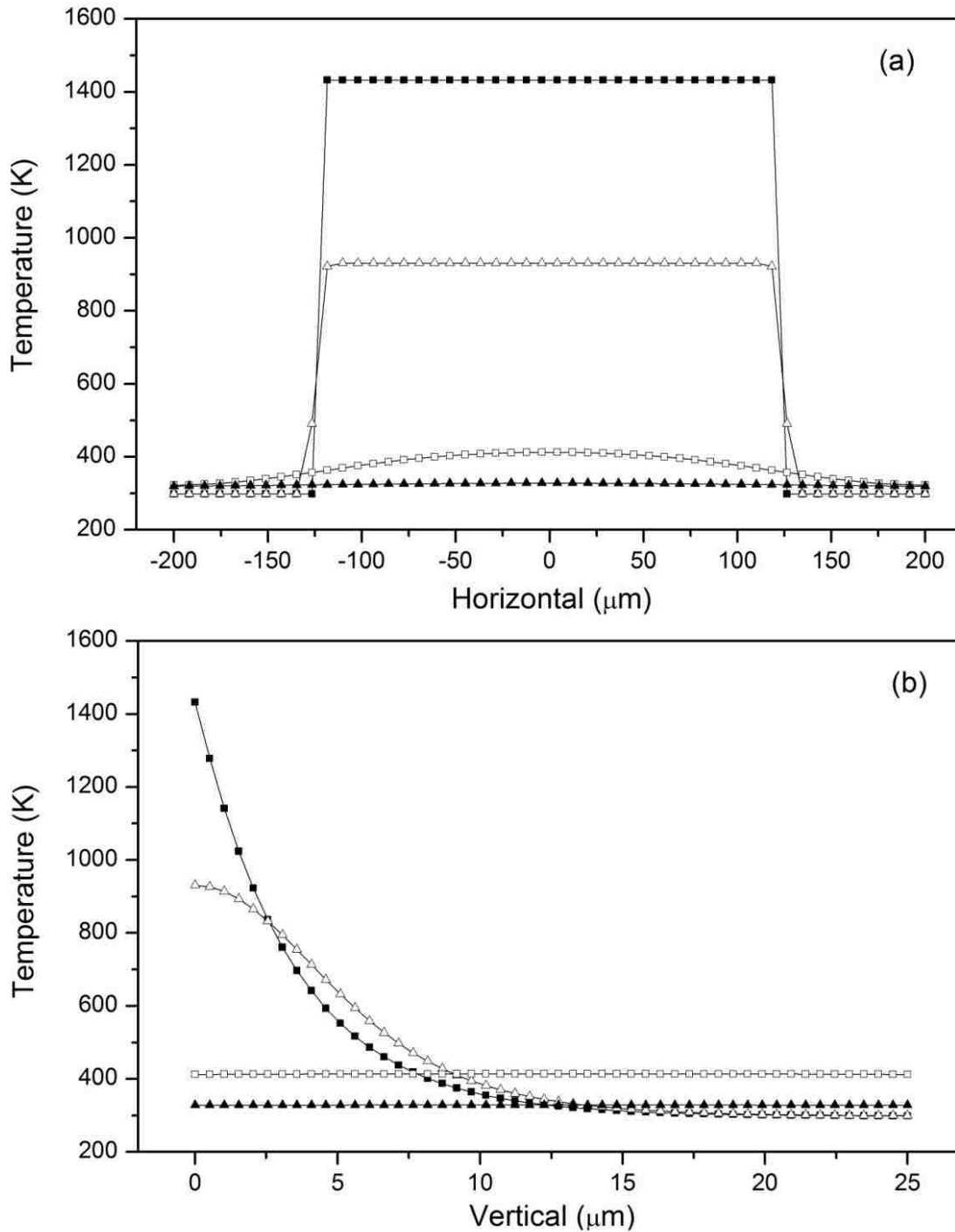


Figure 5-2 Glycerol temperature a) at the surface ($y = 0$) and b) as a function of depth ($x = 0$) for different times (\blacksquare) 5 ns, (\triangle) 50 μs , (\square) 20 ms, and (\blacktriangle) 0.1 s) with a 2.94 μm flat-top laser and 6000 J/m^2 fluence.

Figure 5-2b shows the glycerol temperature as a function of depth at the center of the point of irradiation. This plot shows a rapid drop in temperature within a few micrometers of the surface on the microsecond time scale. From 3 - 15 μm , the temperature at 50 μs is higher than 2 ns due to the thermal conduction. Below 15 μm , the temperature remains close to the initial 298 K at 50 μs , indicating that no heat has diffused to that layer yet in 50 μs . On a millisecond time scale, the lower layers achieve temperatures above 400 K before returning to the original temperature.

FEM simulations were run using parameters corresponding to wavelengths between 2.7 and 3.7 μm . Two plots from simulation of glycerol laser heating at 2.94 μm , corresponding to the glycerol OH stretch absorption, and at 3.4 μm , corresponding to the CH stretch, are shown in Figure 5-3 at 5 ns simulation time. The simulations were made with a flat-top laser profile, 3000 J/m^2 fluence, and 5 ns pulse width. The maximum surface temperature for 2.94 and 3.40 μm was found to be 870 K and 460 K, respectively. The FEM result is in good agreement with a previous estimate of temperatures of 860 K and 434 K for these wavelengths.²⁶ Note that the depth of the heated glycerol is much greater in Figure 5-3b due to the larger laser penetration depth.

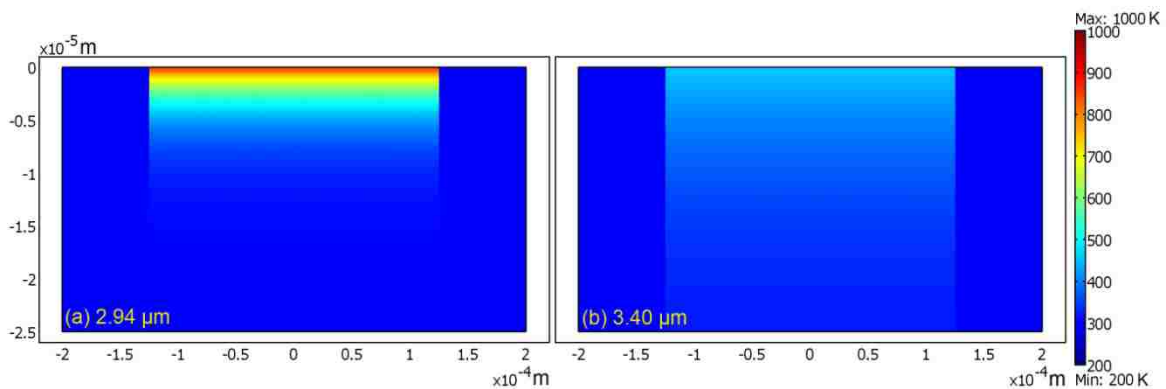


Figure 5-3 Glycerol temperature after 5 ns for a) 2.94 μm and b) 3.4 μm wavelengths at 3000 J/m^2 fluence.

Figure 5-4 shows the glycerol temperature as a function of depth for 2.94 μm (Figure 5-4a) and 3.40 μm wavelength (Figure 5-4b) at different fluences at 5 ns after the beginning of the laser pulse. At all fluences, the surface temperature ($y = 0$) for the 2.94 μm wavelength is greater than that for the 3.40 μm laser due to greater absorption at the OH stretch resonance. Conversely, the heating of the bulk is much greater at the 3.4 μm wavelength that corresponds to the CH stretch absorption.

A plot of the maximum surface temperature at different laser fluences is shown in Figure 5-5. The values correspond to the temperature at the surface 5 ns after the after beginning of the laser pulse. The boiling point of glycerol of 563 K and the point of 90% of the critical temperature at 689 K are indicated with dotted lines in the plot. At temperatures exceeding the boiling point of glycerol, desorption of glycerol will occur. If the temperature exceeds 90% of the critical temperature of glycerol, a volumetric phase change (phase explosion) will occur.¹⁰⁴ Phase explosion will result in the violent ejection of material both as free molecules as well as molecular clusters and particles.³⁸ Figure 5-5 shows that glycerol boiling will occur at 1000 J/m^2 and phase explosion at 2000 J/m^2 if the laser is at the OH stretch absorption at 3.0 μm . If the laser is tuned to the CH stretch at 3.4 μm , glycerol boiling will occur at a fluence of 5000 J/m^2 and phase explosion would require in excess of 6000 J/m^2 . This is consistent with previous particle sizing result, in which the lowest threshold of glycerol particle formation at 3 μm wavelength was found to be 1200 J/m^2 .²⁵ This is also consistent with fast photography studies that indicate a vigorous removal of material at 3 μm whereas tuning the laser off of the OH resonance resulted in a much weaker ablation of material.²⁶

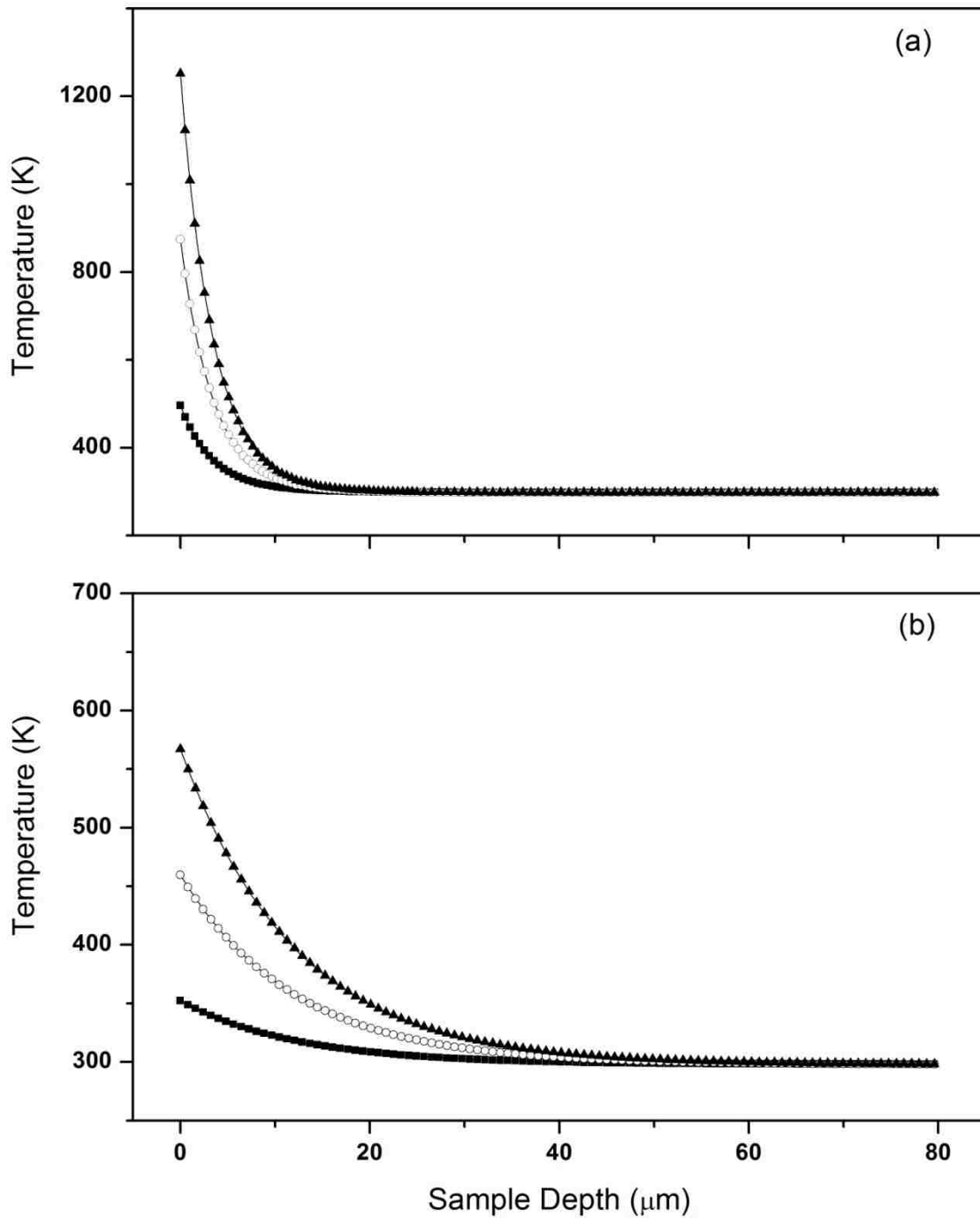


Figure 5-4 Glycerol temperature versus sample depth after 5 ns for a) 2.94 and b) 3.40 μm laser with different fluences: (■) 1000 J/m^2 , (○) 3000 J/m^2 , and (▲) 5000 J/m^2 .

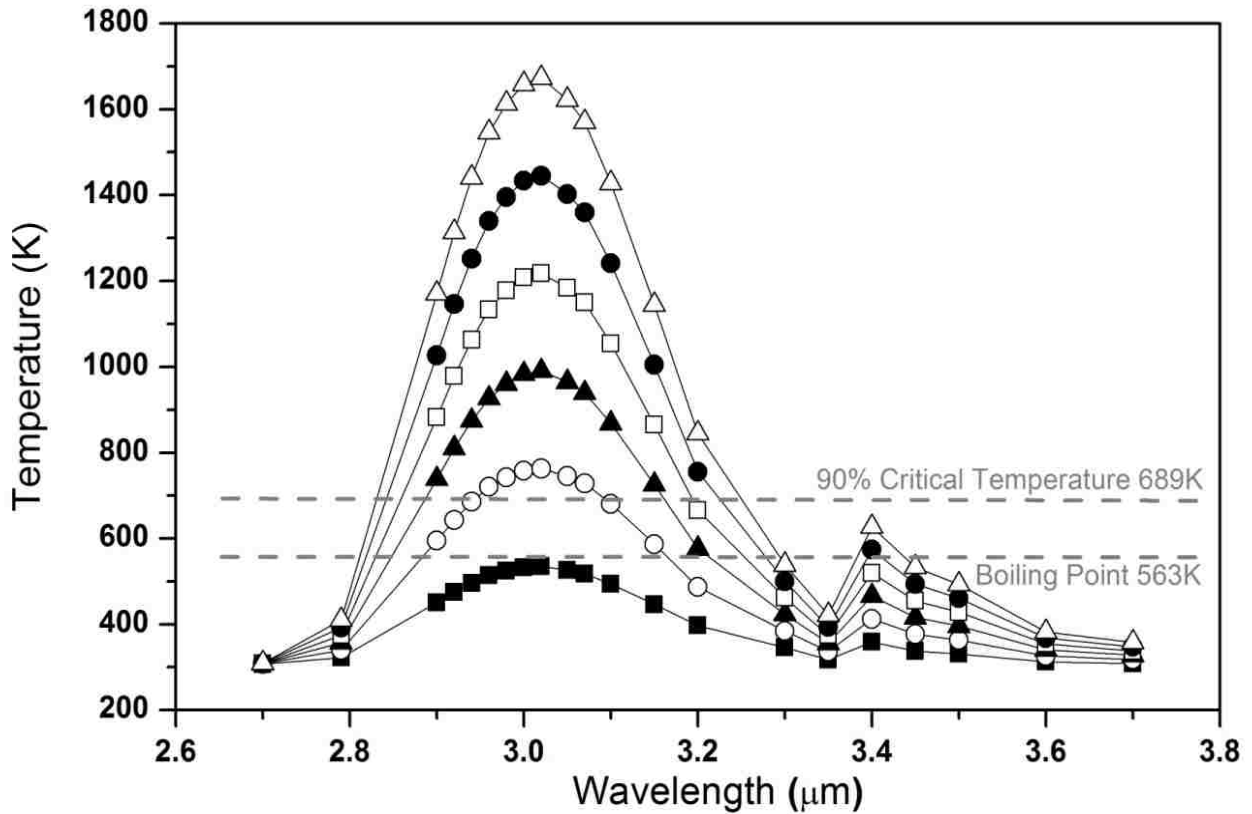


Figure 5-5 Laser wavelength dependence of glycerol surface temperature for fluences: (■) 1000 J/m^2 , (○) 2000 J/m^2 , (▲) 3000 J/m^2 , (□) 4000 J/m^2 , (●) 5000 J/m^2 , and (△) 6000 J/m^2 .

The temperature profile of glycerol obtained from a Gaussian profile laser beam at 2.94 μm is shown in Figure 5-6. The laser pulse energy was 295 μJ and corresponds to the energy of a flat-top profile with a fluence of 6000 J/m^2 . Figure 5-6a can be compared to Figure 5-1b and Figure 5-6b can be compared to Figure 5-2a. For the Gaussian laser profile, the laser energy is concentrated at the center of the beam and the resulting peak temperature of the glycerol is 50% greater than for the flat-top profile.

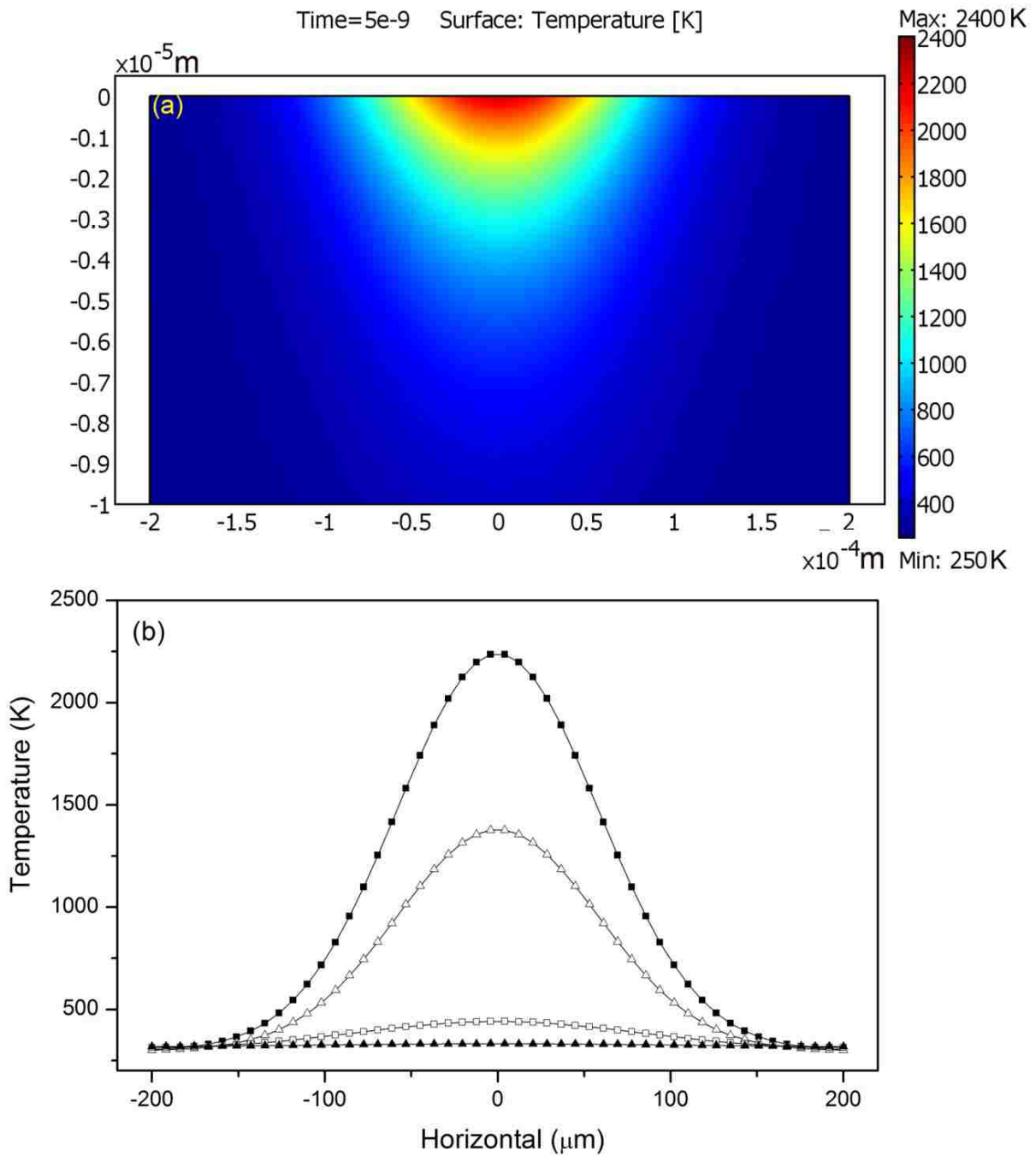


Figure 5-6 Glycerol temperature for a 2.94 μm wavelength Gaussian profile laser: a) temperature profile at 5 ns; b) temperature distribution along at the surface: (■) 5 ns, (Δ) 50 μs , (\square) 20 ms, and (\blacktriangle) 0.1 s.

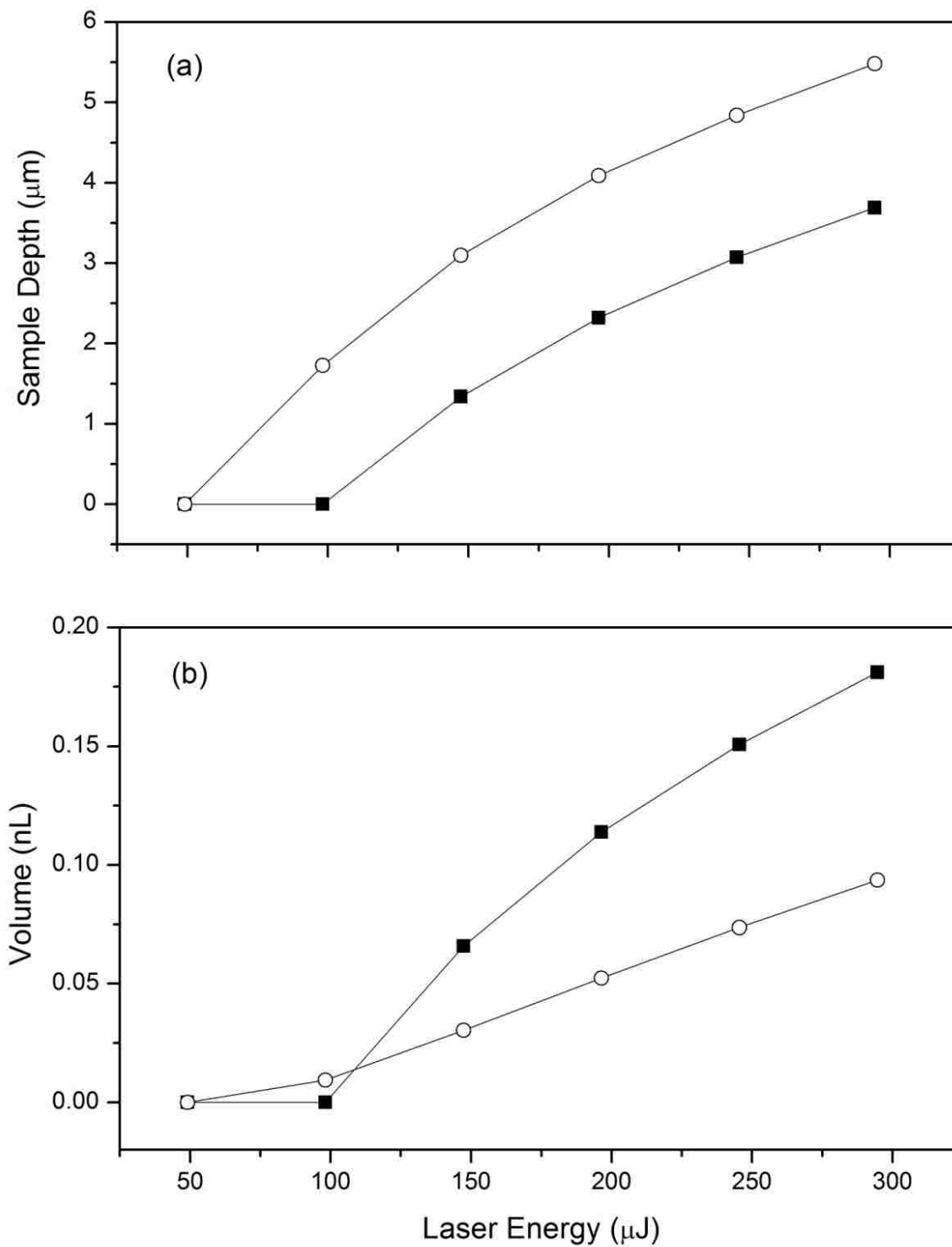


Figure 5-7 Laser energy dependence of the a) depth and b) volume of glycerol subject to phase explosion at 2.94 μm wavelength for flat-top (■) and Gaussian (○) laser profile.

The sample depth and volume subject to volume phase change and resulting phase-explosion can be estimated from the FEM calculations. To make this estimation, the region at which the temperature was greater than 90% of the critical temperature (689 K) was determined for a laser wavelength of 2.94 μm at 5 ns after the beginning of the laser pulse. Results for the sample depth and volume fulfilling this requirement for flat-top and Gaussian laser profile are shown in Figure 5-7.

Figure 5-7a shows sample depth at which phase explosion is anticipated to occur as a function of the laser pulse energy. Note that for the Gaussian profile the center of the laser beam is indicated. If the depth subject to phase explosion can be associated with the ablation depth, the Gaussian beam ablates to about 1 μm greater depth but the flat top beam removes more material once the conditions required for phase-explosion are satisfied. In terms of the model, the Gaussian laser energy is effectively “wasted” heating a small fraction of the glycerol well beyond that required for phase transition. In practice, the glycerol would not be heated in this way, but nonetheless the ejected plume of material might shield the underlying sample. The ablation depth is 5.5 μm for Gaussian and 3.7 μm for flat-top profile at an energy of 295 μJ . The volume ablated for the flat-top profile at this energy is 180 pL and for the Gaussian profile it is 90 pL. As a consequence of the localization of the peak laser energy, conditions for phase explosion can be reached at 3.4 μm at 295 μJ laser energy, although for a smaller volume. A volume of 15 pL reaches 90% of the critical temperature for the Gaussian profile at the energy of 295 μJ . This is consistent with previous fast photography and particle sizing studies, in which a much weaker ablation of glycerol ejection is observed at 3.4 μm compared to 2.94 μm .^{25, 26}

Typically, measurement of the material absorption coefficient α is done at room temperature. However, the thermal and mechanical transients generated by laser ablation

processes are substantial and can result in a significant change of α .⁸⁹ It has been found that α is temperature dependent (dynamic α) and it drops as temperature increases.^{128, 183} The decrease of α leads to a lower temperature as compared to α considered as temperature independent (static α). A 30% lower temperature in the high laser fluence region and 15% lower temperature in the low fluence region for dynamic α study was reported recently in the simulation of TiC ablation.¹²⁸ As mentioned previously, the study shown in this chapter was performed using static α in order to simplify the calculation. Lower glycerol temperatures and higher laser fluences for phase explosion would be expected if using a dynamic α . Assuming there was also a 30% temperature drop for glycerol using dynamic α , the resulting temperature at each wavelength in Figure 5-5 would be lower, and the lowest laser fluence for temperature exceeding 689 K would be 3000 J/m² in OH stretch region at 3.0 μm . On the other hand, the dynamic change of α could be an advantage for a sample with deeply embedded target molecules such as gel and tissue, since higher temperature results in lower α , and thus the laser beam penetrates more deeply into the sample.

5.4. Summary

A 2D finite element model was developed to simulate glycerol heating by a wavelength tunable IR laser under conditions of mass spectrometry applications. The simulation results are in good agreement with previous particle sizing and plume imaging results: the glycerol temperature has a strong dependence on laser wavelength and laser fluence. The highest temperature was obtained at OH stretch absorption of glycerol near 3.0 μm and within the investigated laser fluence range, the calculated temperature is sufficient for phase explosion near

3.0 μm for the flat-top profile and over a broader wavelength range with lower material ejection for the Gaussian profile.

CHAPTER 6. CONCLUSIONS AND FUTURE DIRECTIONS

In this dissertation, fundamental study and developments of ionization methods based on infrared laser desorption and ablation for mass spectrometry analysis of chemical and biological samples were described. Peptide and protein samples were ablated by an IR laser that were subsequently analyzed using a home-built IR/UV two-laser matrix-assisted laser desorption ionization mass spectrometer. A continuous flow IR matrix-assisted laser desorption electrospray ionization interface was designed and coupled with an ion trap mass spectrometer to on-line and off-line study several chemical and biochemical reactions. A simulation model was developed using finite element method to study the processes such as laser-material interaction involved in the IR laser ablation under conditions of AP MALDI or MALDESI, and the simulation results were compared to the previous results of fast plume photography²⁶ and particle sizing²⁵ experiments. The overall results show that the combination of IR lasers are efficient at sample removal, and combining this efficiency with post-ionization techniques can serve as an effective analytical technique for MS study of chemical and biological samples. Fundamental understanding of IR laser ablation can facilitate better optimization of experimental parameters in current applications as well as developments of new IR laser based ionization techniques.

The IR laser ablated particles containing biomolecules that were post-ablated and ionized by a UV laser were presented in Chapter 3. It has been noted that IR lasers are efficient for material removal, and the ejected material in IR laser ablation contains high concentration of particles.^{25, 26} These particles don't form ions under conditions of IR MALDI, and can be problematic since they are not compatible with commercial MALDI instruments operating at vacuum and with high extraction fields.^{19, 20} Adding a second source such as a UV laser to post-ablate and ionize these particles can improve the ionization efficiency. Using a peptide

bradykinin as a standard, it was found that the UV ion yield was strongly dependent on the fluence of IR and UV laser, as well as the delay time between the laser pulses. Protein samples such as cytochrome c and insulin were also tested. It has been stated that large molecules such as protein are difficult to ionize through the absorption of multiple photons due to the efficient energy dissipation in the large number of vibrational degrees of freedom.¹⁴⁵ The observation of protein signal suggests that the ionization undergoes UV MALDI mechanism.

One problem in the IR/UV two-laser MALDI work is that IR laser ablation generated sample plume expands for hundreds of μs , whereas most UV lasers only have a few ns pulse width. Even with the UV laser post-ionization, a large fraction of the sample in the plume is not used and don't make ions due to the temporal mismatch. This problem has been addressed with the development of IR matrix-assisted laser desorption electrospray ionization, which uses a continuous source, electrospray, for ionization.¹² Chapter 4 describes a continuous flow IR MALDESI interface that was developed and coupled to an ion trap mass spectrometer. Samples in aqueous solution were flowed through a silica capillary and a liquid sample bead was formed at the capillary tip. A 2.94 μm IR laser was used for sample ablation, and the ejected sample plume was entrained in an electrospray to form ions. The chelation reaction of 1,10-phenanthroline with iron (II), the denaturation reaction of insulin with 1,4-dithiothreitol (DTT), and tryptic digestion of cytochrome c were on-line and off-line monitored. A band broadening effect was observed for the chelation reaction, which can be attributed to either turbulent mixing or a sample memory effect. This band broadening effect can be reduced by reducing the sample concentration. A detection limit of 7.32 picomole for cytochrome c was calculated. We expect that better detection limit can be obtained by increasing laser intensity, replacing water matrix

with better IR matrices such as glycerol, and coupling CF IR MALDESI to mass analyzers with better sensitivities.

Another important part of this research is the fundamental study of IR laser ablation. There have been numerous applications of laser ablation mass spectrometry since the first use of laser for sample removal, however the mechanisms behind these applications are still under investigation.^{17, 30} Fundamental studies aimed at understanding the physical processes involved in material desorption, ablation, and ion formation can help optimize and extend the applications of IR laser ablation. In Chapter 5, a two-dimensional finite element model was developed to simulate IR laser ablation of glycerol under conditions used for atmospheric pressure MALDI and MALDESI. The laser fluence used in the simulation was varied from 1 to 6 kJ/m², and the wavelength was varied from 2.7 – 3.7 μm that covered the OH and CH stretch absorption region of glycerol. Both flat-top and Gaussian profile laser were studied. The results showed that the glycerol temperature has a strong dependence on laser wavelength and laser fluence. The peak temperature of glycerol was obtained as the laser wavelength tuned to OH stretch absorption at 3 μm. This temperature was sufficient for phase explosion to occur. As the laser wavelength tuned off the OH stretch region, the glycerol temperature quickly dropped and became too low for phase explosion to occur. For the same laser energy, a Gaussian shape laser can generate higher glycerol temperature due to localization of the peak laser energy, whereas a flat-top shape laser can remove more material. The overall FEM simulation data showed a good agreement with previous particle sizing and plume imaging results.^{25, 26}

One problem for this simulation is that the model is not realistic because it simulates the IR laser-glycerol interaction without taking phase transition of glycerol into account. It has been found that as a liquid is superheated to 90% of the critical temperature, phase explosion occurs

and the liquid surface undergoes a rapid and violent transition from superheated liquid to a mixture of vapor and liquid droplets.^{104, 108} In addition, the rapidly expanding vapor plume and the ejected droplets during phase explosion can produce recoil stresses that can induce a secondary material expulsion.^{89, 108} Phase explosion and recoil-induced material ejection have been experimentally observed in many laser ablation studies, such as glycerol,²⁶ water,³⁴ and polystyrene.¹⁰⁹ Another problem for this simulation is that the glycerol absorption coefficient at each laser wavelength used in the model was considered to be temperature independent in order to simplify the calculation, whereas it should be temperature dependent as reported in literature.^{89, 128, 183} One of the future directions thus is the simulation of phase change, material ejection and plume expansion using glycerol dynamic absorption coefficient. By adding simulations of laser-material interaction, material ejection and plume expansion together, an overall picture of IR laser ablation is expected to obtain, and will be used together with the experimental results to explore IR laser ablation mechanism.

The second one of the future directions will focus on designing an interface for coupling microfluidic chips to IR MALDESI for high throughput chemical and biochemical analysis. CF IR MALDESI requires no need for previous purifications, nor isolation for further characterization of reaction species and products, therefore allows the direct study of transient species, intermediates in solution. In addition, water can be used as an IR MALDESI matrix and it is the native environment of most biological samples. The potential application of CF IR MALDESI, therefore, will be the direct analysis of biological fluids under ambient conditions. With the development of a microfluidic chip interface,¹⁸⁶ such as on chip separation, cell culturing, cell lysis, and proteolytic digestion, it is possible to on-line monitor biological reactions on chip using CF IR MALDESI system.

Another one of the future directions will be the development of near-field IR laser ablation for tissue imaging. IR lasers are known to have deep penetration depth that enables them to remove deeply embedded analytes from materials such as thin layer chromatography plates, polyacrylamide gels, and tissue.²²⁻²⁴ Currently MALDI mass spectrometers are capable of imaging tissue at spatial resolution down to 25 μm , which is limited by laser optics, sample preparation, and ion collection efficiency.¹⁸⁷ Applying IR laser ablation in the near field allows imaging resolution down to sub-micron or even nanometer scale, which can potentially bring the biological imaging mass spectrometry to the single cell level. Ongoing studies are focused on the near-field IR laser ablation of biomolecules with droplet capture¹⁸⁸ for off-line nanoelectrospray mass spectrometry. The information obtained from these studies will be used to construct near-field IR laser ablation of cells and tissue imaging.

REFERENCES

1. Georgiou, S.; Hillenkamp, F., Introduction: laser ablation of molecular substrates. *Chem. Rev.* **2003**, 103.
2. Georgiou, S.; Koubenakis, A., Laser-induced material ejection from model molecular solids and liquids: mechanisms, implications, and applications. *Chem. Rev.* **2003**, 103, 349-393.
3. Dass, C., Principles and practice of biological mass spectrometry. *John Wiley & Sons, Inc., New York*, **2001**, Chapter 1&2.
4. Karas, M.; Hillenkamp, F., Laser desorption ionization of proteins with molecular masses exceeding 10000 daltons. *Anal. Chem.* **1988**, 60, 2229-2301.
5. Tanaka, K.; Waki, H.; Ido, Y.; Akita, S.; Yoshida, Y.; Yoshida, T., Protein and polymer analyses up to m/z 100000 by laser ionization time-of-flight mass spectrometry. *Rapid. Commun. Mass Spectrom.* **1988**, 2, 151-153.
6. Weston, D. J., Ambient ionization mass spectrometry: current understanding of mechanistic theory; analytical performance and application areas. *Analyst* **2010**, 135, 661-668.
7. Chen, H.; Gamez, G.; Zenobi, R., What can we learn from ambient ionization techniques? *J. Am. Soc. Mass Spectrom.* **2009**, 20, 1947-1963.
8. Harris, G. A.; Galhena, A. S.; Fernandez, F. M., Ambient sampling/ionization mass spectrometry: applications and current trends *Anal. Chem.* **2011**, 83, 4508-4538.
9. Alberici, R. M.; Simas, R. C.; Sanvido, G. B.; Romao, W.; Lalli, P. M.; Benassi, M.; Cunha, I. B. S.; Eberlin, M. N., Ambient mass spectrometry: bringing MS into the "real world". *Anal. Bioanal. Chem.* **2010**, 398, 265-294.
10. Cody, R. B.; Laramée, J. A.; D., D. H., Versatile new ion source for the analysis of materials in open air under ambient conditions. *Anal. Chem.* **2005**, 77, 2297-2303.
11. Sampson, J. S.; Hawkrige, A. M.; Muddiman, D. C., Generation and detection of multiply-charged peptides and proteins by matrix-assisted laser desorption electrospray ionization (MALDESI) fourier transform ion cyclotron resonance mass spectrometry. *J. Am. Soc. Mass Spectrom.* **2006**, 17, 1712-1716.
12. Rezenom, Y. H.; Dong, J.; Murray, K. K., Infrared laser-assisted desorption electrospray ionization mass spectrometry. *Analyst* **2008**, 133, 226-232.
13. Shiea, J.; Huang, M. Z.; HSu, H. J.; Lee, C. Y.; Yuan, C. H.; Beech, I.; Sunner, J., Electrospray-assisted laser desorption/ionization mass spectrometry for direct ambient analysis of solids. *J. Rapid Commun. Mass Spectrom.* **2005**, 19, 3701-3704.

14. Nemes, P.; Vertes, A., Laser ablation electrospray ionization for atmospheric pressure, in vivo, and imaging mass spectrometry. *Anal. Chem.* **2007**, *79*, 8098-8106.
15. Sampson, J. S.; Murray, K. K.; Muddiman, D. C., Intact and top-down characterization of biomolecules and direct analysis using infrared matrix-assisted laser desorption electrospray ionization coupled to FT-ICR mass spectrometry. *J. Am. Soc. Mass Spectrom.* **2009**, *20*, 667-673.
16. Sampson, J. S.; Hawkrigde, A. M.; Muddiman, D. C., Direct characterization of intact polypeptides by matrix-assisted laser desorption electrospray ionization quadrupole Fourier transform ion cyclotron resonance mass spectrometry. *Rapid Commun. Mass Spectrom.* **2007**, *21*, 1150-1154.
17. Knochenmuss, R.; Zenobi, R., MALDI ionization: the role of in-plume processes. *Chem. Rev.* **2003**, *103*, 441-452.
18. Menzel, C.; Dreisewerd, K.; Berkenkamp, S.; Hillenkamp, F., Mechanisms of energy deposition in infrared matrix-assisted laser desorption/ionization mass spectrometry. *Int. J. Mass Spectrom.* **2001**, *207*, 73-96.
19. Cramer, R.; Burlingame, A. L., Employing target modifications for the investigation of liquid infrared matrix-assisted laser desorption/ionization mass spectrometry. *Rapid. Commun. Mass Spectrom.* **2000**, *14*, 53-60.
20. Rousell, D. J.; Dutta, S. M.; Little, M. W.; Murray, K. K., Matrix-free infrared soft laser desorption/ionization. *J. Mass Spectrom.* **2004**, *39*, 1182-1189.
21. Sampson, J. S.; Murray, K. K.; Muddiman, D. C., Intact and top-down characterization of biomolecules and direct analysis using infrared matrix-assisted laser desorption electrospray ionization coupled to FT-ICR mass spectrometry. *J. Am. Soc. Mass Spectrom.* **2008**, *20*, 667-673.
22. Dreisewerd, K.; Muthing, J.; Rohlfing, A.; Meisen, I.; Vukelic, Z.; Peter-Katalinic, J.; Hillenkamp, F.; Berkenkamp, S., Analysis of gangliosides directly from thin-layer chromatography by infrared matrix-assisted laser desorption/ionization orthogonal time-of-flight mass spectrometry with a glycerol matrix. *Anal. Chem.* **2005**, *77*, 4098-4107.
23. Xu, Y.; Little, M. W.; Murray, K. K., Interfacing capillary gel microfluidic chips with infrared laser desorption mass spectrometry. *J. Am. Soc. Mass Spectrom.* **2006**, *17*, 469-474.
24. Dreisewerd, K.; Lemaire, R.; Pohlentz, G.; Salzet, M.; Wisztorski, M.; Berkenkamp, S.; Fournier, I., Molecular profiling of native and matrix-coated tissue slices from rat brain by infrared and ultraviolet laser desorption/ionization orthogonal time-of-flight mass spectrometry. *Anal. Chem.* **2007**, *79*, 2463-2471.
25. Fan, X.; Little, M.; Murray, K. K., Infrared laser wavelength dependence of particles ablated from glycerol. *Appl. Surf. Sci.* **2008**, *255*, 1699-1704.
26. Fan, X.; Murray, K. K., Wavelength and time-resolved imaging of material ejection in infrared matrix-assisted laser desorption. *J. Phys. Chem. A* **2010**, *114*, 1492-1497.

27. Little, M. W.; Laboy, J.; Murray, K. K., Wavelength dependence of soft infrared laser fesorption and ionization. *J. Phys. Chem. C* **2007**, 111, (3), 1412-1416.
28. Alves, S.; Kalberer, M.; Zenobi, R., Direct detection of particles formed by laser ablation of matrices during matrix-assisted laser desorption/ionization. *Rapid Commun. Mass Spectrom.* **2003**, 17, 2034-2038.
29. Bogaerts, A.; Chen, Z.; Gijbels, R.; Vertes, A., Laser ablation for analytical sampling: what can we learn from modeling? *Spectrochim. Acta Part B* **2003**, 58, 1867-1893.
30. Knochenmuss, R., Ion formation mechanisms in UV-MALDI. *Analyst (Cambridge, U. K.)* **2006**, 131, 966-986.
31. Jackson, S. N.; Kim, J.-K.; Laboy, J. L.; Murray, K. K., Particle formation by infrared laser ablation of glycerol: implications for ion formation. *Rapid. Commun. Mass Spectrom.* **2006**, 20, 1299-1304.
32. Jackson, S. N.; Mishra, S.; Murray, K. K., Characterization of coarse particles formed by laser ablation of MALDI Matrices. *J. Phys. Chem. B* **2003**, 107, 13106-13110.
33. Musapelo, T.; Murray, K. K., Particle formation in ambient MALDI plumes. *Anal. Chem.* **2011**, 83, 6601-6608.
34. Aptiz, I.; Vogel, A., Material ejection in nanosecond Er:YAG laser ablation of water, liver, and skin. *Appl. Phys. A: Mater. Sci. Process* **2005**, 81, 329-338.
35. Leisner, A.; Rohlfing, A.; Rohling, U.; Dreisewerd, K.; Hillenkamp, F., Time-resolved imaging of the plume dynamics in infrared matrix-assisted laser desorption/ionization with a glycerol matrix. *J. Phys. Chem. B* **2005**, 109, 11661-11666.
36. Rohlfing, A.; Leisner, A.; Hillenkamp, F.; Dreisewerd, K., Investigation of the desorption process in UV matrix-assisted laser desorption/ionization with a liquid 3-nitrobenzyl alcohol matrix by photoacoustic analysis, fast-flash imaging, and UV-laser postionization. *J. Phys. Chem. C* **2010**, 114, 5367-5381.
37. Takamizawa, A.; Kajimoto, S.; Hobley, J.; Hatanaka, K.; Ohta, K.; Fukumura, H., Explosive boiling of water after pulsed IR laser heating. *Phys. Chem. Chem. Phys.* **2003**, 5, 888-895.
38. Zhigilei, L. V., Dynamics of the plume formation and parameters of the ejected clusters in short-pulse laser ablation. *Appl. Phys. A* **2003**, 76, 339-350.
39. Grayson, M. A., Measuring mass: from positive rays to proteins. *Atlasbooks* **2005**, p149.
40. Vestal, M. L., Methods of ion generation. *Chem. Rev.* **2001**, 101, 361-375.
41. de Hoffman, E.; Stroobant, V., Mass spectrometry, principles and applications. 2nd ed. *John Wiley & Sons, Inc.* **2002**, West Sussex, UK.

42. Harrison, W. W.; Barshick, C. M.; Kingier, J. A.; Rall, P. H.; Mei, Y., Glow discharge techniques in analytical chemistry. *Anal. Chem.* **1990**, 62, 943A-949A.
43. Hattendorf, B.; Latkoczy, C.; Gunther, D., Laser ablation-ICPMS. *Anal. Chem.* **2003**, 75, 341A-347A.
44. Baldwin, M. A., Mass spectrometers for the analysis of biomolecules. *Methods Enzymol.* **2005**, 402, 3-48.
45. Munson, M. S. B.; Field, F. H., Chemical ionization mass spectrometry. I. General introduction. . *J. Am. Chem. Soc.* **1966**, 88, 2621-30.
46. Vertes, A., Soft laser desorption Ionization - MALDI, DIOS, and Nanostructures. *In Laser Ablation and Its Applications*, **2007**, Phipps, C, R., Ed. Springer: New York, 505-528.
47. Karas, M.; Bachmann, D.; Hillenkamp, F., Influence of the wavelength in high-irradiance ultraviolet laser desorption mass spectrometry of organic molecules. *Anal. Chem.* **1985**, 57, 2935-2939.
48. Hillenkamp, F.; Peter-Jatalinic, J., MALDI MS: A practical guide to instrumentation, methods and applications. . *Wiley-VCH: Weinheim* **2007**.
49. Tang, X.; Dreifuss, P. A.; Vertes, A., New matrixes and accelerating voltage effects in matrix-assisted laser desorption/ionization of synthetic polymers. *Rapid Commun. Mass Spectrom.* **1995**, 9, 1141-1147.
50. Tang, K.; Taranenko, N. I.; Allman, S. L.; Chen, C. H.; Chang, L. Y.; Jacobson, K. B., Picolinic acid as a matrix for laser mass spectrometry of nucleic acids and proteins. *Rapid Commun. Mass Spectrom.* **1994**, 8, 673-677.
51. Hsu, N.-Y.; Yang, W.-B.; Wong, C.-H.; Lee, Y.-C.; Lee, R. T.; Wang, Y.-S.; Chen, C.-H., Matrix-assisted laser desorption/ionization mass spectrometry of polysaccharides with 2',4',6'-trihydroxy-acetophenone as matrix. *Rapid Commun. Mass Spectrom.* **2007**, 21, 2137-2146.
52. Hedrich, H. C.; Isobe, K.; Stahl, B.; Nokihara, K.; Kordel, M.; Schmid, R. D.; Karas, M.; Hillenkamp, F.; Spener, F., Matrix-assisted ultraviolet laser desorption/ionization mass spectrometry applied to multiple forms of lipases. *Anal. Biochem.* **1993**, 211, 288-292.
53. Kirpekar, F.; Berkenkamp, S.; Hillenkamp, F., Detection of double-stranded DNA by IR- and UV- MALDI mass spectrometry. *Anal. Chem.* **1999**, 71, 2334-2339.
54. Schriemer, D. C.; Li, L., Detection of high molecular weight narrow polydisperse polymers up to 1.5 million daltons by MALDI mass spectrometry. *Anal. Chem.* **1996**, 68, 2721-2725.
55. Dreisewerd, K., The desorption process in MALDI. *Chem. Rev.* **2003**, 103, 395-426.

56. Caldwell, K. L.; McGarity, D. R.; Murray, K. K., Matrix-assisted laser desorption/ionization with a tunable mid-infrared optical parametric oscillator. *J. Mass Spectrom.* **1997**, 32, 1374-1377.
57. Overberg, A.; Karas, M.; Bahr, U.; Kaufmann, R.; Hillenkamp, F., Matrix-assisted infrared laser (2940 nm) desorption/ionization mass spectrometry of large biomolecules. . *Rapid. Commun. Mass Spectrom.* **1990**, 4, 293-296.
58. Sadeghi, M.; Olumee, Z.; Tang, X.; Vertes, A.; Jiang, Z. X.; Henderson, A. J.; Lee, H. S.; Doroshenko, V. M.; Prasad, C. R., Compact tunable Cr:LiSAF laser for infrared matrix-assisted laser desorption/ionization. *Rapid. Commun. Mass Spectrom.* **1997**, 11, 393-397.
59. Murray, K. K., Coupling matrix-assisted laser desorption/ionization to liquid separations. *Mass Spectrom. Rev.* **1997**, 16, 283-299.
60. Murray, K. K.; Russell, D. H., Liquid sample introduction for matrix-assisted laser desorption ionization. *Anal. Chem.* **1993**, 65, 2534-2537.
61. Murray, K. K.; Russell, D. H., Aerosol matrix-assisted laser desorption ionization mass spectrometry. *J. Am. Soc. Mass Spectrom.* **1994**, 5, 1-9.
62. Murray, K. K.; Lewis, T. M.; Beeson, M. D.; Russell, D. H., Aerosol Matrix-assisted laser desorption ionization for liquid chromatography/time-of-flight mass spectrometry. *Anal. Chem.* **1994**, 66, 1601-1609.
63. Fei, X.; Murray, K. K., On-line coupling of gel permeation chromatography with MALDI mass spectrometry. *Anal. Chem.* **1996**, 68, 3555-3560.
64. Li, L.; Wang, A. P. L.; Coulson, L. D., Continuous-flow matrix-assisted laser desorption ionization mass spectrometry. *Anal. Chem.* **1993**, 65, 493-495.
65. Lawson, S. J.; Murray, K. K., Continuous flow infrared matrix-assisted laser desorption /ionization with a solvent matrix. *Rapid Commun. Mass Spectrom.* **2000**, 14, 129-134.
66. Knochenmuss, R.; Zhigilei, L. V., What determines MALDI ion yields? A molecular dynamics study of ion loss mechanisms. *Anal. Bioanal. Chem.* **2012**, 402, 2511-2519.
67. Knochenmuss, R.; Zhigilei, L. V., Molecular dynamics simulations of MALDI: laser fluence and pulse width dependence of plume characteristics and consequences for matrix and analyte ionization. *J. Mass Spectrom.* **2010**, 45, 333-346.
68. Karas, M.; Bachmann, D.; Bahr, U.; Hillenkamp, F., Matrix-assisted ultraviolet laser desorption of non-volatile compounds. *Int. J. Mass Spectrom. Ion Processes* **1987**, 78, 53-68.
69. Ehring, H.; Karas, M.; Hillenkamp, F., Role of photoionization and photochemistry in ionization processes of organic molecules and relevance for matrix-assisted laser desorption ionization mass spectrometry. *Org. Mass Spectrom.* **1992**, 27, 472-480.

70. Karas, M.; Kruger, R., Ion formation in MALDI: the cluster ionization mechanism. *Chem. Rev.* **2003**, 103, 427-439.
71. Kruger, R.; Pfenninger, A.; Fournier, I.; Gluckmann, M.; Karas, M., Analyte incorporation and ionization in matrix-assisted laser desorption/ionization visualized by pH indicator molecular probes. *Anal. Chem.* **2001**, 73, 5812-5821.
72. Mowry, C.; Johnston, M. V., Simultaneous detection of ions and neutrals produced by matrix-assisted laser desorption. *Rapid Commun. Mass Spectrom.* **1993**, 7, 569-575.
73. Puretzky, A. A.; Geohegan, D. B., Gas-phase diagnostics and LIF imaging of 3-hydroxypicolinic acid MALDI matrix plumes. *Chem. Phys. Lett.* **1997**, 286, 425-432.
74. Dreisewerd, K.; Schurenberg, M.; Karas, M.; Hillenkamp, F., Influence of the laser intensity and spot size on the desorption of molecules and ions in matrix-assisted laser desorption/ionization with a uniform beam profile. *Int. J. Mass Spectrom.* **1995**, 141, 127-148.
75. Quist, A. P.; Huth-Fehre, T.; Sundqvist, B. U. R., Total yield measurements in matrix-assisted laser desorption using a quartz crystal microbalance. *Rapid Commun. Mass Spectrom.* **1994**, 8, 149-154.
76. Kebarle, P.; Verkerk, U. H., Electrospray: from ions in solution to ions in the gas phase, what we know now. *Mass Spectrom. Rev.* **2009**, 28, 898-917.
77. Fenn, J. B.; Mann, M.; Meng, C. K.; Wong, S. F.; Whitehouse, C. M., Electrospray ionization for mass spectrometry of large biomolecules. *Science* **1989**, 246, 64-71.
78. Dole, M.; Mack, L. L.; Hines, R. L.; Mobley, R. C.; Ferguson, L. D.; Alice, M. B., Molecular beams of macroions. *J. Chem. Phys.* **1968**, 49, 2240-2249.
79. Iribarne, J. V.; Thomson, B. A., On the evaporation of small ions from charged droplets. *J. Chem. Phys.* **1976**, 64, 2287-2294.
80. McMaster, M., LC/MS: a practical user's guide. *Wiley-Interscience, New York* **2005**.
81. Cooks, R. G.; Ouyang, Z.; Takats, Z.; Wiseman, J. M., Ambient mass spectrometry. *Science* **2006**, 311, 1566-1570.
82. Ifa, D. R.; Wu, C.; Zheng, O.; Cooks, R. G., Desorption electrospray ionization and other ambient ionization methods: current progress and preview. *Analyst* **2010**, 135, 669-681.
83. Venter, A.; Nefliu, M.; Cooks, R. G., Ambient desorption ionization mass spectrometry. *Trends Anal. Chem.* **2008**, 27, (284-290).
84. Cody, R. B., Observation of molecular ions and analysis of nonpolar compounds with the direct analysis in real time ion source. *Anal. Chem.* **2009**, 81, 1101-1107.

85. Chrisey, D. B.; Hubler, G. K., *Pulsed Laser Deposition of Thin Films*, Wiley, New York **1994**.
86. Becker, M. F.; Brock, J. R.; Cai, H.; Heneke, D. E.; Keto, J. W.; Lee, J.; Nichols, W. T.; Glicksman, H. D., Metal nanoparticles generated by laser ablation. *Nanostructured Mater.* **1998**, 10, 853-863.
87. Ameer-Beg, S.; Perrie, W.; Rathbone, S.; Wright, J.; Weaver, W.; Champoux, H., Femtosecond laser microstructuring of materials. *Appl. Surf. Sci.* **1998**, 127-129, 875-880.
88. Marcinkevicius, A.; Juodkazis, S.; Watanabe, M.; Miwa, M.; Matsuo, S.; Misawa, H.; Nishii, J., Femtosecond laser-assisted three-dimensional microfabrication in silica. *Opt. Lett.* **2001**, 26, 277-279.
89. Vogel, A.; Venugopalan, V., Mechanisms of pulsed laser ablation of biological tissues. *Chem. Rev.* **2003**, 103, 577-644.
90. Russo, R. E., Laser ablation. *Appl. Spectrosc.* **1995**, 49, 14A-28A.
91. Mao, X.; Russo, R. E., Optimization and calibration of laser ablation inductively coupled plasma atomic emission spectrometry by measuring vertical spatial intensity profiles. *J. Anal. Atom. Spectrom.* **1997**, 12, 177-182.
92. Kabashin, A. V.; Meunier, M., Laser ablation-based nanofabrication in aqueous solutions. *Mater. Res. Soc. Symp. Proc.* **2004**, 850, 217-223.
93. Gunther, D.; Hattendorf, B., Solid sample analysis using laser ablation inductively coupled plasma mass spectrometry. *Trends Anal. Chem.* **2005**, 24, 255-265.
94. Hergenroder, R., Laser-generated aerosols in laser ablation for inductively coupled plasma spectrometry. *Spectrochim. Acta B* **2006**, 61, 284-300.
95. Mokgalaka, N. S.; Gardea-Torresdey, J. L., Laser ablation inductively coupled plasma mass spectrometry: principles and applications. *Appl. Spectrosc. Rev.* **2006**, 41, 131-150.
96. Koch, J.; Gunther, D., Femtosecond laser ablation inductively coupled plasma mass spectrometry achievements and remaining problems. *Anal. Bioanal. Chem.* **2007**, 387, 149-153.
97. Sneddon, J.; Lee, Y.-I., Laser-induced breakdown spectrometry. *Curr. Top. Anal. Chem.* **2004**, 4, 111-117.
98. Babushok, V. I.; Delucia, F. C.; Gottfried, J. L.; Munson, C. A.; Miziolek, A. W., Double pulse laser ablation and plasma: Laser induced breakdown spectroscopy signal enhancement. *Spectrochim. Acta Part B* **2006**, 61B, 999-1014.
99. Harmon, R. S.; Delucia, F. C.; McManus, C. E.; McMillan, N. J.; Jenkins, T. F.; Walsh, M. E.; Miziolek, A., Laser-induced breakdown spectroscopy - An emerging chemical sensor

technology for real-time field-portable, geochemical, mineralogical, and environmental applications. *Appl. Geochem.* **2006**, 21, 730-747.

100. Singh, S., Laser microprobe mass spectrometry. *Nature* **1987**, 329, 183-184.
101. Stump, M. J.; Fleming, R. C.; Gong, W.-H.; Jaber, A. J.; Jones, J. J.; Surber, C. W.; Wilkins, L., C., Matrix-assisted laser desorption mass spectrometry. *Appl. Spectrosc. Rev.* **2002**, 37, 275-303.
102. Zhigilei, L. V.; Garrison, B. J., Microscopic mechanisms of laser ablation of organic solids in the thermal and stress confinement irradiation regimes. *J. Appl. Phys.* **2000**, 88, 1281-1298.
103. Zhigilei, L. V.; Garrison, B. J., Molecular dynamics simulation study of the fluence dependence of particle yield and plume composition in laser desorption and ablation of organic solids. *Appl. Phys. Lett.* **1999**, 74, 1341-1343.
104. Song, K. H.; Xu, X., Explosive phase transformations in excimer laser ablation. *Appl. Surf. Sci.* **1998**, 127-129, 111-116.
105. Miotello, A., Laser-induced phase explosion: new physical problems when a condensed phase approaches the thermodynamic critical temperature. *Appl. Phys. A* **1999**, 69, S67-S73.
106. Fan, X.; Murray, K. K., UV laser irradiation of IR laser generated particles ablated from nitrobenzyl alcohol. *Appl. Surf. Sci.* **2009**, 255, 6297-6302.
107. Bauerle, D., Laser processing and chemistry, 4th edition. *Springer Heidelberg Dordrecht New York* **2011**.
108. Torres, R. D.; Johnston, S. L.; Haglund Jr., R. F.; Hwang, J.; Burn, P. L.; Holloway, P. H., Mechanisms of resonant infrared matrix-assisted pulsed laser evaporation. *Crit. Rev. Solid State Mater. Sci.* **2011**, 36, 16-45.
109. Johnston, S. L.; Bubb, D. M.; Haglund Jr., R. F., Phase explosion and recoil-induced ejection in resonant-infrared laser ablation of polystyrene. *Appl. Phys. A* **2009**, 96, 627-635.
110. Zhigilei, L. V.; Lin, Z.; Ivanov, D. S., Atomistic modeling of short pulse laser ablation of metals: connections between melting, spallation, and phase explosion. *J. Phys. Chem. C* **2009**, 113, 11892-11906.
111. Bencsura, A.; Vertes, A., Dynamics of hydrogen bonding and energy transfer in matrix-assisted laser desorption. *Chem. Phys. Lett.* **1995**, 247, 142-148.
112. Thomas, D. A.; Lin, Z.; Zhigilei, L. V.; Gurevich, E. L., Atomistic modeling of femtosecond laser-induced melting and atomic mixing in Au film - Cu substrate system. *Appl. Surf. Sci.* **2009**, 255, 9605-9612.

113. Schoolcraft, T. A.; Constable, G. S.; Zhigilei, L. V.; Garrison, B. J., Molecular dynamics simulation of the laser disintegration of aerosol particles. *Anal. Chem.* **2000**, *72*, 5143-5150.
114. Knochenmuss, R.; Zhigilei, L. V., Molecular dynamics model of ultraviolet matrix-assisted laser desorption/ionization including ionization processes. *J.Phys. Chem. B* **2005**, *109*, 22947-22957.
115. Knochenmuss, R.; Zhigilei, L. V., What determines MALDI ion yields? A molecular dynamics study of ion loss mechanisms. *Anal. Bioanal. Chem.* **2011**, Online First™, July 3
116. Zhigilei, L. V.; Leveugle, E.; Garrison, B. J.; Yingling, Y. G.; Zeifman, M. I., Computer simulations of laser ablation of molecular substrates. *Chem. Rev.* **2003**, *103*, 321-347.
117. Itina, T. E.; Zhigilei, L. V.; Garrison, B. J., Matrix assisted pulsed laser evaporation of polymeric materials: molecular dynamic simulation. *Nucl. Instr. Meth. B* **2001**, *180*, 238-244.
118. Itina, T. E.; Zhigilei, L. V.; Garrison, B. J., Microscopic mechanisms of matrix assisted laser desorption of analyte molecules: insights from molecular dynamics simulation. *J. Phys. Chem. B* **2002**, *106*, 303-310.
119. Zhigilei, L. V.; Garrison, B. J., Mechanisms of laser ablation from molecular dynamics simulations: dependence on the initial temperature and pulse duration. *Appl. Phys. A* **1999**, *69*, S75-S80.
120. Mao, S. S.; Mao, X.; Greif, R.; Russo, R. E., Initiation of an early-stage plasma during picosecond laser ablation of solids. *Appl. Phys. Lett.* **2000**, *77*, 2464-2466.
121. Mao, X.; Russo, R. E., Observation of plasma shielding by measuring transmitted and reflected laser pulse temporal profiles. *Appl. Phys. A* **1997**, *64*, 1-6.
122. Amoruso, S.; Bruzzese, R.; Velotta, R., Characterization of laser-ablation plasmas. *J. Phys. B: At. Mol. Opt. Phys.* **1999**, *32*, R131-R172.
123. Vertes, A.; Irinyi, G.; Gijbels, R., Hydrodynamic model of matrix assisted laser desorption mass spectrometry. *Anal. Chem.* **1993**, *65*, 2389-2393.
124. Wood, R. F.; Leboeuf, J. N.; Chen, K. R.; Geohegan, D. B.; Puretzky, A. A., Dynamics of plume propagation, splitting, and nanoparticle formation during pulsed-laser ablation. *Appl. Surf. Sci.* **1998**, *127-129*, 151-158.
125. Garrelie, F.; Champeaux, C.; Catherinot, A., Study by a Monte Carlo simulation of the influence of a background gas on the expansion dynamics of a laser-induced plasma plume. *Appl. Phys. A* **1999**, *69*, 45-50.
126. Itina, T. E.; Marine, W.; Autric, M., Monte Carlo simulation of the effects of elastic collisions and chemical reactions on the angular distributions of the laser ablated particles. *Appl. Surf. Sci.* **1998**, *127-129*, 171-176.

127. Oliveira, V.; Vilar, R., Finite element simulation of pulsed laser ablation of titanium carbide. *Appl. Surf. Sci.* **2007**, 253, 7810-7814.
128. Vasantgadkar, N. A.; Bhandarkar, U. V.; Joshi, S. S., A finite element model to predict the ablation depth in pulsed laser ablation. *Thin Solid Films* **2010**, 519, 1421-1430.
129. Tsai, C.-H.; Chen, H.-W., Laser cutting of thick ceramic substrates by controlled fracture technique. *J. Mater. Process Tech.* **2003**, 136, 166-173.
130. Marqa, M.-F.; Colin, P.; Nevoux, P.; Mordon, S. R.; Betrouni, N., Focal laser ablation of prostate cancer: numerical simulation of temperature and damage distribution. *Biomedical Engineering OnLine* **2011**, 10:45.
131. Cotter, R. J., Time-of-flight mass spectrometry: instrumentation and applications in biological research. *American Chemical Society, Washington, D. C.* **1997**.
132. Vestal, M. L., Modern MALDI time-of-flight mass spectrometry. *J. Mass Spectrom.* **2009**, 44, 303-317.
133. March, R. E., An introduction to quadrupole ion trap mass spectrometry. *J. Mass Spectrom.* **1997**, 32, 351-369.
134. Bessoth, F. G.; deMello, A. J.; Manz, A., Microstructure for efficient continuous flow mixing. *Anal. Commun.* **1999**, 36, 213-215.
135. Hillenkamp, F.; Peter-Katalinic, J., MALDI MS-a practical guide to instrumentation and applications. *Wiley-VCH: Weinheim* **2007**.
136. Dreisewerd, K.; Berkenkamp, S.; Leisner, A.; Rohlfing, A.; Menzel, C., Fundamentals of matrix-assisted laser desorption/ionization mass spectrometry with pulsed infrared lasers. *Int. J. Mass Spectrom.* **2003**, 226, 189-209.
137. Murray, K. K., *Infrared MALDI. In: Encyclopedia of Mass Spectrometry. R. M. Caprioli, M. L. Gross, Eds. Elsevier, Amsterdam, Vol. VI* **2006**.
138. Berkenkamp, S.; Karas, M.; Hillenkamp, F., Ice as a matrix for IR-matrix-assisted laser desorption/ionization: mass spectra from a protein single crystal. *Proc. Natl. Acad. Sci. USA* **1996**, 93, 7003-7007.
139. Berkenkamp, S.; Kirpekar, F.; Hillenkamp, F., Infrared MALDI mass spectrometry of large nucleic acids. *Science* **1998**, 281, 260-262.
140. Li, Y.; Shrestha, B.; Vertes, A., Atmospheric pressure molecular imaging by infrared MALDI mass spectrometry. *Anal. Chem.* **2007**, 79, 523-532.
141. Von Seggern, C. E.; Gardner, B. D.; Cotter, R. J., Infrared atmospheric pressure MALDI ion trap mass spectrometry of frozen samples using a Peltier-cooled sample stage. *Anal. Chem.* **2004**, 76, 5887-5893.

142. Tang, X.; Sadeghi, M.; Olumee, Z.; Vertes, A., Matrix-assisted laser desorption/ionization by two collinear subthreshold laser pulses. *Rapid Commun. Mass Spectrom.* **1997**, 11, 484-488.
143. Boesl, U.; Weinkauff, R.; Weickhardt, C.; Schlag, E. W., Laser ion sources for time-of-flight mass spectrometry. *Int. J. Mass Spectrom. Ion Processes* **1994**, 131, 87-124.
144. Grotemeyer, J.; Schlag, E. W., Biomolecules in the gas phase: multiphoton ionization mass spectrometry. *Acc. Chem. Res.* **1989**, 22, 399-406.
145. Schlag, E. W.; Grotemeyer, J.; Levine, R. D., Do large molecules ionize? *Chem. Phys. Lett.* **1992**, 190, 521-527.
146. Carson, P. G.; Neubauer, K. R.; Johnston, M. V.; Wexler, A. S., On-line chemical analysis of aerosols by rapid single-particle mass spectrometry. *J. Aero. Sci.* **1995**, 26, 535-545.
147. Leisner, A.; Rohlfing, A.; Berkenkamp, S.; Hillenkamp, F.; Dreisewerd, K., Infrared laser post-ionization of large biomolecules from an IR-MALD(I) plume. *J. Am. Soc. Mass Spectrom.* **2004**, 15, 934-941.
148. Lin, H.; Murray, K. K., 337 nm Matrix-assisted laser desorption/ionization of single aerosol particles. *J. Mass Spectrom.* **1999**, 34, 909-914.
149. Sinha, M. P., Laser-induced volatilization and ionization of aerosol particles for their mass spectral analysis in real time. *Applied Spectro. in Mater. Sci., David D. Saperstein; Ed* **1991**, Proc. SPIE Vol. 1437, 150-156.
150. Rohlfing, A.; Menzel, C.; Kukreja, L. M.; Hillenkamp, F.; Dreisewerd, K., Photoacoustic analysis of matrix-assisted laser desorption/ionization processes with pulsed infrared lasers. *J. Phys. Chem. B* **2003**, 107, 12275-12286.
151. Ackermann, B. L.; Berna, M. J.; Eckstein, J. A.; Ott, L. W.; Chaudhary, A. K., Current applications of liquid chromatography/mass spectrometry in pharmaceutical discovery after a decade of innovation. *Annu. Rev. Anal. Chem.* **2008**, 1, 357-396.
152. Maurer, H. H., Current role of liquid chromatography mass spectrometry in clinical forensic toxicology. *Anal. Bioanal. Chem.* **2007**, 388, 1315-1325.
153. Tomer, K. B., Separations combined with mass spectrometry. *Chem. Rev.* **2001**, 101, 297-328.
154. Cook, K.; Bennett, K.; Haddix, M., On-line mass spectrometry: a faster route to process monitoring and control. *Ind. Eng. Chem. Res.* **1999**, 38, 1192-1204.
155. Diehl, G.; Karst, U., On-line electrochemistry - MS and related techniques. *Anal. Bioanal. Chem.* **2002**, 373, 390-298.

156. Fabris, D., Mass spectrometric approaches for the investigation of dynamic processes in condensed phase. *Mass Spectrom. Rev.* **2005**, 24, 30-54.
157. Santos, L.; Knaack, L.; Metzger, J., Investigation of chemical reactions in solution using API-MS. *Int. J. Mass Spectrom.* **2005**, 246, 84-104.
158. Eberlin, M. N., Electrospray ionization mass spectrometry: a major tool to investigate reaction mechanisms in both solution and the gas phase. *Eur. J. Mass Spectrom.* **2007**, 13, 19-28.
159. Mirza, U.; Chait, B. T.; Lander, H., Monitoring reactions of nitric oxide with peptides and proteins by electrospray ionization mass spectrometry. *J. Biol. Chem.* **1995**, 270, 17185-17188.
160. Orsnes, H.; Graf, T.; Degn, H.; Murray, K. K., A rotating ball inlet for on-line MALDI mass spectrometry. *Anal. Chem.* **2000**, 72, 251-254.
161. Caprioli, R. M., Analysis of biochemical reactions with molecular specificity using fast atom bombardment mass spectrometry. *Biochemistry* **1998**, 27, 513-521.
162. Caprioli, R. M.; Lin, S. N., On-line analysis of penicillin blood levels in the live rat by combined microdialysis/fast atom bombardment mass spectrometry. *Proc. Natl. Acad. Sci. USA* **1990**, 87, 240-243.
163. Liesener, A.; Karst, U., Monitoring enzymatic conversions by mass spectrometry: a critical review. *Anal. Bioanal. Chem.* **2005**, 382, 1451-1464.
164. Brivio, M.; Fokken, R. H.; Verboom, W.; Reinhoudt, D. N.; Tas, N. R.; Goedbloed, M.; van den Berg, D., Integrated microfluidic system enabling (bio)chemical reactions with on-line MALDI-TOF mass spectrometry. *Anal. Chem.* **2002**, 74, 3972-3976.
165. Petucci, C.; Diffendal, J.; Kaufman, D.; Mekonnen, B.; Terefenko, G.; Musselman, B., Direct analysis in real time for reaction monitoring in drug discovery. *Anal. Chem.* **2007**, 79, 5064-5070.
166. Chen, H.; Wortmann, A.; Zenobi, R., Neutral desorption sampling coupled to extractive electrospray ionization mass spectrometry for rapid differentiation of biosamples by metabolomic fingerprinting. *J. Mass Spectrom.* **2007**, 42, 1123-1135.
167. Zhu, L.; Gamez, G.; Chen, H.; Huang, H.; Chingin, K.; Zenobi, R., Real-time, on-line monitoring of organic chemical reactions using extractive electrospray ionization tandem mass spectrometry. *Rapid Commun. Mass Spectrom.* **2008**, 22, 2993-2998.
168. Peng, I. X.; Loo, R. R. O.; Shiea, J., Reactive-electrospray-assisted laser desorption/ionization for characterization of peptides and proteins. *Anal. Chem.* **2008**, 80, 6995-7003.
169. Dong, J.; Rezenom, Y. H.; Murray, K. K., Desorption electrospray ionization of aerosol particles. *Rapid Commun. Mass Spectrom.* **2007**, 21, 3995-4000.

170. Harris, D. C., *Quantitative Chemical Analysis 6th ed* **2003**.
171. Chait, B. T.; Field, F. H., A rapid, sensitive mass spectrometric method for investigating microscale chemical reactions of surface adsorbed peptides and proteins. *Biochem. & Biophys. Res. Commun.* **1986**, 134, 420-426.
172. Park, Z.-Y.; Russell, D. H., Identification of individual proteins in complex protein mixtures by high-resolution, high-mass-accuracy MALDI TOF-mass spectrometry analysis of in-solution thermal denaturation/enzymatic digestion. *Anal. Chem.* **2001**, 73, 2558-2564.
173. Fischer, W. H.; Rivier, J. E.; Craig, A. G., In situ reduction suitable for matrix assisted laser desorption/ionization and liquid secondary ionization mass spectrometry using tris (2-carboxyethyl) phosphine. *Rapid Commun. Mass Spectrom.* **1993**, 7, 225-228.
174. Russo, R.; Mao, X.; Liu, H.; Gonzalez, J.; Mao, S., Laser ablation in analytical chemistry—a review. *Talanta* **2002**, 57, 425-451.
175. Semaltianos, N., Nanoparticles by Laser Ablation. *Crit. Rev. Solid State Mater. Sci.* **2010**, 35, (2), 105-124.
176. Hergenröder, R., Hydrodynamic sputtering as a possible source for fractionation in LA-ICP-MS. *J. Anal. Atom. Spectrom.* **2006**, 21, 517-524.
177. Radziemski, L. J., From laser to LIBS, the path of technology development. *Spectrochim. Acta Part B* **2002**, 57, 1109-1113.
178. VanVaeck, L.; Poels, K.; DeNollin, S.; Hachimi, A.; Gijbels, R., Laser microprobe mass spectrometry : principle and applications in biology and medicine. *Cell Biol. Int.* **1997**, 21, 634-648.
179. El-Aneed, A.; Cohen, A.; Banoub, J., Mass Spectrometry, Review of the Basics: Electrospray, MALDI, and Commonly Used Mass Analyzers. *Appl. Spectrosc. Rev.* **2009**, 44, 210-230.
180. Eckerskorn, C.; Strupat, K.; Schleuder, D.; Hochstrasser, D.; Sanchez, J.; Lottspeich, F.; Hillenkamp, F., Analysis of proteins by direct-scanning infrared-MALDI mass spectrometry after 2D- PAGE separation and electroblotting. *Anal. Chem.* **1997**, 69, 2888-2892.
181. Xu, Y.; Little, M. W.; Rousell, D. J.; Laboy, J. L.; Murray, K. K., Direct from polyacrylamide gel infrared laser desorption/ionization. *Anal. Chem.* **2004**, 76, (4), 1078-1082.
182. Feldhaus, D.; Menzel, C.; Berkenkamp, S.; Hillenkamp, F.; Dreisewerd, K., Influence of the laser fluence in infrared matrix-assisted laser desorption/ionization with a 2.94 μm Er:YAG laser and a flat-top beam profile. *J. Mass Spectrom.* **2000**, 35, 1320-1328.
183. Johnson, S. L.; Schriver, K. E.; Haglund Jr., R. F.; Bubb, D. M., Effects of the absorption coefficient on resonant infrared laser ablation of poly(ethylene glycol). *J. Appl. Phys.* **2009**, 105, 024901.

184. Laboy, J. L.; Murray, K. K., Characterization of infrared matrix-assisted laser desorption ionization samples by Fourier transform infrared attenuated total reflection spectroscopy. *Appl. Spectro.* **2004**, *58*, 451-456.
185. Bulgakov, A. V.; Bulgakova, N. M., Interaction of laser radiation with matter. Laser plasma: Thermal model of pulsed laser ablation under the conditions of formation and heating of a radiation-absorbing plasma. *Quantum Electron.* **1999**, *29*, 433-437.
186. Lee, J.; Soper, S. A.; Murray, K. K., Microfluidic chips for mass spectrometry-based proteomics. *J. Mass Spectrom.* **2009**, *44*, 579-593.
187. Spraggins, J. M.; Caprioli, R. M., High-speed MALDI-TOF imaging mass spectrometry: rapid ion image acquisition and considerations for next generation instrumentation. *J. Am. Soc. Mass Spectrom.* **2011**, *22*, 1022-1031.
188. Park, S. G.; Murray, K. K., Infrared laser ablation sample transfer for MALDI and electrospray. *J. Am. Soc. Mass Spectrom.* **2011**, *22*, 1352-1362.

APPENDIX A. MATLAB PROGRAM FOR CALCULATING ABLATED SAMPLE VOLUME

The MATLAB program used to calculate the ablated glycerol volume shown in Figure 5-7 is given below. The (x,y) coordinate data set of isothermal lines at 689 K and 563 K for different laser energies were exported from Comsol, and input to MATLAB. The expression of y as a function of x for each laser energy was obtained using a polynomial approximation followed by integration to find the sample volume. The author thanks Zhe Nan from Mathematics Department at LSU for providing valuable information on calculations of sample volume.

```
clear all;
close all;

X=cell(1,11);
Y=cell(1,11);
T=cell(1,11);
[X{1},Y{1},T{1}]=textread('2.94 um 1000 J 5ns 563K.txt','%f%f%u');
[X{2},Y{2},T{2}]=textread('2.94 um 2000 J 5ns 563K.txt','%f%f%u');
[X{3},Y{3},T{3}]=textread('2.94 um 3000 J 5ns 563K.txt','%f%f%u');
[X{4},Y{4},T{4}]=textread('2.94 um 4000 J 5ns 563K.txt','%f%f%u');
[X{5},Y{5},T{5}]=textread('2.94 um 5000 J 5ns 563K.txt','%f%f%u');
[X{6},Y{6},T{6}]=textread('2.94 um 6000 J 5ns 563K.txt','%f%f%u');
[X{7},Y{7},T{7}]=textread('2.94 um 2000 J 5ns 689K.txt','%f%f%u');
[X{8},Y{8},T{8}]=textread('2.94 um 3000 J 5ns 689K.txt','%f%f%u');
[X{9},Y{9},T{9}]=textread('2.94 um 4000 J 5ns 689K.txt','%f%f%u');
[X{10},Y{10},T{10}]=textread('2.94 um 5000 J 5ns 689K.txt','%f%f%u');
[X{11},Y{11},T{11}]=textread('2.94 um 6000 J 5ns 689K.txt','%f%f%u');

X_34um=cell(1,6);
Y_34um=cell(1,6);
T_34um=cell(1,6);
[X_34um{1},Y_34um{1},T_34um{1}]=textread('3.40 um 3000 J 5ns 563K.txt','%f%f%u');
[X_34um{2},Y_34um{2},T_34um{2}]=textread('3.40 um 4000 J 5ns 563K.txt','%f%f%u');
[X_34um{3},Y_34um{3},T_34um{3}]=textread('3.40 um 5000 J 5ns 563K.txt','%f%f%u');
[X_34um{4},Y_34um{4},T_34um{4}]=textread('3.40 um 6000 J 5ns 563K.txt','%f%f%u');
[X_34um{5},Y_34um{5},T_34um{5}]=textread('3.40 um 5000 J 5ns 689K.txt','%f%f%u');
[X_34um{6},Y_34um{6},T_34um{6}]=textread('3.40 um 6000 J 5ns 689K.txt','%f%f%u');

p=cell(1,11);
S=cell(1,11);
mu=cell(1,11);
```

```

p_34um=cell(1,6);
S_34um=cell(1,6);
mu_34um=cell(1,6);

for i=1:11
    p{i}=polyfit(X{i},Y{i},2);
end

f=cell(1,11);

for i=1:11
    f{i}=polyval(p{i},X{i});
end

plot(X{1},Y{1},'o',X{1},f{1},'-')

fprintf('Polynomial Fitting Coefficients: \n ');
fprintf('p1 p2 p3 \n')
for i=1:11

fprintf('%20.16e %20.16e %20.16e \n',p{i}(1),p{i}(2),p{i}(3));
end

root=cell(1,11);
for i=1:11
    root{i}=roots(p{i});
end

rootPos=cell(11,1);
for i=1:11
    rootPos{i}=root{i}(root{i}>0);
end

volume=zeros(1,11);

for i=1:11
    r=rootPos{i};
    p1=p{i}(1);
    p2=p{i}(2);
    p3=p{i}(3);
    volume(i)=-2*pi*(p1*r^4/4 + p2*r^3/3+p3*r^2/2);
end
fprintf('Volume: \n');

for i=1:11
    fprintf('%20.18e \n',volume(i));
end

% computation for the case 3.40 um

```

```

for i=1:6
    p_34um{i}=polyfit(X_34um{i},Y_34um{i},2);
end

f_34um=cell(1,6);

for i=1:6
f_34um{i}=polyval(p_34um{i},X_34um{i});
end

plot(X_34um{1},Y_34um{1},'o',X_34um{1},f_34um{1},'-')

fprintf('Polynomial Fitting Coefficients: \n ');
fprintf('p1 p2 p3 \n')
for i=1:6
fprintf('%20.16e %20.16e %20.16e \n',p_34um{i}(1),p_34um{i}(2),p_34um{i}(3));
end

root_34um=cell(1,6);
for i=1:6
    root_34um{i}=roots(p_34um{i});
end

rootPos_34um=cell(6,1);
for i=1:6
    rootPos_34um{i}=root_34um{i}(root_34um{i}>0);
end

volume_34um=zeros(1,6);

for i=1:6
    r_34um=rootPos_34um{i};
    p1_34um=p_34um{i}(1);
    p2_34um=p_34um{i}(2);
    p3_34um=p_34um{i}(3);
    volume_34um(i)=-2*pi*(p1_34um*r_34um^4/4
p2_34um*r_34um^3/3+p3_34um*r_34um^2/2);
end
fprintf('\Volume: \n');

for i=1:6
    fprintf('%20.18e \n',volume_34um(i));
end

xenergy563_34um=3:6;
xenergy689_34um=5:6;

yvolume563_34um=volume_34um(1:4);
yvolume689_34um=volume_34um(5:6);

```



```
xenergy563=1:6;  
xenergy689=2:6;
```

```
yvolume563=volume(1:6);  
yvolume689=volume(7:11);
```

APPENDIX B. LETTERS OF PERMISSION

JOHN WILEY AND SONS LICENSE

TERMS AND CONDITIONS

Feb 26, 2012

This is a License Agreement between Fan Huang ("You") and John Wiley and Sons ("John Wiley and Sons") provided by Copyright Clearance Center ("CCC"). The license consists of your order details, the terms and conditions provided by John Wiley and Sons, and the payment terms and conditions.

All payments must be made in full to CCC. For payment instructions, please see information listed at the bottom of this form.

License Number	2856691018060
License date	Feb 26, 2012
Licensed content publisher	John Wiley and Sons
Licensed content publication	Rapid Communications in Mass Spectrometry
Licensed content title	Continuous flow infrared matrix-assisted laser desorption electrospray ionization mass spectrometry
Licensed content author	Fan Huang, Kermit K. Murray
Licensed content date	Oct 15, 2010
Start page	2799

End page	2804
Type of use	Dissertation/Thesis
Requestor type	Author of this Wiley article
Format	Print and electronic
Portion	Full article
Will you be translating?	No
Order reference number	
Total	0.00 USD

Terms and Conditions

TERMS AND CONDITIONS

This copyrighted material is owned by or exclusively licensed to John Wiley & Sons, Inc. or one of its group companies (each a "Wiley Company") or a society for whom a Wiley Company has exclusive publishing rights in relation to a particular journal (collectively WILEY"). By clicking "accept" in connection with completing this licensing transaction, you agree that the following terms and conditions apply to this transaction (along with the billing and payment terms and conditions established by the Copyright Clearance Center Inc., ("CCC's Billing and Payment terms and conditions"), at the time that you opened your Rightslink account (these are available at any time at <http://myaccount.copyright.com>)

Terms and Conditions

1. The materials you have requested permission to reproduce (the "Materials") are protected by copyright.
2. You are hereby granted a personal, non-exclusive, non-sublicensable, non-transferable,

worldwide, limited license to reproduce the Materials for the purpose specified in the licensing process. This license is for a one-time use only with a maximum distribution equal to the number that you identified in the licensing process. Any form of republication granted by this licence must be completed within two years of the date of the grant of this licence (although copies prepared before may be distributed thereafter). The Materials shall not be used in any other manner or for any other purpose. Permission is granted subject to an appropriate acknowledgement given to the author, title of the material/book/journal and the publisher. You shall also duplicate the copyright notice that appears in the Wiley publication in your use of the Material. Permission is also granted on the understanding that nowhere in the text is a previously published source acknowledged for all or part of this Material. Any third party material is expressly excluded from this permission.

3. With respect to the Materials, all rights are reserved. Except as expressly granted by the terms of the license, no part of the Materials may be copied, modified, adapted (except for minor reformatting required by the new Publication), translated, reproduced, transferred or distributed, in any form or by any means, and no derivative works may be made based on the Materials without the prior permission of the respective copyright owner. You may not alter, remove or suppress in any manner any copyright, trademark or other notices displayed by the Materials. You may not license, rent, sell, loan, lease, pledge, offer as security, transfer or assign the Materials, or any of the rights granted to you hereunder to any other person.

4. The Materials and all of the intellectual property rights therein shall at all times remain the exclusive property of John Wiley & Sons Inc or one of its related companies (WILEY) or their respective licensors, and your interest therein is only that of having possession of and the right to reproduce the Materials pursuant to Section 2 herein during the continuance of this Agreement. You agree that you own no right, title or interest in or to the Materials or any of the intellectual property rights therein. You shall have no rights hereunder other than the license as provided for above in Section 2. No right, license or interest to any trademark, trade name, service mark or other branding ("Marks") of WILEY or its licensors is granted hereunder, and you

agree that you shall not assert any such right, license or interest with respect thereto.

5. NEITHER WILEY NOR ITS LICENSORS MAKES ANY WARRANTY OR REPRESENTATION OF ANY KIND TO YOU OR ANY THIRD PARTY, EXPRESS, IMPLIED OR STATUTORY, WITH RESPECT TO THE MATERIALS OR THE ACCURACY OF ANY INFORMATION CONTAINED IN THE MATERIALS, INCLUDING, WITHOUT LIMITATION, ANY IMPLIED WARRANTY OF MERCHANTABILITY, ACCURACY, SATISFACTORY QUALITY, FITNESS FOR A PARTICULAR PURPOSE, USABILITY, INTEGRATION OR NON-INFRINGEMENT AND ALL SUCH WARRANTIES ARE HEREBY EXCLUDED BY WILEY AND ITS LICENSORS AND WAIVED BY YOU.

6. WILEY shall have the right to terminate this Agreement immediately upon breach of this Agreement by you.

7. You shall indemnify, defend and hold harmless WILEY, its Licensors and their respective directors, officers, agents and employees, from and against any actual or threatened claims, demands, causes of action or proceedings arising from any breach of this Agreement by you.

8. IN NO EVENT SHALL WILEY OR ITS LICENSORS BE LIABLE TO YOU OR ANY OTHER PARTY OR ANY OTHER PERSON OR ENTITY FOR ANY SPECIAL, CONSEQUENTIAL, INCIDENTAL, INDIRECT, EXEMPLARY OR PUNITIVE DAMAGES, HOWEVER CAUSED, ARISING OUT OF OR IN CONNECTION WITH THE DOWNLOADING, PROVISIONING, VIEWING OR USE OF THE MATERIALS REGARDLESS OF THE FORM OF ACTION, WHETHER FOR BREACH OF CONTRACT, BREACH OF WARRANTY, TORT, NEGLIGENCE, INFRINGEMENT OR OTHERWISE (INCLUDING, WITHOUT LIMITATION, DAMAGES BASED ON LOSS OF PROFITS, DATA, FILES, USE, BUSINESS OPPORTUNITY OR CLAIMS OF THIRD PARTIES), AND WHETHER OR NOT THE PARTY HAS BEEN ADVISED OF THE POSSIBILITY OF SUCH DAMAGES. THIS LIMITATION SHALL APPLY NOTWITHSTANDING ANY FAILURE OF ESSENTIAL PURPOSE OF ANY LIMITED REMEDY PROVIDED HEREIN.

9. Should any provision of this Agreement be held by a court of competent jurisdiction to be

illegal, invalid, or unenforceable, that provision shall be deemed amended to achieve as nearly as possible the same economic effect as the original provision, and the legality, validity and enforceability of the remaining provisions of this Agreement shall not be affected or impaired thereby.

10. The failure of either party to enforce any term or condition of this Agreement shall not constitute a waiver of either party's right to enforce each and every term and condition of this Agreement. No breach under this agreement shall be deemed waived or excused by either party unless such waiver or consent is in writing signed by the party granting such waiver or consent. The waiver by or consent of a party to a breach of any provision of this Agreement shall not operate or be construed as a waiver of or consent to any other or subsequent breach by such other party.

11. This Agreement may not be assigned (including by operation of law or otherwise) by you without WILEY's prior written consent.

12. Any fee required for this permission shall be non-refundable after thirty (30) days from receipt.

13. These terms and conditions together with CCC's Billing and Payment terms and conditions (which are incorporated herein) form the entire agreement between you and WILEY concerning this licensing transaction and (in the absence of fraud) supersedes all prior agreements and representations of the parties, oral or written. This Agreement may not be amended except in writing signed by both parties. This Agreement shall be binding upon and inure to the benefit of the parties' successors, legal representatives, and authorized assigns.

14. In the event of any conflict between your obligations established by these terms and conditions and those established by CCC's Billing and Payment terms and conditions, these terms and conditions shall prevail.

15. WILEY expressly reserves all rights not specifically granted in the combination of (i) the license details provided by you and accepted in the course of this licensing transaction, (ii) these terms and conditions and (iii) CCC's Billing and Payment terms and conditions.

16. This Agreement will be void if the Type of Use, Format, Circulation, or Requestor Type was misrepresented during the licensing process.

17. This Agreement shall be governed by and construed in accordance with the laws of the State of New York, USA, without regards to such state's conflict of law rules. Any legal action, suit or proceeding arising out of or relating to these Terms and Conditions or the breach thereof shall be instituted in a court of competent jurisdiction in New York County in the State of New York in the United States of America and each party hereby consents and submits to the personal jurisdiction of such court, waives any objection to venue in such court and consents to service of process by registered or certified mail, return receipt requested, at the last known address of such party.

Wiley Open Access Terms and Conditions

All research articles published in Wiley Open Access journals are fully open access: immediately freely available to read, download and share. Articles are published under the terms of the [Creative Commons Attribution Non Commercial License](#), which permits use, distribution and reproduction in any medium, provided the original work is properly cited and is not used for commercial purposes. The license is subject to the Wiley Open Access terms and conditions: Wiley Open Access articles are protected by copyright and are posted to repositories and websites in accordance with the terms of the [Creative Commons Attribution Non Commercial License](#). At the time of deposit, Wiley Open Access articles include all changes made during peer review, copyediting, and publishing. Repositories and websites that host the article are responsible for incorporating any publisher-supplied amendments or retractions issued

subsequently.

Wiley Open Access articles are also available without charge on Wiley's publishing platform, **Wiley Online Library** or any successor sites.

Use by non-commercial users

For non-commercial and non-promotional purposes individual users may access, download, copy, display and redistribute to colleagues Wiley Open Access articles, as well as adapt, translate, text- and data-mine the content subject to the following conditions:

- The authors' moral rights are not compromised. These rights include the right of "paternity" (also known as "attribution" - the right for the author to be identified as such) and "integrity" (the right for the author not to have the work altered in such a way that the author's reputation or integrity may be impugned).
- Where content in the article is identified as belonging to a third party, it is the obligation of the user to ensure that any reuse complies with the copyright policies of the owner of that content.
- If article content is copied, downloaded or otherwise reused for non-commercial research and education purposes, a link to the appropriate bibliographic citation (authors, journal, article title, volume, issue, page numbers, DOI and the link to the definitive published version on Wiley Online Library) should be maintained. Copyright notices and disclaimers must not be deleted.
- Any translations, for which a prior translation agreement with Wiley has not been agreed, must prominently display the statement: "This is an unofficial translation of an article that appeared in a Wiley publication. The publisher has not endorsed this translation."

Use by commercial "for-profit" organisations

Use of Wiley Open Access articles for commercial, promotional, or marketing purposes requires further explicit permission from Wiley and will be subject to a fee. Commercial purposes include:

- Copying or downloading of articles, or linking to such articles for further redistribution, sale or licensing;
- Copying, downloading or posting by a site or service that incorporates advertising with such content;
- The inclusion or incorporation of article content in other works or services (other than normal quotations with an appropriate citation) that is then available for sale or licensing, for a fee (for example, a compilation produced for marketing purposes, inclusion in a sales pack)
- Use of article content (other than normal quotations with appropriate citation) by for-profit organisations for promotional purposes
- Linking to article content in e-mails redistributed for promotional, marketing or educational purposes;
- Use for the purposes of monetary reward by means of sale, resale, licence, loan, transfer or other form of commercial exploitation such as marketing products
- Print reprints of Wiley Open Access articles can be purchased

from: corporatesales@wiley.com

Other Terms and Conditions:

BY CLICKING ON THE "I AGREE..." BOX, YOU ACKNOWLEDGE THAT YOU HAVE READ AND FULLY UNDERSTAND EACH OF THE SECTIONS OF AND PROVISIONS SET FORTH IN THIS AGREEMENT AND THAT YOU ARE IN AGREEMENT WITH AND ARE WILLING TO ACCEPT ALL OF YOUR OBLIGATIONS AS SET FORTH IN THIS AGREEMENT.

v1.7

If you would like to pay for this license now, please remit this license along with your payment made payable to "COPYRIGHT CLEARANCE CENTER" otherwise you will be invoiced within 48 hours of the license date. Payment should be in the form of a check or money order referencing your account number and this invoice number RLNK500727005.

Once you receive your invoice for this order, you may pay your invoice by credit card. Please follow instructions provided at that time.

Make Payment To:

Copyright Clearance Center

Dept 001

P.O. Box 843006

Boston, MA 02284-3006

For suggestions or comments regarding this order, contact RightsLink Customer

Support: customercare@copyright.com or +1-877-622-5543 (toll free in the US) or +1-978-646-2777.

Gratis licenses (referencing \$0 in the Total field) are free. Please retain this printable license for your reference. No payment is required.



ELSEVIER LICENSE
TERMS AND CONDITIONS

Feb 26, 2012

This is a License Agreement between Fan Huang ("You") and Elsevier ("Elsevier") provided by Copyright Clearance Center ("CCC"). The license consists of your order details, the terms and conditions provided by Elsevier, and the payment terms and conditions.

All payments must be made in full to CCC. For payment instructions, please see information listed at the bottom of this form.

Supplier	Elsevier Limited The Boulevard, Langford Lane Kidlington, Oxford, OX5 1GB, UK
Registered Company Number	1982084
Customer name	Fan Huang
Customer address	232 Choppin Hall, Baton Rouge, LA 70803
License number	2856700490397
License date	Feb 26, 2012
Licensed content publisher	Elsevier
Licensed content publication	International Journal of Mass Spectrometry

Licensed content title	Matrix-assisted laser desorption ionization of infrared laser ablated particles
Licensed content author	Fan Huang,Xing Fan,Kermit K. Murray
Licensed content date	15 July 2008
Licensed content volume number	274
Licensed content issue number	1–3
Number of pages	4
Start Page	21
End Page	24
Type of Use	reuse in a thesis/dissertation
Portion	full article
Format	both print and electronic
Are you the author of this Elsevier article?	Yes
Will you be translating?	No
Order reference number	
Title of your thesis/dissertation	Infrared Laser Ablation for Biological Mass Spectrometry
Expected completion date	Apr 2012
Estimated size (number of pages)	120
Elsevier VAT number	GB 494 6272 12
Permissions price	0.00 USD
VAT/Local Sales Tax	0.0 USD / 0.0 GBP

Total

0.00 USD

[Terms and Conditions](#)

INTRODUCTION

1. The publisher for this copyrighted material is Elsevier. By clicking "accept" in connection with completing this licensing transaction, you agree that the following terms and conditions apply to this transaction (along with the Billing and Payment terms and conditions established by Copyright Clearance Center, Inc. ("CCC"), at the time that you opened your Rightslink account and that are available at any time at <http://myaccount.copyright.com>).

GENERAL TERMS

2. Elsevier hereby grants you permission to reproduce the aforementioned material subject to the terms and conditions indicated.

3. Acknowledgement: If any part of the material to be used (for example, figures) has appeared in our publication with credit or acknowledgement to another source, permission must also be sought from that source. If such permission is not obtained then that material may not be included in your publication/copies. Suitable acknowledgement to the source must be made, either as a footnote or in a reference list at the end of your publication, as follows:

“Reprinted from Publication title, Vol /edition number, Author(s), Title of article / title of chapter, Pages No., Copyright (Year), with permission from Elsevier [OR APPLICABLE SOCIETY COPYRIGHT OWNER].” Also Lancet special credit - “Reprinted from The Lancet, Vol. number, Author(s), Title of article, Pages No., Copyright (Year), with

permission from Elsevier.”

4. Reproduction of this material is confined to the purpose and/or media for which permission is hereby given.

5. Altering/Modifying Material: Not Permitted. However figures and illustrations may be altered/adapted minimally to serve your work. Any other abbreviations, additions, deletions and/or any other alterations shall be made only with prior written authorization of Elsevier Ltd. (Please contact Elsevier at permissions@elsevier.com)

6. If the permission fee for the requested use of our material is waived in this instance, please be advised that your future requests for Elsevier materials may attract a fee.

7. Reservation of Rights: Publisher reserves all rights not specifically granted in the combination of (i) the license details provided by you and accepted in the course of this licensing transaction, (ii) these terms and conditions and (iii) CCC's Billing and Payment terms and conditions.

8. License Contingent Upon Payment: While you may exercise the rights licensed immediately upon issuance of the license at the end of the licensing process for the transaction, provided that you have disclosed complete and accurate details of your proposed use, no license is finally effective unless and until full payment is received from you (either by publisher or by CCC) as provided in CCC's Billing and Payment terms and conditions. If full payment is not received on a timely basis, then any license preliminarily granted shall be deemed automatically revoked and shall be void as if never granted. Further, in the event that you breach any of these terms and conditions or any of CCC's Billing and Payment terms and conditions, the license is automatically revoked and shall be void as if never granted. Use of materials as described in a revoked license, as

well as any use of the materials beyond the scope of an unrevoked license, may constitute copyright infringement and publisher reserves the right to take any and all action to protect its copyright in the materials.

9. Warranties: Publisher makes no representations or warranties with respect to the licensed material.

10. Indemnity: You hereby indemnify and agree to hold harmless publisher and CCC, and their respective officers, directors, employees and agents, from and against any and all claims arising out of your use of the licensed material other than as specifically authorized pursuant to this license.

11. No Transfer of License: This license is personal to you and may not be sublicensed, assigned, or transferred by you to any other person without publisher's written permission.

12. No Amendment Except in Writing: This license may not be amended except in a writing signed by both parties (or, in the case of publisher, by CCC on publisher's behalf).

13. Objection to Contrary Terms: Publisher hereby objects to any terms contained in any purchase order, acknowledgment, check endorsement or other writing prepared by you, which terms are inconsistent with these terms and conditions or CCC's Billing and Payment terms and conditions. These terms and conditions, together with CCC's Billing and Payment terms and conditions (which are incorporated herein), comprise the entire agreement between you and publisher (and CCC) concerning this licensing transaction. In the event of any conflict between your obligations established by these terms and conditions and those established by CCC's Billing and Payment terms and conditions, these terms and conditions shall control.

14. Revocation: Elsevier or Copyright Clearance Center may deny the permissions

described in this License at their sole discretion, for any reason or no reason, with a full refund payable to you. Notice of such denial will be made using the contact information provided by you. Failure to receive such notice will not alter or invalidate the denial. In no event will Elsevier or Copyright Clearance Center be responsible or liable for any costs, expenses or damage incurred by you as a result of a denial of your permission request, other than a refund of the amount(s) paid by you to Elsevier and/or Copyright Clearance Center for denied permissions.

LIMITED LICENSE

The following terms and conditions apply only to specific license types:

15. **Translation:** This permission is granted for non-exclusive world **English** rights only unless your license was granted for translation rights. If you licensed translation rights you may only translate this content into the languages you requested. A professional translator must perform all translations and reproduce the content word for word preserving the integrity of the article. If this license is to re-use 1 or 2 figures then permission is granted for non-exclusive world rights in all languages.

16. **Website:** The following terms and conditions apply to electronic reserve and author websites:

Electronic reserve: If licensed material is to be posted to website, the web site is to be password-protected and made available only to bona fide students registered on a relevant course if:

This license was made in connection with a course,

This permission is granted for 1 year only. You may obtain a license for future website posting,

All content posted to the web site must maintain the copyright information line on the bottom of each image,

A hyper-text must be included to the Homepage of the journal from which you are licensing at <http://www.sciencedirect.com/science/journal/xxxxx> or the Elsevier homepage for books at <http://www.elsevier.com> , and

Central Storage: This license does not include permission for a scanned version of the material to be stored in a central repository such as that provided by Heron/XanEdu.

17. **Author website** for journals with the following additional clauses:

All content posted to the web site must maintain the copyright information line on the bottom of each image, and

the permission granted is limited to the personal version of your paper. You are not allowed to download and post the published electronic version of your article (whether PDF or HTML, proof or final version), nor may you scan the printed edition to create an electronic version,

A hyper-text must be included to the Homepage of the journal from which you are licensing at <http://www.sciencedirect.com/science/journal/xxxxx> , As part of our normal production process, you will receive an e-mail notice when your article appears on Elsevier's online service ScienceDirect (www.sciencedirect.com). That e-mail will include the article's Digital Object Identifier (DOI). This number provides the electronic link to the published article and should be included in the posting of your personal version. We ask that you wait until you receive this e-mail and have the DOI to do any posting.

Central Storage: This license does not include permission for a scanned version of the

material to be stored in a central repository such as that provided by Heron/XanEdu.

18. **Author website** for books with the following additional clauses:

Authors are permitted to place a brief summary of their work online only.

A hyper-text must be included to the Elsevier homepage at <http://www.elsevier.com>

All content posted to the web site must maintain the copyright information line on the bottom of each image

You are not allowed to download and post the published electronic version of your chapter, nor may you scan the printed edition to create an electronic version.

Central Storage: This license does not include permission for a scanned version of the material to be stored in a central repository such as that provided by Heron/XanEdu.

19. **Website** (regular and for author): A hyper-text must be included to the Homepage of the journal from which you are licensing

at <http://www.sciencedirect.com/science/journal/xxxxx>. or for books to the Elsevier

homepage at <http://www.elsevier.com>

20. **Thesis/Dissertation:** If your license is for use in a thesis/dissertation your thesis may be submitted to your institution in either print or electronic form. Should your thesis be published commercially, please reapply for permission. These requirements include permission for the Library and Archives of Canada to supply single copies, on demand, of the complete thesis and include permission for UMI to supply single copies, on demand, of the complete thesis. Should your thesis be published commercially, please reapply for permission.

21. **Other Conditions:**

v1.6

If you would like to pay for this license now, please remit this license along with your payment made payable to "COPYRIGHT CLEARANCE CENTER" otherwise you will be invoiced within 48 hours of the license date. Payment should be in the form of a check or money order referencing your account number and this invoice number RLNK500727014.

Once you receive your invoice for this order, you may pay your invoice by credit card. Please follow instructions provided at that time.

Make Payment To:

Copyright Clearance Center

Dept 001

P.O. Box 843006

Boston, MA 02284-3006

For suggestions or comments regarding this order, contact RightsLink Customer Support: customercare@copyright.com or +1-877-622-5543 (toll free in the US) or +1-978-646-2777.

Gratis licenses (referencing \$0 in the Total field) are free. Please retain this printable license for your reference. No payment is required.

VITA

Fan Huang was born in Beijing, China. He graduated from Peking University with a Bachelor of Science degree in chemistry in 2000. One year later, he enrolled at University of Science and Technology of China (USTC) where he majored in physical chemistry as a graduate student. His research project was *study of anion emitting material $12\text{CaO}\cdot 7\text{Al}_2\text{O}_3$* . During that time at USTC, he was once awarded the Guanghai Education Scholarship, an award that is granted to the top 5% of students. In 2005, he graduated with a Master of Science Degree from USTC and five publications, two of which were of first-author. In the same year, he decided to extend his study to the doctoral level in chemistry at Louisiana State University. In 2006, he joined Dr. Kermit Murray's research group to study mass spectrometry. The research interest during his doctoral program mainly focused on infrared laser ablation for biological mass spectrometry. He was involved in various research projects to develop ionization methods for mass spectrometry analysis of chemical and biomolecules. He is currently a member of the American Chemical Society (ACS) and the American Society for Mass Spectrometry (ASMS). He has presented his research at eight national conferences, and he has two publications and one manuscript in preparation as the first author. He is currently a candidate for the degree of Doctor of Philosophy in chemistry, which will be awarded at the May 2012 commencement.